Response to reviewers comments for the paper "**Quantifying the volatility of organic aerosol in the southeastern U.S.**" by Provat K. Saha et al.

To Whom It May Concern:

We would like to thank the two reviewers for their thoughtful and helpful comments. In addressing these comments, we feel we have substantially improved the manuscript. Here we provide a point-by-point response to review comments.

Please find below detailed responses in normal text (with direct quotes from the revised manuscript shown in *italics*) to the comments and suggestions (shown in **blue text**) offered by the two reviewers. The changes made in the revised manuscript and SI are marked-up with red text.

Best regards,

The Authors

Anonymous Referee #1

General Comments:

R1.0. Saha and co-authors present a well-articulated investigation of the volatility properties of organic aerosol at two sites in the southeast United States. The opportunity at Centerville, AL during SOAS is uniquely favorable since there were so many collocated measurements (of meteorological metrics and AMS factors, for example). The authors do a good job motivating the juxtaposition of these data to other data they have collected in Raleigh, albeit at a different time of year. Overall, I find the goal of the work and its presentation quality to be acceptable for ACP and important for the scientific community. However, I have some concerns about the discussion. For example, I think the issue of solubility, while not specifically addressed by their measurements, should be better woven throughout their discussions in the manuscript to make it clearer that the properties of volatility and solubility simultaneously affect the gas-particle partitioning of organic compounds. I look forward to discussing the following issues with the authors:

A1.0. We thank the reviewer for his/her review and useful comments. All of the items mentioned here are addressed in response to specific comments below.

R1.1. Page 2, Line 15: Although it is well-known that volatility plays a pivotal in gasparticle partitioning, I think it is worth mentioning that solubility will also be critical for this phenomenon, especially in places like the southeast US. Admittedly, solubility is outside the scope of this paper (and the RH of the observations is maintained relatively low at 30-40%). It is of course still vital and useful to gain an in-depth knowledge of the partitioning behavior of compounds to the "dry" organic phase. However, please also be careful throughout the text about statements like in line 17-18: "vapor pressure determines whether an organic compound is found in the particle- or gas-phase" since this is not exactly true for many compounds, which are highly volatile and highly soluble, for example. This should be reworded for completeness.

AR1.1. We thank the reviewer for pointing out the role of solubility in OA gas-particle partitioning. We certainly agree with the reviewer that solubility in water may also play an important role in the gas-particle partitioning of many organic species (e.g., isoprene related species). We have revised the text to address this point.

"*At equilibrium, volatility of organic species, specifically, saturation vapor pressure (or equivalently, saturation concentration, C^*; $\mu g\ m^{-3}$) plays a vital role in determining their gas-particle partitioning (Donahue et al., 2006; Pankow, 1994). Solubility in water may also be critical for gas-particle partitioning for many species (Hennigan et al., 2009), especially in places with higher relative humidity, for example, in the southeast U.S. Enthalpies of vaporization (ΔH_{vap}) dictate the change in partitioning with temperature (Donahue et al., 2006; Epstein et al., 2010). Although gas-particle partitioning is determined by the basic thermodynamic properties of OA species – their C^*, ΔH_{vap}, and solubility– these, along with the impacts of non-ideal mixing on individual species, are generally unknown for ambient OA.*"

R1.2. Did the authors size select the particles before entry to the TD units? It does not appear so. Could they comment on their method of incorporating the size distribution information into their model? Did they use a moving sectional, fixed sectional, or a modal algorithm? Or was only a single diameter used as is implied on page 6, line 13? If this is the case, can the authors provide some insight into how the inaccuracies introduced in their model results from the width of the

distributions (as seen in Fig. S6c,d)? Are there significant size-dependent particle losses in the system and are these temperature dependent?

AR1.2. We did not size select the particles before entry to the TD units. We heated a polydisperse distribution of particles in TDs and observed the changes in total volume/mass concentrations as a function of temperatures and residence times.

In our TD kinetic modeling, we assumed the volume median diameter (VMD) as a representative size for a polydisperse aerosol; a reasonable assumption to extract average properties of aerosol. This assumption has been examined in the past (Park et al., 2013) and shown to have a minuscule effect on modeled particle evaporation. For example, Park et al. (2013) tested this assumption (Fig. S4, SI in Park et al.) for a similar model formulation to ours and showed that assumptions of poly- and monodisperse size distributions to represent a single-mode aerosol lead to virtually indistinguishable model results. In our dual-TD method characterization paper (Saha et al., 2015), we included a sensitivity analysis (SI; section S.6) to explore the potential influence of changes in particle VMD within a generous range (which would have a much larger effect than simply including a polydisperse aerosol population). We have shown that sensitivity of VMD within this range does not substantially alter our derived volatility parameter values.

Regarding particle losses, we have applied empirically determined particle loss correction factors derived using non-volatile NaCl aerosol (this approach was discussed in Saha et al., 2015). Particle mass and number transmission through TDs is temperature dependent. The size dependence is much stronger for particle number transmission than mass/volume transmission. This is because of the substantial diffusional loss of smaller size particles which contribute relatively little to the particle mass/volume concentrations. We conducted our NaCl loss characterization experiments with a size distribution that was broadly comparable to the ambient distribution. Therefore, correcting our data with the mass transmission factors derived from laboratory-generated NaCl aerosol introduces minimal additional uncertainty.

R1.3. Page 6, Line 19-21: what is the reason for putting only the fi sets that have been "accepted" against the TS-TD data through the VRT-TD analysis? What sets are undetected by not doing both applications for every set and then taking the best performers? On a related note, what initial fi values were used as input to the solver and how dependent was the "accepted"

solution on these values? Were these initial conditions varied at all? Why are the authors confident they have evaluated the entire space of volatility distributions?

AR1.3. For a given input temperature (T) and residence time (Rt), the evaporation kinetic model predicts a mass fraction remaining; MFR (T, Rt). In our method, the fitting can be done in one step (fitting all data from TS-TD and VRT-TD together) or two steps. We have found that the two-step fitting approach gives essentially identical results to fitting all data simultaneously. We, therefore, decided to use a two-step fitting approach because it narrows down the parameter space substantially in the first step, which reduces the computational requirements substantially. An additional advantage to applying the 'two-step' approach in this work is that it distinctly demonstrates the benefit of adding the additional dimension (Rt) to the traditional TD measurement space (T) via goodness of fit quantification across the [γ_e, ΔH_{vap}] space at each step (Fig. 3). Thus, this approach/presentation gives insight into the range of parameter values that can be used to explain observations from 'single-dimensional' perturbations (only T) in typical TD arrangements used in various past/ongoing studies.

For solving for f_i distributions, we have used a non-linear constrained optimization solver (*fmincon* in Matlab). We tested our model with different initial guesses for f_i distributions, and optimal solutions were found to be insensitive to the initial guess for a given set of inputs. A constraint of $\Sigma f_i = 1$ was used. We have provided constraint for the lower (f_i minimum = 0.02) and upper (f_i maximum = 0.4) boundary for a f_i value in each C^* bin. This choice of a wide solution space for solving a f_i value in each C^* bin would address any sensitivity of the error to an optimum solution of f_i.

We have not evaluated the entire volatility distributions space using our method, and did not indicate this in the paper. However, we explicitly did mention that our selected C^* bin range was based on our measurement conditions; specifically, the highest TD operating temperature and the average ambient OA loading provide limitations on the lower and upper C* bins we consider, respectively. Within this predefined range, our approach provides an empirical OA volatility distribution that explains the observed evaporation of bulk OA in our dual-TD system.

R1.4. Page 7, Line 8-9: How do the enthalpies of vaporization used in this WRF-Chem simulation compare with those derived from the observations here (could they add this to the methods section)? What are the implications of comparing the volatility distribution from a

model to observations when they are using different enthalpies? Is this something that other researchers should take seriously when comparing model output to TD data? On Page 15, Lines 20-24, the authors provide some discussion of this issue. However, they seem to be assessing the sensitivity of the enthalpies in the model independently of the mass yields being used. Is this appropriate?

AR1.4. In our CTM evaluation, we focused on comparing our observed OA volatility distribution against the WRF/Chem output using the current treatment of OA in models. Therefore, we used the VBS parametrizations (e.g., C* bin range), SOA yields and ΔH_{vap} that are currently being used in the research community. For enthalpies of vaporization, the semi-empirical correlation by Epstein et al. (2010) ($\Delta H_{vap,\,i} = 130\text{-}11\log10C^{*}_{i,298}$) was used in the WRF/Chem simulation (discussed in section 2.5). Our TD parameter fitting used a generalized functional form for ΔH_{vap} ($\Delta H_{vap,\,i}$ = intercept-slope ($\log10C^{*}_{i,298}$)), where intercept and slope were fit parameters. We found that a $\Delta H_{vap,\,i} = 100\text{-}0$ ($\log10C^{*}_{i,298}$) relationship 'best' explained the observed temperature sensitivity of bulk OA in our TDs (See Fig. 3 and discussion in section 3.3).

It should be noted here that the reference VBS temperature was 25ºC for both WRF/Chem run and TD fits. The difference in ΔH_{vap} used in WRF/Chem runs and our TD-derived value would not have a significant effect on the comparison shown in Fig.10. This is because the modeled-measured OA volatility comparison was made at temperatures (SOAS campaign average T= 24.7ºC; WRF/Chem simulated campaign average T= 23.8ºC @ 2 m) that are very close to the VBS reference temperature (25ºC). Murphy et al. (2011) also reported a low sensitivity of ΔH_{vap} when predicting surface OA loading during the FAME-08 study using a 2D-VBS framework. However, the effect of ΔH_{vap} could be very significant when simulating OA loading at high altitudes. Therefore, we recommend that researchers should take the influence of ΔH_{vap} seriously, especially when comparing an OA volatility distribution from a CTM at a temperature that is very different from the reference temperature of VBS. We included relevant discussions in our revised manuscript in page 16, Lines 15-20. *"The difference in ΔH_{vap} values used in WRF/Chem and our TD-derived values should not have a significant effect on the comparison shown in Fig.10. This is because the modeled-measured OA volatility comparison was made at temperatures (SOAS campaign average T= 24.7ºC; WRF/Chem simulated campaign average T= 23.8ºC) very close to the VBS reference temperature (25ºC). Murphy et al. (2011) also reported*

a low sensitivity of ΔH_{vap} when predicating surface OA loading during the FAME-08 study using a 2D-VBS framework. However, the effect of ΔH_{vap} could be significant when simulating OA loading at low ambient temperatures and high altitudes."

Ideally, yields parameterization and ΔH_{vap} should be internally consistent for a CTM input. Traditionally yields parameterization and ΔH_{vap} have not been coupled and constrained consistently. Typically a ΔH_{vap} of 30 - 40 KJ mol^{-1} has been assumed for atmospheric modeling. A derivation of consistent parameterizations for yields and ΔH_{vap} as CTM inputs are not within the scope of our paper. Following previous work (Farina et al., 2010; Murphy et al., 2011), we briefly discussed the sensitivity of ΔH_{vap} to provide some insights into the influence of ΔH_{vap} in a qualitative sense.

R1.5. Page 9, Line 8-9: I'm not familiar with the term "condensation sink diameter". Could the authors please explain it and potentially provide an equation in the supporting info for this quantity? How is it related to the more common term, condensation sink which is in units of inverse time?

AR1.5. Yes, the concept of condensation sink diameter (d_{cs}) is related to condensation sink (CS). This concept is first described in Lehtinen et al. (2003). According to Lehtinen et al.,

"The condensation sink diameter of a distribution of particles with total number concentration N_{tot}, is the diameter where a monodisperse population of particles of number concentration N_{tot} should be placed to obtain the same total condensation sink (CS) as for the polydisperse distribution of interest."

Mathematically, $2\,\pi\,\mathrm{D} d_{cs} F(d_{cs}) N_{tot} = 2\,\pi\,\mathrm{D} \sum F(d_{p,i}) d_{p,i} N_i = CS$

Where, D is the diffusion coefficient, F is the Fuchs and Sutugin correction factor, N_i is the number concentration of particles in size bin of $d_{p,i}$. A new section (Sec. S2) has been added to the SI detailing the estimation of condensation sink diameter.

R1.6. Do the authors have an explanation for why the 80-0 and 80-4 cases with evaporation coefficient equal to 0.5 and 1.0 performed acceptably for the Raleigh cases and not for the Centerville cases? How close were they to being accepted with the VRT-TD data? It perhaps appears that they performed better for the TS-TD data at Centerville than they did at Raleigh (or at least the cases around them with discernible colors did).

AR1.6. Although the observed campaign-average evaporation in both data sets were indistinguishable at higher TD temperatures, there was a slight difference in evaporation profiles at various Rt at lower temperatures (see Figs 2.b and c). This slight differences in the observed evaporation profiles at 60 and 90 ºC as shown in Figs. 2b and c are likely the cause of the differences between optimal parameter sets. We cannot comment on the factors leading to this difference, as our estimated volatility parameter values are empirical estimates that optimally describe bulk volatility properties in combination with the assumed values of other parameters (D, σ, ρ, *MW)*.

R1.7. Page 10, Lines 5-10: The low enthalpies used in models are based on observation data (e.g. Offenberg et al. 2006; Pathak et al. 2007; Stanier et al., 2008) of so-called "effective" enthalpies, so please consider mentioning this for completeness; Stanier et al. (2008) were a bit higher than others and in line with the lower bound explored in this study. It has been argued that low enthalpies of vaporization result from describing systems with too few volatility surrogates (Riipinen et al., 2010). Could the authors comment on what they attribute the void between their high enthalpies and historical low enthalpies to? If they run their model with only two surrogates, for example, do they get low enthalpies as well?

AR1.7. We thank the reviewers for the suggestion. We added these references in our paper. As the reviewer correctly pointed out, these are not real enthalpies, but "effective" ones. The reported "effective" enthalpies are often much lower than enthalpies of chemical compounds relevant to atmospheric aerosols. By reducing the number of surrogate compounds, the system moves further away from realistic enthalpies. As a mixture evaporates, it is progressively enriched in less volatile compounds, slowing down evaporation in terms of the total mixture mass. Thus, the apparent sensitivity of the aerosol mass to temperature appears to be low. This translates to a low enthalpy of vaporization if one uses, for example, one surrogate compound. We have not tested the dependence of the apparent ΔH_{vap} values on the number of surrogate compounds, as our purpose was to describe the aerosol using the VBS representation with a commonly used number of bins.

R1.8. Can the authors please provide some statistics to go along with the comparison in Fig. 4? For example, it would be useful to have mean bias, correlation coefficient and root mean square error so that future studies would have something succinct to use as a benchmark.

AR1.8. We have added values of coefficient of determination (r^2) and root mean square error (RMSE) for the measured and modeled MFRs in Fig 4.a and Fig.S9.

R1.9. In Fig. 4a, is the COA that of the ambient (unheated) sample? There does appear to be systematic overprediction for low COA cases compared to high COA cases. Is this true? Could the authors provide some statistics stratified by COA to assess this? If there is a relationship, could they comment on why it emerges from their approach?

AR1.9. Yes, the C_{OA} in Fig.4a is the measured ambient OA concentrations.

We explored the relationship between C_{OA} and extracted volatility. Fig.AR.1 shows the scatter plot of (a) mean C^* vs. ambient C_{OA} and (b) C^*_{eff} vs. ambient C_{OA} (this Fig. is included in SI as Fig.S12). In a few low C_{OA} instances, the mean C^* was found to be higher, but this trend is not consistent. The relative contribution of MO-OOA (more-oxidized oxygenated-OA) in C_{OA} in many of these instances was low (yellow/orange points in Fig. AR.1a, which likely influences this observation. However, there is large amounts of scatter in mean C* in the lowest C_{OA} range, so a consistent relationship is not evident. The C^*_{eff} vs. ambient C_{OA} plot shows an increasing trend of C^*_{eff} with C_{OA}. This is because the C^*_{eff} only considers the particle-phase components and was estimated following equilibrium partitioning theory – therefore this mild increase of C^*_{eff} is consistent with increasing partitioning of semi-volatile species to the particle-phase with increased C_{OA}.

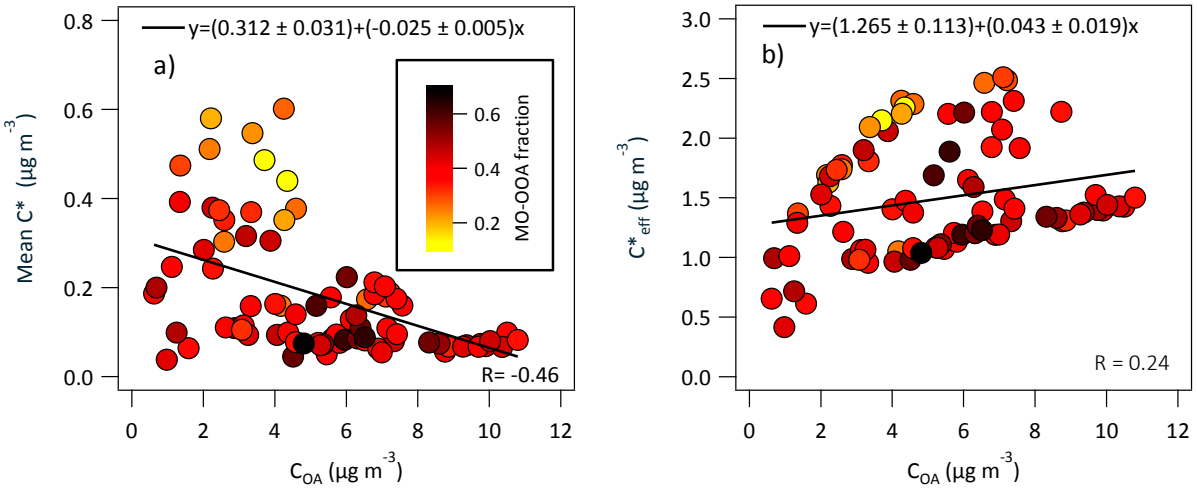

Fig.AR.1: Scatter plot of (a) mean C* vs. ambient OA loading (C_{OA}); (b) C^*_{eff} vs. ambient OA loading (C_{OA}). Results are shown from the Centreville campaign.

R1.10. Page 13, Line 8: Please avoid using the word "relatively" and opt instead for a quantification of the difference between the afternoon and early morning.

AR1.10. Revised text. "*OA appeared less volatile in the afternoon than early morning for both sites (Centreville: campaign average* $\overline{C^*}$ *(μg m^{-3}) in the morning ~ 0.25; afternoon ~ 0.13 and Raleigh: morning ~ 0.2; afternoon ~ 0.12)*."

R1.11. Sections 3.4-3.5: The authors have defined both mean(C*) and C*eff and chose the former for their analysis of time series and diurnal profiles. I think this may have been an unfortunate choice. This value, as they say, accounts for both particle- and gas-phase compounds. It is not very surprising to me that it would be a more stable quantity, throughout the SOAS campaign at least. I wonder if they would capture the trends they are after better by using the C*eff which just accounts for the particle-phase material. This at least would seem to make more sense for correlating with AMS factors (Isoprene-OA, LO-OOA, and MO-OOA) since those apply just to the particle phase and not the total organic burden. Using this alternative approach would theoretically introduce a temperature and dilution dependence that might result in a more striking and meaningful variability. Of course, it may on the other hand yield a rather invariant trend similar to what they have already shown.

AR1.11. According to our definition, the mean C* is a log-mean of the volatility bins of organic species (particles + vapor) ($\overline{C^*} = 10^{\sum f_i \log_{10} C_i^*}$), which gives a description of where the mass (center) of different volatility compounds is located. Therefore, the mean C* is a simpler representation of the volatility basis set (VBS). On the other hand, C*_eff is another simplified representation of OA volatility ($C^*_{eff} = \sum x_i C_i^*$) derived based on the Raoult's law and using arithmetic averaging. The C*_eff would indicate a current state of OA volatility and temperature- and dilution-dependence. We elected to use the mean C* for our extended analysis because we consider the log-mean a better representation of the volatility of ambient OA, not only what is measured in particle instruments.

We explored the correlation between different OA factors and bulk OA volatility using both metrics (mean C* and C*_eff). As an example, Fig. AR.2 shows the scatter plot of (a) mean C* vs. MO-OOA fraction and (b) C*_eff vs. MO-OOA fraction C_{OA} (this Fig. is now included in the

SI as Fig.S13). While the exact correlations of course vary, the correlation coefficients and thus our general conclusions on the correlation between different OA factors and bulk OA volatility remain unchanged.

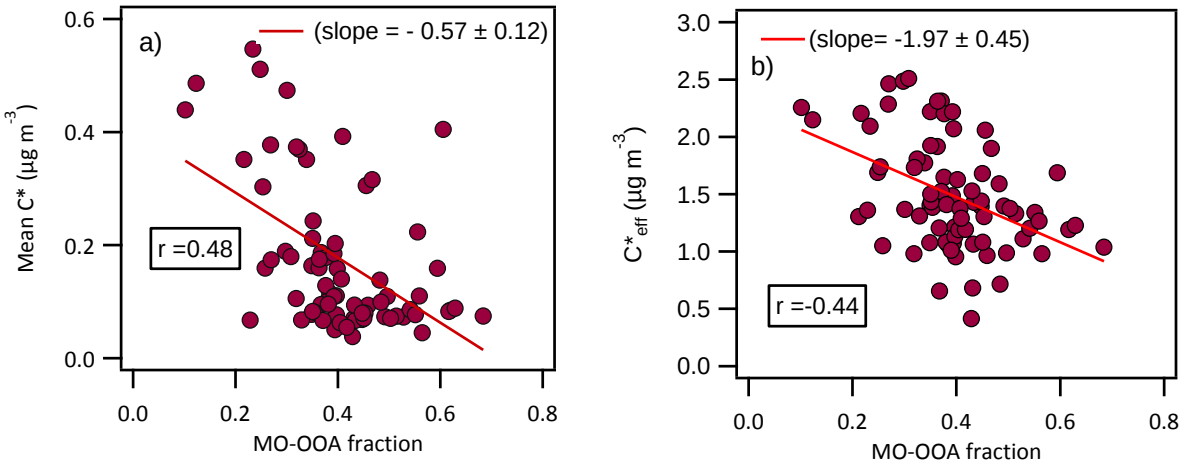

Fig.AR.2: Scatter plot of (a) mean C* vs. MO-OOA fraction in C_{OA}; (b) C^*_{eff} vs. MO-OOA fraction in C_{OA}. Results are shown from the Centreville campaign.

Minor Changes/Typos:

R1.12. Pg 1, Line 11: Consider mentioning solubility as well. "quantitative estimates of the thermodynamic (volatility, water solubility, etc)"

AR1.12. We revised the text as suggested.

R1.13. Pg 1, Line 14: "one at a biogenic: : :"

AR1.13. We revised the text

R1.14. Pg 2, Line 6-7: Of course SOA has also been shown to be introduced from oxidation of primary SVOCs and IVOCs followed by condensation and aqueous phase reactions of high soluble compounds. Depending on your definition of "secondary", it is also formed by heterogeneous oxidation of POA without evaporation. Please mention these here or don't be so specific about the VOCs role.

AR1.14. We revised the text. Page 2, Lines 5-6*: "Secondary OA (SOA) is formed in the atmosphere via oxidation reactions of gas-phase organic species; it may also be formed by reactions in the particle (condensed) phase"*

R1.15. Pg 5, Line 16-17: The VBS approach does not assume unity activity coefficients. Instead the activity coefficient are assumed to be lumped into the Cvap, making it C*. And so the activity coefficients have a value, but that value is assumed not to change from the lab or field to other mixtures or conditions.

AR1.15. We revised the text. Page5, Lines 22-23: *"The VBS approach is based on an effective saturation concentration (C*) where the activity coefficient is assumed to be lumped into the saturation concentration."*

R1.16. Page 6, Line 10: I disagree that the model is applied in an "inverse sense", as it appears that the authors are solving the evaporation problem in the forward way, brute-force, for all of their free parameter combinations and then comparing output to the observations. This could perhaps be labelled reverse engineering, but I think associating it with inverse modeling is inaccurate.

AR1.16. We used a non-linear constrained optimization solver ('*fmincon*' in Matlab) to extract OA volatility distribution by matching measured and modeled evaporation data.

We revised the text. *"The model is applied to extract OA properties such as the volatility distribution, ΔH_{vap}, and γ_e as fitting parameters by matching measured and modeled evaporation data."*

R1.17. Page 6, Line 27: "common means to improve the performance of OA prediction in chemical transport models"

AR1.17. We revised the text as suggested.

R1.18. Fig. 2b,c: There is no explanation or legend for the colors of the trends. The text claims they distinguish different residence times but isn't this described by the x-axis? Please clarify this point.

AR1.18. Fig. 2a shows an OA MFR vs. temperature plot. A colour scale was used for Fig.2a to distinguish TD measurements data with different residence times across studies. It was mentioned in Fig.2 caption. The x-axis of Figs. 2b and c are residence times. Thus we do not need a residence time colour scale for these two panels. To clarify the legend issue, we added a sentence in Fig.2 caption: "*Legend shown next to panel (a) applies to all panels (a-c).*"

R1.19. Page 9, Line 14: Just write "volatility". Having the "/C*" is unnecessary. Page 15, Line

7 as well. Page 9 and Fig. 3: Neither the description in the text nor the figure caption should claim that the figure depicts the fi values. As far as I can tell, it does not.

AR1.19. We revised the text as suggested.

We agree with the reviewer that Fig.3 visually does provide information about our fitted f_i distributions. To clarify it we revised Fig.3 caption as, "*Extraction process of OA gas-particle partitioning parameter (ΔH_{vap}, γ_e and f_i) values. A f_i distribution was solved for each combination of (ΔH_{vap}, γ_e) via evaporation kinetic model fits to campaign-average dual-TD observations*"

R1.20. Page 9, Line 18: Please indicate here, and throughout the text, that this C* is at Tref (presumably 298 or 300 K). This should especially be made clear for any references to mean C*.

AR1.20. We revised the text as suggested. "*A reference temperature (T_{ref}) of 298 K is assumed. Any C* value reported in this paper should be considered at 298 K, unless otherwise specified."*

R1.21. Page 10 and Fig. 2: The notation for Ceff is not consistent with Csat_eff.

AR1.21. We revised the text as suggested.

R1.22. Page 13, Line 26-27: You do not really need this final sentence since the section you refer to comes directly next.

AR1.22. We revised the text as suggested.

R1.23. Page 16, Line 16: Please be quantitative rather than saying "Relatively less volatile".

AR1.23. We removed the word 'relatively'. Quantitative data is stated in page 13, Lines 16-18; **"***OA appeared less volatile in the afternoon than early in the morning for both sites (Centreville: campaign average $\overline{C^*}$ ($\mu g\ m^{-3}$) in the morning ~ 0.25; afternoon ~ 0.13 and Raleigh: morning ~ 0.2; afternoon ~ 0.12)*"

R1.24. Page 16, Line 30: Murphy et al. (2011) compared predictions with the 2D-VBS in a Lagrangian column CTM against the FAME data reported by Lee et al.

We thank the reviewer for the information. We cut that sentence and added the Murphy et al. (2011) reference.

Anonymous Referee #2

General Comments:

R2.0. This manuscripts presents measurements and analysis of the evaporation behavior of organic aerosol (OA) measured at two different locations – one more rural, one more urban, but both influenced by significant concentrations of BVOCs. Measurements were taken with a dual thermodenuder system in which both the temperature and residence time were varied. Main conclusions of the work include that the OA evaporation behavior was fairly similar at the two sites and did not vary much over the course of the measurement campaign, and also that much of the OA is in low-volatility bins which are currently not represented in (most) air-quality models. The manuscript is well written and generally well argued, and overall the topic and quality of the manuscript makes it suitable for publication in ACP. However, I have a few concerns about the analysis and interpretation as explained below which I suggest the authors should address before publication.

A2.0. We thank the reviewer for his/her review and useful comments. We address the specific comments below.

Major comments:

R2.1. The authors focus on the "best fit solution" and address to some extent the sensitivity of the error (SSR) to changes in dHvap and gamma (e.g. Fig. 3). I request that they also address the sensitivity of the error to changes in the fi. I am particularly worried that the fi in the lower C* bins may not be well constrained by the data.

AR2.1. For solving a f_i distribution, we have used a non-linear constrained optimization solver (*fmincon* in Matlab). We provided constraint for the lower (f_i minimum = 0.02) and upper (f_i maximum = 0.4) boundary for a f_i value in each C^* bin. This choice of a wide solution space for solving a f_i value in each C^* bin should address any sensitivity of the error to an optimum solution of f_i.

As we discussed in our manuscript that our selected C^* bin range was based on our measurement conditions; specifically, the highest TD operating temperature and the average ambient OA loading provide limitations on the lower and upper C* bins we consider, respectively. Page 6, Lines 5-6, "*With the above C^* bin limits, materials having $C^* < 10^{-4}$ μg m^{-3} are lumped into the lowest bin……*"

Bins lower than ~10^{-4} are not constrained in our data set because maximum TD operating temperature was 180ºC. Materials those survived at 180 ºC may well be even lower volatility, but we need to see it evaporate to be able to say anything quantitative about volatility. The key point is that within this predefined range, our approach provides an empirical OA volatility distribution that explains the observed evaporation of bulk OA in our dual-TD system.

R2.2. Regarding higher C* bins, on page 6 lines 1-2 the stated reason for not including C*>10 _g/m3 is that less than 5% of the materials would be present in the condensed phase at the average COA of 5 _g/m3. Common VBS bins used range from 0.1 to 100 _g/m3 for ambient OA concentration of _10 _g/m3. Elevated OA episodes (OA > 10 _g/m3) were observed, especially at the Raleigh site (Figure S7). It would be reasonable to include the 100 _g/m3 bin in the model to account for these episodes. Have the authors investigated the effects of including higher volatility bins on the fitted model parameters? As referee #1 pointed out and according to Riipinen et al. (2010), a two-surrogate product model could lead to very different conclusions about dHvap. How does the inclusion of more and lower volatility bins affect modeled dHvap? In other words, does bin selection introduce bias in to model results (and if so, how much)?

AR2.2. As noted in the manuscript and above (AR1.3), the selection of C^* bin range in our fitting was based on our measurement conditions, specifically the highest TD operating temperature and average ambient OA loading. We performed sensitivity analysis on the selection of C* bin range. Fig. AR.3 shows an example result showing the comparison between fits with ranges of C^*= [10^{-4} to 10 µg m^{-3}] (base case used in our paper) versus C^*= [10^{-3} to 10^2 µg m^{-3}] of the Raleigh campaign average TD observations. Result indicates that C^*= [10^{-3} to 10^2 µg m^{3}] fails to recreate the observed evaporations at higher TD temperature and that there is an indistinguishable change at lower temperature conditions (where the C* = 10^2 µg m^{-3} would have any influence on the fit).

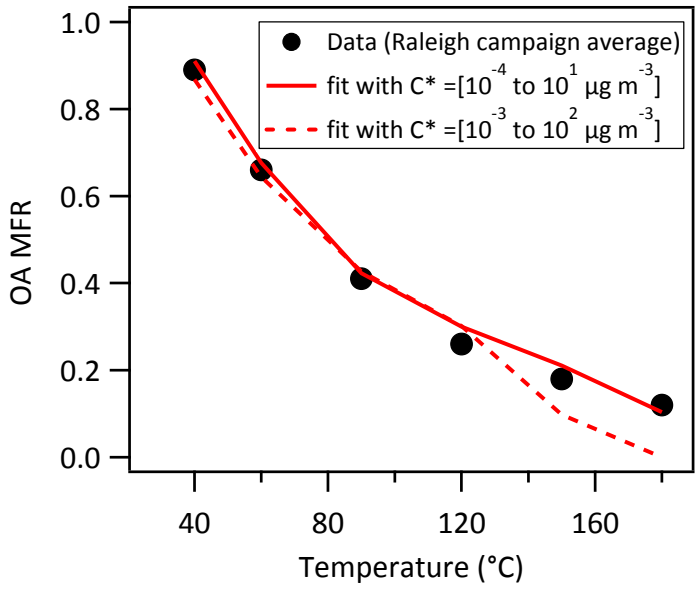

Fig.AR.3: Sensitivity of C* bin range in fitting TD data using an evaporation kinetic model. The best fitted curves with (ΔH_{vap} = 100 kj mol^{-1} and γ_e = 0.5) are shown.

The reviewer correctly pointed out that there were a few elevated C_{OA} episodes ($\geq$ 10 µg m^{-3}) during the Raleigh campaign. However, these episodes were for a relatively short period of time (2-3 hours) and the time required for collecting a complete set of thermograms using our TD setup was ~ 4-5 hours, we were not been able to capture a complete set of data under a consistently elevated C_{OA} which could be fitted to constrain higher volatility bins.

As we discussed earlier in response to reviewer #1 (AR1.7) Comment, by reducing the number of surrogate compounds, the system representation would potentially move further away from realistic enthalpies. Therefore, we focused to describe the aerosol using the VBS representation with a commonly-used number of bins. We have not tested the dependence of the apparent ΔH_{vap} values on the number of surrogate compounds. Our goal of this study was to describe ambient OA within this pre-defined framework. In our fitting, we represented ΔH_{vap} as a function of C* bin (ΔH_{vap} = intercept-slope ($\log_{10}$C*)) and found that a relatively 'shallow' $\log_{10}C^*$ dependence (slope ~ 0, 4) better explain the observed temperature sensitivity of bulk OA in TDs. This suggests that an effective ΔH_{vap} required to explain the observed temperature sensitivity of bulk OA would be less sensitive to an inclusion of higher/lower C* bins within a realistic range. However, we do recommend that further work explores the sensitivity of the apparent ΔH_{vap} to the number of surrogate bins in future studies considering the use of basis sets with fewer bins.

R2.3. Page 6 Line 21-23: Have the authors attempted to apply the two models in a different order (VRT-TD first then TS-TD)? How much does this change the results?

AR2.3. The order of model application has no effect on derived parameters. We have used the same model for fitting data from TS-TD and VRT-TD. For a given input temperature (T) and residence time (Rt), the evaporation kinetics model predicts a mass fraction remaining; MFR (T, Rt). In our method, the fitting can be done in one step (fitting all data from TS-TD and VRT-TD together) or two steps. We have found that the two-step fitting approach gives identical results to fitting all data simultaneously. We, therefore, elected to use a two-step fitting approach because it narrows down the parameter space substantially in the first step, which reduces the computational requirements substantially. An additional advantage to applying the 'two-step' approach in this work is that it distinctly demonstrates the benefit of the additional dimension (Rt) we have added to the traditional TD measurement space (T) via goodness of fit quantification across the [γ_e, ΔH_{vap}] space at each step (Fig. 3).

R2.4. Page 13 Line 1-6: mean C* is perhaps not a suitable metric to correlate with the fraction of isoprene OA. If isoprene OA was in fact much less volatile, its overall contribution to mean C* would be minor; the calculated mean C* value would be dominated by fi values of more volatile surrogate compounds. Using Ceff would present similar issues. It seems more appropriate to investigate the correlation between isoprene OA and individual bin fi's.

A2.4. We thank the reviewer for this suggestion. We have performed this additional analysis and a summary result is shown below:

$\log_{10}C^*$ bin	-4	-3	-2	-1	0	10	mean C^*	C^*_eff
Pearson R value (Iso-OA fraction vs f_i's)	0.02	0.29	-0.07	-0.06	-0.14	0.04	-0.06	0.19

Based on our analysis we did not find any statistically-significant relationship between isoprene-OA fraction and fi's in any individual C^* bin. This result is consistent with our original observation of no correlation between mean C* of bulk OA and the fractional contribution of isoprene-OA to C_{OA}. This new result is included in Table S2 and discussed on Page 13, Lines 29-

30: *"Neither were statistically-significant relationships found between the isoprene-OA fraction and f_i's in any particular C^* bin (see Table S2)."*

R2.5. Page 6, line 7: Was a constant collection efficiency of 0.5 also applied to all thermally denuded data? Evaporating part of the organic aerosol (and therefore changing the org/sulfate ratio) could change the collection efficiency, which would bias MFR measurements. The authors could partially address this issue by comparing total SMPS and ACSM measurements (mass), i.e. the ACMS/SMPS ratio in the bypass and after the thermodenuder.

AR2.5. Yes, we have analyzed both bypass and heated (TD) ACSM data using a constant collection efficiency (CE) of 0.5. A comparison of ACSM/SMPS ratio in the bypass (slope = 0.95±0.006) and after the TD (slope = 0.91±0.009) data is shown in panels c and d in Fig S1. A slightly lower slope for the heated measurements suggest that CE could be ~4-8 % lower for the aerosol that passes through the TD. We did not attempt to use a different CE value for the thermodenuded aerosol based on this analysis because the SMPS measurement also could be affected by a potential change in particle morphology and shape upon heating. However, the bottom line is that the potential uncertainty that may arise from using a constant CE would be very low compared to the overall observed variability in measurements.

R2.6. Fig S7 seems to assume that all nitrate measured in the ACSM is inorganic. This seems to contradict discussion earlier in the manuscript of the potential importance of organic nitrates. Previous work has shown that the ratio of NO+ to NO2+ fragments measured by AMS or ACSM instruments is quite different for organic nitrates and ammonium nitrate, and that the ratio can be used to estimate the fraction of measured nitrate due to organic nitrates. I suggest the authors use these measurements from the ACSM to estimate how much of the measured nitrate is organic vs. inorganic. Assuming full neutralization of sulfate by ammonium (which is reasonable in the presence of ammonium nitrate) could also be used to calculate the nitrate attributable to ammonium nitrate and, therefore, the nitrate due to organic nitrates.

AR2.6. The Nitrate measured by an ACSM would be a combination of both organic and inorganic nitrate. We changed the axis label for panel (b and d) of Fig.S7 from 'inorganic' to 'SO_4, NO_3, NH_4'. We explored the NO+ to NO2+ ratio from our ACSM measurements as suggested by the reviewer. A summary is given below:

Measurements	NO+ to NO2+ ratio (campaign average ± 1 SD)
Centreville	10.02 ± 3.47
Raleigh	5.93 ± 1.96
Pure ammonium nitrate (Cal aerosol)	3.58 ± 0.84

The NO+: NO2+ ratios in both campaigns were significantly higher than that of pure ammonium nitrate aerosol in our instrument. This is consistent with a substantial contribution from organic nitrate and with our discussion of the potential importance of organic nitrates. However, an absolute quantification of organic nitrate is not critical for our analysis, as our paper focuses on the volatility of bulk OA as identified by the ACSM/AMS.

R2.7. Page 4 Line 12: "All Rts reported here are calculated assuming plug flow at room temperature" This implies that a plug flow (as opposed to parabolic) velocity profile is assumed in the evaporation model. Is this correct? It was suggested by (Cappa, 2010) that assuming plug flow profile would lead to underestimation of dHavp and overestimation of Csat. Have the authors explored different assumptions for gas velocity profile in the model?

A2.7. The Cappa (2010) paper discussed the effect of the laminar vs. plug flow assumptions on the derived saturation vapor pressure and enthalpy of vaporization of a single component aerosol. The author notes that the effect of this assumption changes with the compound saturation vapor pressure. It is not clear what effect this assumption would have if a multi-component aerosol is considered. It should be noticed that a plug flow approximation is widely used (Lee et al., 2010; Riipinen et al., 2010; Saleh et al., 2008), with the residence time and non-uniform temperature effects on derived quantities being relatively small (Park et al., 2013). Based on the sensitivity analysis result presented in our earlier dual-TD method characterization paper (Saha et al., 2015) and a detailed two-dimensional laminar flow modeling effort in Park et al. (2013), this plug-flow assumption has relatively smaller influences on evaporation in a TD relative to values of (C*, ΔH_{vap}, and γ_e).

Minor comments:

R2.8. Page 5 Line 2: Please expand on what "instrumental inter-calibration factors" entail

AR2.8. To get directly comparable SMPS concentration data from 3 SMPSs running in parallel with our dual TD system, we ran them periodically in parallel to determine an inter-calibration factor. The inter-calibration factor is determined from a scatter plot of SMPS inter-comparison data collected by running 3 SMPSs in parallel on the bypass line. Among the 3 SMPS, we chose one as a reference upon which all corrections were based. The reference SMPS system was selected based on which yielded counts most consistent with the median of those measured during a group SMPS inter-comparison test of 8 systems from different laboratories during the SOAS field campaign. We added this discussion briefly in the paper: *"To get directly comparable SMPS concentration data from 3 SMPSs running in parallel with our dual TD system, we ran them periodically in parallel on the bypass line to determine inter-calibration factors. Further details on SMPS inter-comparison are discussed in Saha et al (2015).*"

R2.9. Page 6 Line 23-24: Please clarify on how variability is calculated. Is it based on measured MFR values or OA measurements? Is it calculated over small intervals or over the entire course of campaign?

AR2.9. We added this discussion to the paper: *"Variability is based on measured MFR data. Raw data at each (T, Rt) condition were averaged over 20-30 minutes. At given TD operating conditions (T, Rt), we defined ±1 standard deviation of MFR data (20-30 minute resolution) from the whole campaign as an indicator of observed variability."*

R2.10. Page 8 Line 31: Please provide references for previous field studies.

AR2.10. Page 9; Line 12-13: References to field studies ("Häkkinen et al., 2012; Huffman et al., 2009; Lee et al., 2010; Paciga et al., 2015; Xu et al., 2016") are added.

R2.11. Page 10 Line 8-10: Please add discussion on why observed slope may be different from the empirical relation determined by Epstein et al.

AR2.11. The Epstein et al. correlation was determined from range of compounds with known ΔHvap. However, it has been found that for this and other complex OA systems, a correlation other than the Epstein correlation better explains observations. For example, Ranjan et al.(2012) reported dH_{vap} = 85-11logC* for gas–particle partitioning of POA emissions from diesel engine; May et al.(2013) reported dH_{vap} = 85-4logC* for biomass burning POA emission. A key point is that like results from Ranjan et al. (2012), May et al. (2013) and many others, our estimated

dH_{vap} correlation for ambient OA is an empirical estimate, which explain our observations better than the Epstein correlation. We added this discussion in the paper. Page10, Line 28-33:

"The Epstein et al. correlation was determined from range of compounds with known ΔH_{vap}. Several recent studies of complex OA systems (May et al., 2013; Ranjan et al., 2012) have found that a correlation other than that from Epstein et al. better explains observations. For example, Ranjan et al.(2012) reported ΔH_{vap} = 85-11logC for gas–particle partitioning of POA emissions from a diesel engine; May et al.(2013) reported ΔH_{vap} = 85-4logC* for biomass burning POA emissions. Similar to these and other studies, our ΔH_{vap} correlation for ambient OA is an empirical estimate which best explains our observations."*

R2.12. Page 2 line 6: ": : :SOA is formed in the atmosphere via condensation of low volatility products: : :" This statement is not inclusive enough. Please revise.

AR2.12. We revised the text. Page 2; Line 5-6: *"Secondary OA (SOA) is formed in the atmosphere via oxidation reactions of gas-phase organic species; it may also be formed by reactions in the particle (condensed) phase."*

References:

Cappa, C. D.: A model of aerosol evaporation kinetics in a thermodenuder, Atmos. Meas. Tech., 3(3), 579–592, doi:10.5194/amt-3-579-2010, 2010.

Farina, S. C., Adams, P. J. and Pandis, S. N.: Modeling global secondary organic aerosol formation and processing with the volatility basis set: Implications for anthropogenic secondary organic aerosol, J. Geophys. Res. Atmospheres, 115(D9), D09202, doi:10.1029/2009JD013046, 2010.

Hennigan, C. J., Bergin, M. H., Russell, A. G., Nenes, A. and Weber, R. J.: Gas/particle partitioning of water-soluble organic aerosol in Atlanta, Atmos Chem Phys, 9(11), 3613–3628, doi:10.5194/acp-9-3613-2009, 2009.

Lee, B. H., Kostenidou, E., Hildebrandt, L., Riipinen, I., Engelhart, G. J., Mohr, C., DeCarlo, P. F., Mihalopoulos, N., Prevot, A. S. H., Baltensperger, U. and Pandis, S. N.: Measurement of the ambient organic aerosol volatility distribution: application during the Finokalia Aerosol Measurement Experiment (FAME-2008), Atmos Chem Phys, 10(24), 12149–12160, doi:10.5194/acp-10-12149-2010, 2010.

Lehtinen, K., Korhonen, H., Maso, M. D. and Kulmala, M.: On the concept of condensation sink diameter, Boreal Env. Res, 8, 405–411, 2003.

May, A. A., Levin, E. J. T., Hennigan, C. J., Riipinen, I., Lee, T., Collett, J. L., Jimenez, J. L., Kreidenweis, S. M. and Robinson, A. L.: Gas-particle partitioning of primary organic aerosol emissions: 3. Biomass burning, J. Geophys. Res. Atmospheres, 118(19), 11,327–11,338, doi:10.1002/jgrd.50828, 2013.

Murphy, B. N., Donahue, N. M., Fountoukis, C. and Pandis, S. N.: Simulating the oxygen content of ambient organic aerosol with the 2D volatility basis set, Atmos Chem Phys, 11(15), 7859–7873, doi:10.5194/acp-11-7859-2011, 2011.

Offenberg, J. H., T. E. Kleindienst, M. Jaoui, M. Lewandowski, and E. O. Edney (2006), Thermal properties of secondary organic aerosols, Geophys. Res. Lett., 33, L03816, doi:10.1029/2005GL024623.
Park, S. H., Rogak, S. N. and Grieshop, A. P.: A Two-Dimensional Laminar Flow Model for Thermodenuders Applied to Vapor Pressure Measurements, Aerosol Sci. Technol., 47(3), 283–293, doi:10.1080/02786826.2012.750711, 2013.

Ranjan, M., Presto, A. A., May, A. A. and Robinson, A. L.: Temperature Dependence of Gas–Particle Partitioning of Primary Organic Aerosol Emissions from a Small Diesel Engine, Aerosol Sci. Technol., 46(1), 13–21, doi:10.1080/02786826.2011.602761, 2012.

Riipinen, I., Pierce, J. R., Donahue, N. M. and Pandis, S. N.: Equilibration time scales of organic aerosol inside thermodenuders: Evaporation kinetics versus thermodynamics, Atmos. Environ., 44(5), 597–607, doi:10.1016/j.atmosenv.2009.11.022, 2010.

Saha, P. K., Khlystov, A. and Grieshop, A. P.: Determining Aerosol Volatility Parameters Using a “Dual Thermodenuder” System: Application to Laboratory-Generated Organic Aerosols, Aerosol Sci. Technol., 49(8), 620–632, doi:10.1080/02786826.2015.1056769, 2015.

Saleh, R., Walker, J. and Khlystov, A.: Determination of saturation pressure and enthalpy of vaporization of semi-volatile aerosols: The integrated volume method, J. Aerosol Sci., 39(10), 876–887, doi:10.1016/j.jaerosci.2008.06.004, 2008.

Stanier, Donahue, and Pandis (2008), Parameterization of secondary organic aerosol mass fractions from smog chamber data, Atmos. Environ. 42, 10, 2276-2299, doi:10.1016/j.atmosenv.20

Quantifying the volatility of organic aerosol in the southeastern U.S.

Provat K. Saha[1], Andrey Khlystov[2], KhairunnisaYahya[3], Yang Zhang[3], Lu Xu[4], Nga L. Ng[4,5], and Andrew P. Grieshop[1]

[1]Department of Civil, Construction and Environmental Engineering, North Carolina State University, Raleigh, NC, USA
[2]Division of Atmospheric Sciences, Desert Research Institute, Reno, Nevada, USA
[3]Department of Marine Earth and Atmospheric Sciences, North Carolina State University, Raleigh, NC, USA
[4]School of Chemical and Biomolecular Engineering, Georgia Institute of Technology, Atlanta, GA, USA
[5]School of Earth and Atmospheric Sciences, Georgia Institute of Technology, Atlanta, GA, USA

Correspondence to: Andrew P. Grieshop (apgriesh@ncsu.edu)

Abstract. The volatility of organic aerosols (OA) has emerged as a property of primary importance in understanding their atmospheric lifecycle, and thus abundance and transport. However, quantitative estimates of the thermodynamic (volatility, water solubility) and kinetic parameters dictating ambient OA gas-particle partitioning, such as saturation concentrations (C^*), enthalpy of evaporation (ΔH_{vap}) and evaporation coefficient (γ_e), are highly uncertain. Here, we present measurements of ambient OA volatility at two sites in the southeastern U.S., one at a biogenic-volatile-organic-compound (BVOC)-dominated rural setting in Alabama as part of the Southern Oxidant and Aerosol Study (SOAS) in June-July, 2013, and another at a more anthropogenically-influenced urban location in North Carolina during October-November, 2013. These measurements applied a dual-thermodenuder (TD) system, in which temperature and residence times are varied in parallel, to constrain equilibrium and kinetic aerosol volatility properties. Gas-particle partitioning parameters were determined via evaporation kinetic model fits to the dual-TD observations. OA volatility parameters values derived from both datasets were similar despite the fact that measurements were collected in distinct settings and seasons. The OA volatility distributions also did not vary dramatically over the campaign period nor strongly correlate with OA components identified via positive matrix factorization of aerosol mass spectrometer data. A large portion (40-70%) of measured ambient OA at both sites was composed of very low volatility organics ($C^* \leq 0.1$ μg m^{-3}). An effective ΔH_{vap} of bulk OA of ~ 80-100 kJ mol^{-1} and a γ_e value of ~ 0.5 best describe the evaporation observed in the TDs. This range of ΔH_{vap} values is substantially higher than that typically assumed for simulating OA in atmospheric models (30-40 kJ mol^{-1}). TD data indicate that γ_e is on the order of 0.1 to 0.5, indicating that repartitioning timescales for atmospheric OA are on the order of several minutes to an hour under atmospheric conditions. The OA volatility distributions resulting from fits were compared to those simulated in the Weather, Research and Forecasting model with Chemistry (WRF/Chem) with a current treatment of SOA formation. The substantial fraction of low-volatility material observed in our measurements is largely missing from simulations, and OA mass concentrations are underestimated. The large discrepancies between simulations and observations indicate a need to treat low volatility OA in atmospheric models. Volatility parameters extracted from ambient measurements enable evaluation of emerging treatments for OA (e.g., secondary OA using the volatility basis set or formed via aqueous chemistry) in atmospheric models.

1. Introduction

Organic aerosol (OA) is a dominant component of atmospheric fine particulate matter ($PM_{2.5}$) (Jimenez et al., 2009; Zhang et al., 2007), which is linked with adverse human health and uncertain climate effects. Atmospheric OA is a complex mixture of thousands of individual organic compounds originating from a range of natural and anthropogenic sources. Primary OA (POA) is emitted directly into the atmosphere. Secondary OA (SOA) is formed in the atmosphere via oxidation reactions of gas-phase organic species; it may also be formed by reactions in the particle (condensed) phase (Kroll and Seinfeld, 2008). A large fraction of SOA in many parts of the globe, e.g., in the southeast U.S., is formed from biogenic-VOCs (BVOCs) (Goldstein et al., 2009; Goldstein and Galbally, 2007). However, the mechanisms responsible for SOA production from BVOCs (Budisulistiorini et al., 2015; Goldstein and Galbally, 2007, 2007; Marais et al., 2016; Xu et al., 2015a, 2015b), its chemical composition and many important physical properties are largely undetermined (Goldstein et al., 2009; Schichtel et al., 2008; Weber et al., 2007). Therefore their representation in current atmospheric and climate models are highly uncertain (Hallquist et al., 2009; Liao et al., 2007; Pye et al., 2015; Pye and Seinfeld, 2010).

One of the major sources of uncertainty in predicting SOA concentrations in atmospheric models arises from the poor understanding of gas-particle partitioning of chemical species comprising SOA (Hallquist et al., 2009; Jimenez et al., 2009; Seinfeld and Pankow, 2003). Gas-particle partitioning plays a central role in determining OA lifecycle and thus its atmospheric abundance, transport, and impacts (Donahue et al., 2006; Jimenez et al., 2009). At equilibrium, the volatility of organic species, specifically saturation vapor pressure (or equivalently, saturation concentration, C^*; $\mu g\ m^{-3}$), plays a vital role in determining their gas-particle partitioning. (Donahue et al., 2006; Pankow, 1994). Solubility of organic species in water may also be critical for gas-particle partitioning for many species (Hennigan et al., 2009), especially in places with higher relative humidity, for example, in the southeast US. Enthalpies of vaporization (ΔH_{vap}) dictate the change in partitioning with temperature (Donahue et al., 2006; Epstein et al., 2010). Although gas-particle partitioning is determined by the basic thermodynamic properties of OA species – their C^*, ΔH_{vap}, and solubility– these, along with the impacts of non-ideal mixing on individual species, are generally unknown for ambient OA. Under changing conditions, gas-particle partitioning is also influenced by the kinetics of gas/particle exchange, for example due to barriers to mass transfer in solid or viscous particles or molecular accommodation at a particle surface (Kroll and Seinfeld, 2008). The overall kinetic limitation to mass transfer during repartitioning is typically described by an evaporation coefficient (γ_e) (also often called mass accommodation coefficient), which is highly uncertain for ambient OA and can dictate time-scales for partitioning (Saleh et al., 2013). Though current models assume OA to be at equilibrium within a model prediction time-step (several minutes to an hour) during atmospheric simulations, several studies have indicated that partitioning time scales could be as long as days or months ($\gamma_e << 0.1$) due to a highly viscous and/or glassy aerosol (Vaden et al., 2011; Zobrist et al., 2008).

Quantitative measures of ambient OA gas-particle partitioning parameters are needed to provide inputs for, and to evaluate, atmospheric models. However, methods to quantitatively determine ambient OA volatility are in their infancy and the resulting estimates of parameters dictating OA volatility are highly uncertain (Cappa and Jimenez, 2010). Thermodenuder

(TD) systems have been previously applied to measure ambient OA volatility (Burtscher et al., 2001; Huffman et al., 2009; Lee et al., 2010; Paciga et al., 2015; Xu et al., 2016). A TD system measures evaporation of sampled aerosol at various temperature perturbations by systematically comparing the size distribution and/or aerosol mass concentration measured after heating in a TD and at a reference ("bypass") condition (Huffman et al., 2008). Several efforts have been made to infer ambient OA volatility distributions by fitting observed evaporation in a TD using a model of evaporation kinetics (Cappa and Jimenez, 2010; Lee et al., 2010). However, since OA evaporation in a TD is dictated by a large number of independent parameters (e.g., C^*, ΔH_{vap}, and γ_e) (Cappa and Jimenez, 2010; Lee et al., 2010), it is difficult to constrain all parameters with a single-dimensional perturbation (e.g. varying TD temperature) to the initial equilibrium. Saha et al. (2015) showed that operating two TDs in parallel (dual-TD) that vary both temperature and residence time can provide tighter constraint on estimates of volatility parameter values (C^*, ΔH_{vap}, and γ_e) for single component OA via kinetic model fits to the observations. In Saha and Grieshop (2016), this approach was applied to determine volatility and phase-partitioning parameter values for laboratory α-pinene SOA. The resulting parameters are consistent with recent observations of low-volatility SOA (Jokinen et al., 2015; Zhang et al., 2015) and evaporation rates (Vaden et al., 2011; Wilson et al., 2015) observed by several techniques. TD perturbations alone cannot give insights into the solubility of OA components, though may be used in concert with other techniques to do so (Cerully et al., 2015).

This paper describes the application of the dual-TD approach during ambient observations from two different settings in the southeastern U.S. Measurements at a rural site during the Southern Oxidant and Aerosol Study (SOAS-2013) (https://soas2013.rutgers.edu/) leverage the range of complementary measurements available during this large field study. To provide a contrast, measurements were also taken several months later, under cooler conditions, in Raleigh, U.S., a small metropolitan area in a similar ecological zone, but with stronger influence from local anthropogenic emissions. The objectives of the study were to: (i) determine a set of volatility parameter values, such as OA volatility distribution using the Volatility Basis Set (VBS) framework (Donahue et al., 2006, 2012) and ΔH_{vap} and γ_e, that describe observations, (ii) examine the variability and consistency in ambient OA volatility distributions across diverse settings and conditions, (iii) examine relationships between extracted volatility distributions and OA composition and source contributions, and (iv) evaluate a model treatment of OA volatility by comparing the measured OA volatility distribution with that simulated by a chemical transport model using a current implementation of the VBS framework.

2. Methods

2.1. Measurement sites

Ambient OA volatility measurements were conducted at two locations in the southeastern U.S., one in a forested rural setting and another in an urban location. Six weeks (June 1 to July 15, 2013) of continuous measurements were conducted in rural Alabama during the Southern Oxidant and Aerosol Study (SOAS-2013) field campaign. The SOAS field campaign occurred

in summer 2013 at several locations in the southeastern U.S. in order to study the interaction of biogenic and anthropogenic atmospheric compounds with a focus on BVOCs and organic aerosols. The measurements reported here are from the main SOAS ground site (32.903°N, 87.250°W), near Talladega National Forest and Centreville, Alabama. The Centreville, Alabama site is an ideal location to study volatility of OA dominated by secondary OA from BVOC precursors (Warneke et al., 2010) in the presence of a range of anthropogenic influences. An additional four weeks (October 18 to November 20, 2013) of ambient OA volatility measurements were conducted at the North Carolina State University (NCSU) main campus (35.786°N, 78.669°W) in Raleigh, USA. The NCSU site, while in an area with plentiful tree cover and BVOC emissions, receives a substantially stronger influence from anthropogenic emissions due to its location within the Raleigh metro area. Section 3.1 includes further comparison between two study areas. Here-in-after, the two data sets are referred to as 'Centreville' and 'Raleigh'.

2.2. Dual thermodenuder operation and sampling strategy

Measurements were collected using the dual TD experimental setup introduced in Saha et al. (2015) and only briefly described here. Two TDs operated in parallel, one at various temperature settings (temperature stepping TD; TS-TD) with a fixed, relatively longer residence time (Rt) and another at fixed temperature and various Rt settings (variable residence time TD; VRT-TD). The TS-TD temperature settings were 40, 60, 90, 120, 150, and 180 ℃ with ~50 s Rt, while the VRT-TD operated at 60 or 90℃ with Rt varying between 1 to 40 s (5-8 settings). All Rts reported here are calculated assuming plug flow at room temperature. Temperature effects on Rt were included during modeling of evaporation kinetics (discussed below) as $Rt(T_{TD}) = Rt(T_{ref})\times(T_{ref}/T_{TD})$, where T_{ref} and T_{TD} are the reference (e.g., room temperature) and TD temperature in K, respectively (Cappa, 2010). The time to run through all temperatures and Rt steps during measurements was ~ 4-5 hours.

A schematic of the experimental setup is shown in Fig.1. Three Scanning Mobility Particle Sizers (SMPS, TSI Inc; Model 3081 DMAs; Model 3010/3787 CPCs) simultaneously measured aerosol size distributions (10-600 nm) in 3 parallel lines (two TDs and one bypass). An Aerosol Chemical Speciation Monitor (ACSM, Aerodyne Research Inc.) alternated between the bypass and TS-TD lines at ~ 20-30 minute intervals using an automated 3-way valve system. The ACSM measured the sub-micron aerosol (~ 75-650 nm) mass concentration of non-refractory chemical species (organic, sulfate, nitrate, ammonium, and chloride) (Ng et al., 2011a).

All aerosol instruments and TD inlets were inside a temperature-controlled (25˚±2) trailer in Centreville, and laboratory room in Raleigh. Ambient air was continuously sampled through a sampling inlet located on the rooftop of a trailer/building (~5 m above ground level). The sampling inlet included a $PM_{2.5}$ cyclone (URG Corp, 16.7 L min^{-1}) followed by a ~ 8 mm inner diameter copper sample line. A silica gel diffusion dryer upstream of TD inlets and aerosol instruments maintained relative humidity (RH) < 30-40%. The dryer is required for instrument operation under these humid conditions but may induce some loss of water-soluble OA components (El-Sayed et al., 2016).

2.3. Quantifying OA evaporation

Evaporation of bulk OA at a particular TD operating temperature and residence time is described in terms of mass fraction remaining (MFR). OA MFR is the ratio of OA mass concentration measured after passing through TD to that measured via the bypass (room temperature) line. For quantitative assessment of aerosol volatility, such as during modeling of aerosol evaporation, the initial OA concentration (C_{OA}) and particle size are also needed. Empirically estimated particle loss correction factors as a function of TD temperatures and residence times (Saha et al., 2015) and instrumental inter-calibration factors were applied in MFR calculations. To get directly comparable SMPS concentration data from 3 SMPSs running in parallel with our dual TD system, we ran them periodically in parallel on the bypass line to determine inter-calibration factors. Further details on SMPS inter-comparison are discussed in Saha et al. (2015). Since the VRT-TD line was measured with the SMPS only (Fig.1), it provided only information on evaporation of submicron aerosol in terms of its volume concentration. We estimated the OA MFR from VRT-TD/SMPS data assuming measured aerosol volume was comprised of OA and ammonium sulfate (AS) only. This is a reasonable assumption under these conditions because more than 90% of measured aerosol volume concentrations can be explained by OA+AS for both sites (see supplementary information; SI, Fig. S1). Our calculations also assumed that AS did not evaporate at the VRT-TD operating temperatures (60 or 90˚C) (Fig. S2). For further detail on the estimation of approximate OA MFR from VRT-TD/SMPS data, see SI, section S.1.

2.4. Determining OA gas-particle partitioning parameters

We apply a previously described volatility parameter extraction framework (Saha et al., 2015; Saha and Grieshop, 2016) to extract a set of volatility parameter (C^*, ΔH_{vap}, γ_e) values via inversion of dual-TD data using an evaporation kinetics model. The approach is outlined briefly below. The resulting fit describes OA using a $\log_{10}$ volatility basis set (VBS) framework (Donahue et al., 2006, 2012), where material is lumped into volatility bins separated by orders of magnitude in C^* space at a reference temperature (T_{ref}). The volatility distribution extracted using this approach is an empirical estimate describing the bulk volatility behavior of OA, assuming absorptive partitioning (Donahue et al., 2006, 2012). The VBS approach is based on an effective saturation concentration (C*) where the activity coefficient is assumed to be lumped into the saturation concentration. In the VBS approach, total OA concentration (C_{OA}; μg m^{-3}) is modeled using Eq. 1.

$$C_{OA} = C_{tot} \sum_i f_i \left(1 + \frac{C_i^*}{C_{OA}} \right)^{-1} \quad (1)$$

Here, C_{tot} is the total organic material (vapor + aerosol) in phase equilibrium with C_{OA}; f_i is the fraction of C_{tot} in each volatility ($\log_{10}C^*$) bin. Thus, $f_i = C_{tot,i}/C_{tot}$, describes the distribution of organics in volatility space and is usually called the 'volatility distribution'.

The Clausius-Clapyeron equation (Eq. 2) is used to represent temperature dependent C*.

$$C_i^*(T) = C_i^*(T_{ref}) \exp\left[-\frac{\Delta H_{vap,i}}{R}\left(\frac{1}{T}-\frac{1}{T_{ref}}\right)\right]\frac{T_{ref}}{T} \quad (2)$$

Where R is the gas constant and ΔH_{vap} is the enthalpy of vaporization.

To extract the volatility distribution of OA from ambient measurements, we select lower and upper C^* (T_{ref}) bins of 10^{-4} and 10^1 μg m^{-3}, respectively. A reference temperature (T_{ref}) of 298 K is assumed. All C* values reported in this paper should be considered at 298 K, unless otherwise specified. The selection of the lower and upper bins are determined by the highest TD operating temperature (180 ˚C) and the average ambient OA loading (C_{OA} ~ 5 μg m^{-3}), respectively. With the above C^* bin limits, materials having $C^* < 10^{-4}$ μg m^{-3} are lumped into the lowest bin, while materials having $C^* > 10$ μg m^{-3} are not represented. Note, if a C^* bin of 100 μg m^{-3} is included, Eq. 1 indicates less than 5% of the material in this bin will be in the condensed-phase at C_{OA} ~ 5 μg m^{-3}. Therefore, C^* bins > 10 μg m^{-3} are not well constrained by our TD data and are not included in our analysis.

The general approach to fitting a volatility parameterization employed in this study is similar to that applied to laboratory aerosol systems (Saha et al., 2015; Saha and Grieshop, 2016). Briefly, the kinetic model tracks both particle- and gas-phase concentrations of model species (each represented by a VBS bin) as they proceed through TD operated at a particular temperature and residence time. The model takes inputs of several aerosol properties (e.g., C^* distribution, ΔH_{vap}, diffusion coefficient (D), surface tension (σ), molecular weight (MW) and density (ρ)), total aerosol loading (C_{OA}) and particle diameter (d_p) and determines how much aerosol mass concentration will evaporate for a set of input parameters at a particular TD temperature and residence time. Non-continuum effects on mass transfer are represented using the Fuchs−Sutugin correction factor, which depends on γ_e. The model is applied to extract OA properties such as the volatility distribution, ΔH_{vap}, and γ_e as fitting parameters by matching measured and modeled evaporation data. Values of D, σ, MW, and ρ generally have a smaller influence on observed evaporation (Cappa and Jimenez, 2010; Saha et al., 2015), and are approximated from literature values (Table S-1). Volume median diameter was used as a representative d_p. For simplicity, a large (ΔH_{vap}, γ_e) space was considered for fitting a f_i distribution of measured OA. Following previous work (Epstein et al., 2010; May et al., 2013), a linear relationship was assumed between ΔH_{vap} and $\log_{10}C^*$ with $\Delta H_{vap,i}$ = intercept-slope ($\log_{10}C^*_{i,298}$), where intercept and slope are fit parameters. Values for ΔH_{vap} intercept = [50, 80, 100, 130, 200] and slope = [0, 4, 8, 11] KJ mol^{-1} were applied along with γ_e = [0.01, 0.05, 0.1, 0.25, 0.5, 1]. γ_e was assumed constant over all bins, and is an effective parameter representing all kinetic limitations within the condensed-phase and at the particle surface.

A distribution of f_i was solved for each combination of (ΔH_{vap}, γ_e) applying the non-linear constrained optimization solver '*fmincon*' in Matlab (Mathworks, Inc.) by first fitting TS-TD data; 'accepted' solutions were then further refined by fitting VRT-TD observations. A constraint of $\Sigma f_i = 1$ was used. The goodness of fit was quantified in terms of the sum of squared residual (SSR) values. For the campaign average fit, an 'acceptance' threshold value for SSR was selected based on observed variability (±one standard deviation) in measurements. A parameter set (f_i, ΔH_{vap}, and γ_e) was considered a finally 'accepted'

solution if it optimally reproduced both TS-TD and VRT-TD observations within the observed variability. Raw data at each (T, Rt) condition were averaged over 20-30 minutes. At given TD operating conditions (T, Rt), we defined ±1 standard deviation of MFR data (20-30 minute resolution) from the whole campaign as an indicator of the observed variability. The '*best fit*' is defined as that with the lowest SSR value among all the accepted combinations.

2.5 Simulation of OA in a chemical transport model

Considering that VBS-based parameterizations are becoming common means to improve the performance of OA prediction in chemical transport models (CTMs) (Farina et al., 2010; Lane et al., 2008b; Matsui et al., 2014; Murphy et al., 2011; Shrivastava et al., 2013), measurements of OA volatility provide a useful means by which to evaluate these simulations. We compared OA volatility distributions measured in this study to those resulting from CTM simulations with a current VBS-based parameterization implemented in a modified version of the Weather, Research and Forecasting model with Chemistry (WRF/Chem) v3.6.1 (Wang et al., 2015; Yahya et al., 2016b). The WRF/Chem simulation uses the Carbon Bond version 6 (CB6) gas-phase mechanism (Yarwood et al., 2010) coupled by Wang et al. (2015) to the Model for Aerosol Dynamics for Europe – Volatility Basis Set (MADE/VBS) (Ackermann et al., 1998; Ahmadov et al., 2012; Shrivastava et al., 2011). The CB6-MADE/VBS treatment includes semivolatile POA and SOA, as well as a fragmentation and functionalization treatment for multi-generational OA aging based on Shrivastava et al. (2013). The fragmentation and functionalization treatment in this case assumes 25% fragmentation for the third and higher generations of oxidation (Shrivastava et al., 2013). The ranges of C^* values used in WRF/Chem simulation are defined based on current SOA and semi-volatile POA parametrizations and were 10^0 to 10^3 μg m^{-3} for ASOA (anthropogenic-SOA) and BSOA (biogenic-SOA), 10^{-2} to 10^6 μg m^{-3} for POA and 10^{-2} to 10^5 μg m^{-3} for SVOA (semi-volatile OA), where SVOA refers to oxidized OA from evaporated POA. The semi-empirical correlation for ΔH_{vap} by Epstein et al. (2010) was used to estimate temperature-dependent partitioning.

The simulations are performed at a horizontal resolution of 36-km with 148 × 112 horizontal grid cells over the continental U.S. domain and parts of Canada and Mexico, and a vertical resolution of 34 layers from the surface to 100-hPa. Anthropogenic emissions in 2010 are based on the 2008 National Emissions Inventory (NEI) from the Air Quality Model Evaluation International Initiative (AQMEII) project (Pouliot et al., 2015). Biogenic emissions are simulated online by the Model of Emissions of Gases and Aerosols from Nature v2.1 (MEGAN2.1) (Guenther et al., 2012). The chemical initial and boundary conditions (ICs/BCs) come from the modified Community Earth System Model/ Community Atmosphere Model (CESM/CAM v5.3) with updates by He and Zhang (2014) and Gantt et al.(2014). The meteorological ICs/BCs come from National Center for Environmental Protection Final Analysis (FNL) data.

3. Results

3. 1. Overview of campaign characteristics

The two field campaigns were conducted in settings with distinct local emission sources and metrological conditions. The Centreville campaign was during summer (T=24.7 ± 3.3˚C, RH = 83.1 ± 15.3%). Local organic emissions surrounding the Centreville site are dominated by BVOCs since this site is located in a forest and biogenic emissions substantially increase with temperature (Lappalainen et al., 2009; Tarvainen et al., 2005; Warneke et al., 2010). In contrast, Raleigh measurements were in a setting with substantially stronger anthropogenic emissions during fall/winter (T=12.7 ± 6.0˚C, RH = 65.7 ± 18.8%). Comparison of long-term data from an air quality monitoring station near the Raleigh site shows substantially higher NO_x (5-10 fold) and CO (2-4 fold) concentrations relative to those observed at Centreville (See Fig. S3). However, the Raleigh-Durham metropolitan area has plentiful tree cover and thus substantial local BVOC emissions. For instance, α- and β-pinene concentrations measured in summer at Centreville and Duke Forest (about 40 km Northwest of the Raleigh site) are in the same range (Fig. S4). However, since the Raleigh campaign was conducted at lower temperature conditions, local BVOC emissions are expected to be lower by a factor of 3 to 4 (Fig S.4). Measurements in such diverse but similar ecological settings allows us to examine the consistency of OA volatility under varying levels of biogenic and anthropogenic influence.

Figs. S5 to S7 show average meteorological conditions, submicron aerosol size distributions, chemical composition and their temporal variations over the campaign periods. Ambient submicron particle number concentrations (10-600 nm) were higher in Raleigh (Centreville: 1500-3000 cm^{-3}, Raleigh: 3000-6000 cm^{-3}) and particle size was relatively smaller (volume median diameter, Centreville: 275 ± 30 nm, Raleigh: 227 ± 34 nm) (Fig. S6). Organic species were the dominant component in non-refractory submicron aerosol (PM_1) as measured by the ACSM at both sites (Centreville: 71± 10 %, Raleigh: 76 ± 8 %). The campaign average ± one standard deviation of ACSM-derived OA mass concentrations were 5.2 ± 3.0 μg m^{-3} in Centreville and 6.7 ± 3.6 μg m^{-3} in the Raleigh campaign, assuming a collection efficiency (CE) of 0.5. Application of the 'coarse' tracer *m/z* based factor analysis approach to decompose OA mass spectra (Ng et al., 2011b), the majority of OA measured at both sites was oxygenated-OA (OOA). While approximately 7% of campaign averaged OA mass concentration in Raleigh was classified as hydrocarbon-like OA (HOA), the HOA contribution at the Centreville site was negligible. Positive matrix factorization (PMF) results from high-resolution mass spectra collected at the Centerville site (Xu et al., 2015a, 2015b) and their linkage with the measured OA volatility are discussed in sections 3.3 and 3.4, below.

3. 2. Observed campaign average evaporation of OA

Fig.2 shows the campaign average OA MFR as a function of TD temperature and residence time. (1-MFR) at a TD temperature and residence time indicates what fraction of bulk OA mass evaporates at that condition. It is important to note that MFR at a given temperature is not a consistent descriptor of OA volatility because it depends on many parameters related to TD experimental conditions (e.g., *Rt*) and sampled aerosol (e.g., C_{OA}, d_p). Therefore, MFR data should not be interpreted as a direct measure of OA volatility or even directly compared (unless experiments are conducted under identical conditions).

Fig. 2a (MFR vs. temperature, frequently called a thermogram plot) shows TS-TD measurements from this study along with one other measurement from SOAS (Hu et al., 2016) and several previous field and laboratory measurements. The campaign average OA MFRs measured at the two sites in the southeastern US, under relatively consistent C_{OA} ~ 5 μg m^{-3}, were found to be quite similar. Approximately 60 -70% of OA mass evaporated after heating at 100℃ with a residence time of 50 s. The campaign average T_{50} and T_{90} (temperature at which 50% and 90% of OA mass evaporate, respectively) with a residence time of 50 s were ~ 78℃ and ~ 180℃, respectively. Data from α-pinene chamber SOA experiments collected using the same dual-TD setup at atmospheric conditions (dark ozonolysis, C_{OA} ~ 5 μg m^{-3}), described in Saha and Grieshop (2016), are also shown. Relative to the ambient observations, the lab SOA data show similar evaporation behavior in the lower temperature range (40-90 ˚C), but relatively greater evaporation at higher temperatures.

Fig. 2b and 2c show the campaign-average estimated OA MFRs at various residence times with the VRT-TD operated at 60˚C and 90˚C, respectively. Results show increased evaporation with longer residence time. In Fig. 2a, data are color coded by the TD residence time used in each study. A substantial effect of residence time on the observed evaporation is consistent with that observed across TD measurements from several previous field studies (Häkkinen et al., 2012; Huffman et al., 2009; Lee et al., 2010; Paciga et al., 2015; Xu et al., 2016). This effect of residence time on observed MFR strongly suggests that comparisons of OA volatility across studies should not be made based on measured MFRs. Doing so may bias inferences about differences in aerosol volatility. Observed evaporation depends on TD residence time and many physical and chemical properties of sampled aerosol (Cappa, 2010; Riipinen et al., 2010; Saleh et al., 2011), unless the aerosol reaches equilibrium inside a TD (saturates the gas phase across the volatility range). The equilibration time of aerosol in a TD is dictated by many parameters including particle size distribution, diffusion coefficient (D) and evaporation coefficient (γ_e) and is typically several minutes or more under atmospheric (low C_{OA}) conditions (Saleh et al., 2011, 2013).

Following the method of Saleh et al. (2013), the estimated characteristic equilibration times for the sampled aerosol in the Centreville and Raleigh measurements are 147-470 s and 150-450 s, respectively, assuming unhindered mass transfer ($\gamma_e = 1$). These calculations are based on the interquartile ranges of particle number concentrations (N_p) and condensation sink diameter (d_{cs}) measured in Centreville (N_p ~ 1500-3000 cm^{-3}, d_{cs} ~ 125- 170 nm) and Raleigh (N_p ~ 3000-6000 cm^{-3}, d_{cs} ~ 80- 105 nm), $D = 3.5 \times 10^{-6}$ m^2 s^{-1} and $MW = 200$ g mol^{-1}. The condensation sink diameter (d_{cs}) is estimated following Lehtinen et al. (2003); further detail is given in the SI. A factor-of-ten reduction in γ_e relative to ideal accommodation ($\gamma_e = 0.1$) increases equilibration time by an order of magnitude. The observed continuous downward slope of MFR versus residence time (Fig. 2b, c) suggests that equilibrium was not reached in the TD during the maximum *Rt* of 50 s. This result implies that TD measurements in an ambient setting are essentially a measure of the evaporation rate of sampled aerosol, rather than one of volatility, an equilibrium thermodynamic property. Therefore, an evaporation kinetic model is needed to extract volatility parameter values from ambient TD data.

3.3. Extracted OA volatility parameter values

Fig. 3 presents the results of the extraction process used to determine parameters dictating gas-particle partitioning (f_i, ΔH_{vap}, γ_e); the example shown is for a fit to the Centreville campaign-average data, though the same process was conducted for all fits. Fig. S8 shows a similar plot for the Raleigh data set. Fitting results show that a broad range of γ_e (0.05 to 1) can reproduce the TS-TD observation within observed variability (i.e., error bars in Fig. 2) for several ΔH_{vap} combinations (accepted TS-TD fits are shown with filled inner circles). The inclusion of VRT-TD data provides additional constraints for parameter fitting. Only the points with white crosses (x) in Fig. 3 recreate both TD data sets; a larger sized 'x' represents a better fit. Thus, VRT-TD data help to narrow the possible solution space. Fig. 3 shows that ΔH_{vap} = 100 KJ mol^{-1} and γ_e = 0.5 provide the overall *best fit* for the Centreville data set. For the Raleigh data set, ΔH_{vap} of both 80 (marginally better) and 100 KJ mol^{-1} with γ_e = 0.5 provide similarly good fits (Fig S8). For simplicity, ΔH_{vap} = 100 KJ mol^{-1} and γ_e = 0.5 are considered as best estimates for both data sets for the next portion of the paper.

These results are inconsistent with a very small value of OA evaporation coefficient (e.g., $\gamma_e << 0.1$) that would indicate significant resistance to mass transfer during evaporation, which has been suggested previously based on dilution (Grieshop et al., 2007, 2009; Vaden et al., 2011) and heating (Lee et al., 2011) experiments. Our best estimate of $\gamma_e \sim 0.5$ is consistent with the observations of Saleh et al. (2012), in which they report an $\gamma_e \sim 0.28$ to 0.46 for ambient aerosols in Beirut, Lebanon via measured equilibration profiles of concentrated ambient aerosols ($C_{OA} \sim$ 200-300 μg m^{-3}) after heating in a TD at 60 ˚C. Our results show that an effective $\gamma_e \sim 0.1$ to 1 can explain dual-TD data to within observed variability, suggesting that there is no extreme resistance to mass transfer such as what might be encountered due to a glassy-solid or highly-viscous aerosol. Some previous assertions of highly inhibited evaporation (Grieshop et al., 2007; Vaden et al., 2011) were likely biased as they assumed volatility distributions based on smog-chamber yield experiments that likely overestimated the volatility, and thus expected evaporation rate of lab OA (Saha and Grieshop, 2016; Saleh et al., 2013).

Our fitting results show that a ΔH_{vap} intercept of 80 -130 KJ mol^{-1} and slopes of 0 or 4 KJ mol^{-1} can be used to explain campaign average observations (Fig. 3, Fig. S6). These ΔH_{vap} values are consistent with those of atmospherically-relevant low-volatility organics such as dicarboxylic acids (Bilde et al., 2015), but distinct from those typically assumed (30 - 40 KJ mol^{-1}) for atmospheric modeling (Farina et al., 2010; Lane et al., 2008b; Pye and Seinfeld, 2010). The low enthalpies assumed in models are based on temperature sensitivity observations from smog chamber SOA experiments (Offenberg et al., 2006; Pathak et al., 2007; Stanier et al., 2008). The semi-empirical correlation based fit from Epstein et al. (2010) (ΔH_{vap}=130-11 $\log_{10}C^*$) has steeper $\log_{10}C^*$ dependence than those able to explain our observations (Figs. 3, S8). The Epstein et al. correlation was determined from range of compounds with known ΔH_{vap}. Several recent studies of complex OA systems (May et al., 2013; Ranjan et al., 2012) have found that a correlation other than that from Epstein et al. better explains observations. For example, Ranjan et al.(2012) reported ΔH_{vap} = 85-11logC* for gas–particle partitioning of POA emissions from a diesel engine; May et al.(2013) reported ΔH_{vap} = 85-4logC* for biomass burning POA emissions. Similar to these and other studies, our ΔH_{vap} correlation for ambient OA is an empirical estimate which best explain our observations.

Although several ΔH_{vap} and γ_e combinations can recreate observations from both TDs within variability (Figs. 3, S8), to enable comparison of C^* distributions we adopt our *best* estimates of ΔH_{vap} and γ_e (ΔH_{vap} = 100 KJ mol^{-1} and γ_e = 0.5) for further analysis of data from both campaigns. Campaign-average f_i distributions corresponding to that (ΔH_{vap}, γ_e) are the basis for model fits shown in Fig. 2. The 'campaign-average' f_i distribution was derived by fitting campaign-average dual-TD observations (Fig. 2) and using campaign-average C_{OA} and d_p. A f_i distribution was also fit based on all the individual measurements from the campaign (*MFR*, C_{OA}, d_p; 20-30 minute time resolution) using ΔH_{vap} = 100 KJ mol^{-1} and γ_e = 0.5; we term this the 'unified' fit. The 'campaign-average' and 'unified' f_i distributions for the Centreville and Raleigh data set are listed in Table 1. In addition to the volatility distribution (f_i), we also show estimates of mean C^* ($\overline{C^*}$; estimated as $\overline{C^*} = 10^{\sum f_i \log_{10} C_i^*}$) to quantify the center of mass (central tendency) of different volatility distributions. Another way to collapse a distribution to a single value (also reported in Table 1) is the effective C^* (C_{eff}^*) of the ensemble, estimated as, $C_{eff}^* = \sum x_i C_i^*$, where x_i is the condensed-phase mass fraction in each C_i^* bin and Σ x_i =1. While the volatility parameter values reported in Table 1 are the *best* fit results, other parameter sets can reproduce observations within variability. Application of f_i distributions reported in Table 1 must be with reported γ_e and ΔH_{vap} values. Sensitivities of the estimated volatility parameter values to assumed values of D, σ, *MW,* and ρ are discussed in Saha et al.(2015) and Saha and Grieshop(2016). These assumed parameters have relatively minor effects on observed evaporation in a TD compared to C^*, γ_e, and ΔH_{vap}.

The extracted campaign-average and unified-fit OA volatility distributions (f_i) and corresponding $\overline{C^*}$ and C_{eff}^* from Centreville and Raleigh data sets are quite similar (see Table 1). A large portion of the measured OA (40-70%) at both sites is composed of very low-volatility organics (LVOCs; $C^* \leq 0.1$ μg m^{-3}, Donahue et al., 2012). It is somewhat surprising that results from two field campaigns, which occurred in distinct scenarios with varying level of biogenic and anthropogenic emissions, results in such similar OA volatility distributions. This finding is consistent with those of Kolesar et al.(2015a), who report similar mass thermograms for laboratory SOA formed from a variety of anthropogenic and biogenic VOCs under different oxidant (O_3, OH) conditions. Our extracted ambient OA volatility distributions are also comparable to those previously derived from TD measurement in Mexico City (Cappa and Jimenez, 2010) and Finokalia, Greece (Lee et al., 2010). However, the ambient OA volatility distributions determined here are relatively less volatile than those from chamber-generated fresh SOA from α-pinene ozonolysis (Table 1).

Fig. 4a demonstrates a forward modeling exercise to show how the extracted average volatility parameter values (f_i, ΔH_{vap}, and γ_e; those listed in Table 1) can reproduce individual measurements from the whole Centreville campaign as well as TD data from other groups (Cerully et al., 2015; Hu et al., 2016) during SOAS. The results show that a single set of volatility parameter values (campaign average/unified fit f_i, γ_e = 0.5 and ΔH_{vap} = 100 KJ mol^{-1}) reproduce individual observations from the whole campaign within approximately ± 20% (coefficient of determination, r^2 = 0.83; root mean squared error, RMSE: 0.11). These parameter values also closely reproduced the measured campaign average OA MFRs from the University of Colorado TD (Rt ~ 15 s) (Hu et al., 2016) and Georgia Tech TD (Rt ~ 7 s) (Cerully et al., 2015) collected during the Centreville campaign (see solid blue squares and cyan triangles in Fig. 4a). MFRs reported in Cerully et al. (2015) are for the total

submicron aerosol species. These were converted to OA MFRs applying the method given in SI Sec. S1 to enable direct comparison with modeled OA MFRs.

Fig 4b shows a comparison of the extracted campaign-average OA volatility distribution from this study with those from two other independent approaches during the Centreville campaign (Hu et al., 2016; Lopez-Hilfiker et al., 2016). Hu et al. (2016) report OA volatility distributions from observed evaporation in a TD during the Centreville campaign fit using the method given by Faulhaber et al.(2009). In this method, TD evaporation observations at different temperatures are translated to a volatility distribution using an empirically derived calibration curve based on evaporation of known compounds and their C^* (Faulhaber et al., 2009). Our derived distribution from dual-TD observations coupled with evaporation kinetic model is comparable to that from Hu et al. (2016), although this distribution is slightly less volatile than ours. Lopez-Hilfiker et al. (2016) derived an OA volatility distribution from Centreville measurements with the Filter Inlet for Gases and AEROsols-Chemical Ionization Mass Spectrometer (FIGAERO-CIMS), which thermally desorbs filter-bound aerosol into a CIMS. The FIGAERO-derived distribution is several orders of magnitude less volatile than ours; all OA in it has $C^* \leq 10^{-4}$ μg m^{-3}. Therefore, in Fig.4b the Centreville campaign-average C_{OA} of ~ 5 μg m^{-3} is assigned to the log10C* ≤ -4 bin to enable direct comparison with TD-ACSM/AMS measurements (this study and Hu et al.). However, in reality FIGAERO-CIMS observations accounted for ~50% of AMS organic mass concentrations measured at Centreville (Lopez-Hilfiker et al. 2016), indicating half the OA was not quantified. The discrepancy between FIGAERO- and TD-based distributions would be reduced if this unmeasured OA is distributed in higher volatility bins, thus re-assigning material shown in the lowest volatility bin in Fig. 4b. Lopez-Hilfiker et al. (2016) reported that heating OA at higher temperatures has the potential to introduce artifacts into quantification of its volatility, for example if it causes oligomer decomposition leading to artificially high volatility. If this occurs, this may bias any heating-based measurement approaches, including TD measurements.

A test for these various parameter values is to use them to recreate data from other (non-heating-based) perturbations of gas-particle partitioning. Fig. 5 shows evaporation kinetics of OA upon continuous stripping of vapors under isothermal (25 ˚C) conditions simulated using volatility parameter values from multiple independent approaches. The simulation framework used here is described elsewhere (Saha and Grieshop, 2016). The shaded region in Fig.5 shows the prediction range applying dual-TD derived parameter values from this study within estimated uncertainty ranges (campaign average and unified fits of f_i, γ_e = 0.1 to 1) with initial C_{OA} values from 2 to 10 μg m^{-3} and d_p = 100 nm and 150 nm. Simulations are also shown with the OA volatility distribution from Hu et al.(2016) and FIGAERO-CIMS-derived OA volatility distribution (Lopez-Hilfiker et al., 2016) from Centreville measurements. The room temperature evaporation data from Vaden et al. (2011) measurements of ambient aerosols during the Carbonaceous Aerosols and Radiative Effects Study (CARES-2010) field campaign in Sacramento, California are also shown. This study attributed the observed slower-than-expected evaporation to extreme kinetic limitations to mass transfer ($\gamma_e << 0.1$). Although a direct comparison of observations collected in California and simulations based on volatility distributions from Centreville is not ideal, the consistency of volatility behavior across our and other sites (Fig. 2; Table 1) suggests it is reasonable. Fig. 5 shows that these data fall within the range of values simulated using our TD-

estimated volatility parameter values ($\gamma_e \geq 0.1$). The Hu et al. (2016) volatility distribution with $\gamma_e = 1$ also recreates these data. In contrast, simulations with the FIGAERO-CIMS-derived OA volatility distribution (Lopez-Hilfiker et al., 2016) from Centreville measurements (assuming $\gamma_e = 1$) predict almost zero evaporation (dashed black line in Fig. 5). This distribution thus appears to be inconsistent with our observations and those from room temperature evaporation experiments.

3.4 Temporal variation of OA volatility

A time series of OA volatility distributions extracted over the campaign period is shown in Figs. 6 (Centreville) and S10 (Raleigh). The volatility distributions (f_i) were extracted as described above from ~ 6-hour windows with fixed ΔH_{vap} = 100 KJ mol^{-1} and $\gamma_e = 0.5$ based on the best estimates from campaign-average fits. The average and (95% confidence interval) of $\overline{C^*}$ (μg m^{-3}) are 0.18 (0.05 - 0.54) and 0.16 (0.04 - 0.43) for the Centreville and Raleigh data sets, respectively, in line with values from the campaign-average and unified fits. The OA volatility distributions do not vary dramatically over the campaign period for either site.

Ambient OA concentrations (C_{OA}) shown in Fig. 6a (Centreville) and S10a (Raleigh). Fig. 6b shows a time series of the fractional contribution of isoprene-derived OA and more-oxidized oxygenated OA (MO-OOA) (Xu et al., 2015a, 2015b) to total OA during the Centreville campaign. In a few low C_{OA} instances, $\overline{C^*}$ was found to be higher, but there was no strong relation between these two quantities (see Fig. S12; scatter plot of mean C* vs C_{OA}). The relative contribution of MO-OOA to C_{OA} in many of these higher-$\overline{C^*}$ instances was low likely leading to more-volatile aerosol during these periods. Isoprene was the dominant biogenic VOC (> 80% of total VOC mass) measured during Centreville campaign (Xu et al., 2015b), and is the biogenic VOC with greatest global emissions (Sindelarova et al., 2014). Isoprene-derived OA contributed ~ 17-18% to the campaign average C_{OA} at the Centreville site during the SOAS (Hu et al., 2015; Xu et al., 2015a, 2015b) while MO-OOA contributed ~ 39% (Xu et al., 2015a, 2015b). Lopez-Hilfiker et al. (2016) reported isoprene-derived OA was more volatile than the remaining OA using FIGAERO-CIMS measurements at the Centreville site. This result contradicts with Hu et al. (2016), who reported a lower volatility of isoprene-derived OA than the bulk OA using TD measurements at the same site. Since our derived volatility distributions are for the bulk OA, we cannot make a specific comment on the volatility of isoprene-derived OA. However, if the volatility of isoprene-derived OA differs substantially from the remaining bulk, OA volatility might be expected to co-vary with the fractional contribution of isoprene-OA to C_{OA}. Fig. 6c shows extracted bulk OA volatility distributions and their mean C^* over the Centreville campaign period. Fig.6d shows a scatter plot of mean C^* versus the fractional contribution of isoprene-OA to C_{OA}; the two show no correlation. Neither were statistically significant relationships found between the isoprene-OA fraction and f_i's in any particular C^* bin (see table S2). These results indicates that the effective volatility of isoprene-OA may not be substantially different than the remaining bulk OA. If there is a difference we cannot differentiate this effects from bulk OA volatility, potentially due to the contributions of other components to bulk OA.

Diurnal trends in OA volatility distributions are shown in Figs. 7 (Centreville) and S11 (Raleigh). Results show that OA appeared less volatile in the afternoon than early in the morning for both sites (Centreville: campaign average $\overline{C^*}$ (μg m^{-3}) in

the morning ~ 0.25; afternoon ~ 0.13 and Raleigh: morning ~ 0.2; afternoon ~ 0.12). This trend is consistent with previous field measurements in Mexico City (MILAGRO) and Riverside (SOAR-1) (Huffman et al., 2009). Fig. 7a shows diurnal trends of OA factors derived from PMF analysis during the Centreville campaign (Xu et al., 2015a, 2015b). Less-oxidized oxygenated-OA (LO-OOA; average O:C ~ 0.63) dominated in the early morning (~40-50 %) while more-oxidized oxygenated-OA (MO-OOA; average O:C ~ 1.02) was the largest OA component in the afternoon (~50%). Xu et al.(2015a) hypothesized that oxidation of monoterpenes forms a large portion of observed LO-OOA in the Southeastern U.S. via NO_x and O_3 (NO_3 radical) pathways, and that organo-nitrates contribute substantially to LO-OOA (20-30%). Laboratory chamber experiments also suggest that nitrate-containing species make a significant contribution to SOA formed during terpene photooxidation/ozonolysis under high NO_x conditions (Ng et al., 2007; Presto et al., 2005), and from reactions with nitrate radicals (Boyd et al., 2015). Lee et al. (2011) observed greater evaporation in a TD of α-pinene and β-pinene ozonolysis SOA formed under high NOx conditions than under low NOx condition. Thus the higher volatility observed in the morning can likely be linked with the prevalence of LO-OOA and possible contributions from organo-nitrates. In contrast, bulk OA was dominated by MO-OOA in the afternoon. That OA is relatively less volatile in the afternoon is consistent with the observation that OA volatility often decreases with increased oxidation (during functionalization) (Jimenez et al., 2009). Fig. 8 shows scatter plots of $\overline{C^*}$ versus LO-OOA and MO-OOA fractions of OA during the Centreville campaign. Although the average slopes of the scatter plots show an increase (decrease) of $\overline{C^*}$ with increasing LO-OOA (MO-OOA) fraction, respectively, these correlations are not strong (correlation coefficient; r ~ 0.5). Similar levels of correlation were found with effective C* (Fig. S13). A poor correlation between $\overline{C^*}$ and OA factors is also observed in the Raleigh data set. For example, Fig. S14 shows scatter plots of $\overline{C^*}$ versus tracer *m/z* based HOA fraction and OOA fraction estimates (Ng et al., 2011b) with an average slope of – 0.3 ± 0.16 (r ~ 0.2) for HOA and - 0.12 ± 0.11 (r ~ 0.1) for OOA.

3.5 Average volatility and oxidation state of OA

Fig. 9 explores the link between average carbon oxidation state, $\overline{OS_c}$, calculated as 2× O:C - H:C (Kroll et al., 2011), and $\overline{C^*}$. O:C and H:C are estimated from an empirical parameterization of OA elemental ratio from unit mass resolution data, given by Canagaratna et al. (2015) as a function of f_{44} (O:C = 0.079 + 4.31× f_{44}) and f_{43} (H:C = 1.12 + 6.74 ×f_{43} – 17.77 × f_{43}^2) , respectively. f_{44} and f_{43} are the fractional ion intensity at *m/z* 44 and 43, respectively, taken from ACSM measurements. The estimated OA elemental ratios using the above empirical parameterizations are in relatively good agreement with those determined via elemental analysis of the high resolution mass spectra data (HRToF-AMS) collected by other groups during SOAS. For example, our estimated campaign average O:C during Centreville campaign (0.68 ± 0.07) is within 1-2 standard deviation of that determined in Xu et al.(2015b) (~ 0.78).

The scatter plot of $\overline{OS_c}$ versus $\overline{C^*}$ (Fig. 9) shows a mild downward trend, which is suggestive of lower-volatility OA being associated with higher oxidation state. However, the correlation is not statistically robust (r < 0.3). This is consistent with the observations of Xu et al.(2016) and Paciga et al. (2015) who reported weak association between average oxidation state and

volatility for OA measured in the London and Paris areas, respectively. The campaign-average $\overline{OS_c}$ during the Centreville measurements (-0.18 ± 0.15) was higher than in Raleigh (-0.42 ± 0.16) (p-value << 0.0001), whereas campaign-average $\overline{C^*}$ values were essentially identical (Centreville: 0.18 ± 0.14, Raleigh: 0.16 ± 0.12 μg m^{-3}; p-value > 0.1).

3.6 Application of measured volatility distribution to evaluate simulated OA in a CTM

Fig. 10 compares the measured and simulated OA volatility distributions at Centreville for June, 2013. The simulated OA volatility distribution in the C^* bins between 10^0 and 10^1 μg m^{-3} agrees reasonably well with observations. The model predicts a dominance of BSOA in the two bins, consistent with observations in the Centreville region. However, large discrepancies exist between the observed and simulated OA volatility distribution in the C* bins between 10^{-2} and 10^{-1} μg m^{-3}. The model tends to greatly underpredict the OA concentrations in this volatility range. WRF/Chem did not reproduce the observed portion of the mass of OA in the lower C^* bins, from 10^{-4} to 10^{-1} μg m^{-3}, because the VBS SOA module in this version of WRF/Chem does not treat volatility in this range. Consistent with the measurement results from this study, a number of laboratory (Ehn et al., 2014; Jokinen et al., 2015; Kokkola et al., 2014; Zhang et al., 2015) and field (Hu et al., 2016; Lopez-Hilfiker et al., 2016) studies have reported a significant fraction of SOA from biogenic precursors is low-volatility. These low volatility materials are missing in the WRF/Chem simulation.

The simulated total OA mass concentration (C_{OA}) was underpredicted by a factor of 2 to 3 at Centreville during the SOAS period. Several factors may contribute to this underprediction. Comparison of WRF/Chem predictions of most relevant meteorological variables and major precursor VOCs with measurements collected during the SOAS shows a relatively good performance (Yahya et al., 2016a). For example, the mean biases for simulated temperature at 2 m, relative humidity at 2 m, and wind speed at 10 m are -0.9 ºC, -0.8%, and 0.3 m s^{-1}, respectively. The normalized mean bias (NMB) of the simulated planetary boundary layer height (PBLH) is -38%, which would tend to bias OA concentrations high, suggesting that the underprediction in PBLH is not responsible for the underpredictions of OA. In terms of VOC concentrations, the model performs well for β-pinene and formaldehyde with NMBs of -8.5% and -4.3%, respectively, but underpredicts α-pinene with an NMB of -51.7% and significantly overpredicts limonene with an NMB of 249% (Figure not shown). The WRF/Chem simulation only considers the SOA formed from a few BVOCs including isoprene, α-pinene, β-pinene, limonene, humulene, and ociene and does not account for contributions from other BSOA precursors such as other sesquiterpenes. Therefore, underestimation of precursor VOC emissions and missing precursors may contribute to OA underprediction. Other sources of uncertainty in the VBS treatment in WRF/Chem include the coarse spatial resolution in the model simulation, the assumed fraction of OA added for each oxidation/aging step, the assumed fragmented and functionalized percentages of organic condensable vapors, as well as the uncertainties in the dry and wet deposition velocities of SOA and SOA precursors. These factors can also contribute to the discrepancies between the model and observed C_{OA} at Centreville.

One likely contributor to the model's under-prediction is issues with the SOA yield parameterizations in the model. Smog chamber growth-experiment-derived mass yield coefficients (i.e., distributions of product mass yield in different volatility/C^*

bins) (Pathak et al., 2007) are used to model SOA in a CTM. The estimated SOA yield from a traditional smog chamber experiment could be underestimated due to wall losses of condensable vapors. For example, Zhang et al. (2014) showed up to a factor of 4 yield underestimation for toluene SOA due to this fact. The high and low NO_x mass yields used in WRF/Chem simulations for ASOA and BSOA are based on traditional smog chamber yield experiments, taken from Lane et al.(2008b). These distributions do not consider mass yields from the C* bins 10^{-4} to 10^{-1} μg m^{-3}, where a significant portion of the OA mass was observed. The substantial amounts of low volatility materials are typically missing in these traditional yield measurement based distributions (Kolesar et al., 2015b; Saha and Grieshop, 2016). Our recent dual-TD-based effort to determine the SOA mass yield distribution for α-pinene ozonolysis (Saha and Grieshop, 2016) indicates products are substantially less volatile than the parameterizations used in current models (including that discussed above). This α-pinene product distribution suggests a factor of 2-4 more SOA yield under atmospherically relevant conditions compared to traditional distributions from smog chamber growth experiments. Updating SOA mass yield coefficient data is likely required for all known precursors, and may lead to large improvements in model predictions of both C_{OA} and OA volatility distributions.

The WRF/Chem simulation used the semi-empirical ΔH_{vap} correlation derived by Epstein et al. (2010) (ΔH_{vap} = 130 - $11\log_{10}C^*_{,298K}$), which gives higher values, with a steeper $\log_{10}C^*$ dependence, than our TD-derived values (~80-100 kJ mol^{-1}). The difference in ΔH_{vap} values used in WRF/Chem and our TD-derived values should not have a significant effect on the comparison shown in Fig.10. This is because the modeled-measured OA volatility comparison was made at temperatures (SOAS campaign average T= 24.7ºC; WRF/Chem simulated campaign average T= 23.8ºC) very close to the VBS reference temperature (25ºC). Murphy et al. (2011) also reported a low sensitivity of ΔH_{vap} when predicating surface OA loading during the FAME-08 study using a 2D-VBS framework. However, the effect of ΔH_{vap} could be significant when simulating OA loading at low ambient temperatures and high altitudes.

4. Conclusions and Implications

This paper presents results from ambient OA volatility measurements from two sites in the southeastern U.S. under diverse conditions. Measurement campaigns were conducted at a BVOC-dominated forested rural setting during summer and another more anthropogenically-influenced, but forested urban location under cooler conditions. This study applied a dual-thermodenuder (dual-TD) setup that varied temperature and residence time in parallel. Ambient OA gas-particle partitioning parameters (C^*, $\Delta H_{vap,}$ γ_e) value were extracted by fitting observed dual-TD data using an evaporation kinetic model. The OA volatility distribution derived via inverse modeling is sensitive to $\Delta H_{vap,}$ and γ_e values. The addition of variable residence time TD (VRT-TD) data provided tighter constraints on the extracted parameter values. A ΔH_{vap} of ~ 100 KJ $mole^{-1}$ and γ_e of 0.5 best explain observations collected at both sites, under diverse conditions. An effective γ_e value of ~ 0.1 to 1 can explain observed evaporations within variability while a very small γ_e value ($\gamma_e << 0.1$) cannot fit the observations from both TDs. The Epstein et al. (2010) ΔH_{vap} correlation, which was determined based on measured properties of a variety of known compounds also did not reproduce the evaporation observed in this study.

While measurement campaigns were conducted under different meteorological conditions at locations with differing levels of biogenic and anthropogenic emissions, the derived OA volatility distributions are found to be very similar. A substantial amount of OA (40-70%) at both sites was found to be of very low volatility ($C^* \leq 0.1$ μg m^{-3}) so will remain predominantly in the particle-phase (effectively non-volatile) under typical atmospheric conditions. OA volatility distributions also did not vary substantially over the campaign period. Our derived OA volatility parameterizations appear to be broadly consistent with observations of room temperature evaporation (Vaden et al., 2011) during CARES-2010 in California. The observed consistency in OA volatility across diverse settings is an important finding, which implies that OA in the atmosphere formed from a variety of sources can exhibit similar volatility properties and chemical signatures. This result also suggests that measurements of OA volatility distributions such as derived here could provide good diagnostics for overall model representativeness, but may not be as useful for diagnosing differences across sites and conditions.

The diurnal profile of extracted OA volatility showed that bulk OA was less volatile in the afternoon than early in the morning. This trend is consistent with the prevalence of LO-OOA (less oxidized) in the morning and MO-OOA (more oxidized) in the afternoon. However, while average O:C and/or oxidation state ($\overline{OS_c}$) of bulk OA is often considered linked to volatility, in our data sets correlations between mean oxidation state ($\overline{OS_c}$) and mean volatility ($\overline{C^*}$) were weak ($r < 0.3$). This observed weak correlation and the fact that atmospheric OA is a complex mixture of organics of a broad range of volatilities and oxidation states, reinforces the need to measure and understand the distribution of both volatility and oxidation states. The 2D-VBS framework (Donahue et al., 2012) offers one way to constrain these parameters in atmospheric models. While determination of OA volatility distributions was the focus of this study, future efforts also should measure distributions of volatility and oxidation states comprising ambient OA.

The gas-particle partitioning parameters (C^*, ΔH_{vap}, γ_e) extracted from these measurements have important implications for the treatment and evaluation of OA in current atmospheric models. Since a CTM incorporating the VBS framework predicts OA concentrations in each volatility ($\log_{10}C^*$) bin (i.e., OA volatility distribution), comparison of simulated and measured OA volatility distribution is an useful means for model evaluation beyond only comparing total OA concentration (C_{OA}). Here, we compared our measured OA volatility distribution with that simulated by WRF/Chem. This evaluation indicates that OA volatility distributions predicted in WRF/Chem are inconsistent with measurements over the C^* range from 10^{-4} to 10^{-1} μg m^{-3}. This may give important clues towards the root causes of the model's underestimation of C_{OA} by a factor of 2 to 3. In comparison to our TD-derived OA volatility distribution and other recent evidence (Ehn et al., 2014; Hu et al., 2016, 2016; Jokinen et al., 2015; Kokkola et al., 2014; Lopez-Hilfiker et al., 2016; Saha and Grieshop, 2016), low-volatility materials are mostly missing from the WRF/Chem predictions. Recent evidence of SOA from aqueous-phase oxidation in presence of abundant particle water (Carlton and Turpin, 2013; Marais et al., 2016), formation of oligomers and large molecular compounds directly in the gas- phase (Ehn et al., 2014) and via condensed phase chemistry (Kroll et al., 2015; Kroll and Seinfeld, 2008) suggest that complex and multi-phase formation and evolution processes produce SOA in the atmosphere. Many of these processes can produce very low-volatility organics and most are not included in current CTMs. These low-

volatility organics appear to make significant contributions to the atmospheric OA budget and cloud condensation nuclei formation (Jokinen et al., 2015).

The ΔH_{vap} and γ_e values extracted here for atmospheric OA in the Southeastern U.S. also have important implications for predicting OA concentrations in a CTM. First, a ΔH_{vap} value of 30-40 KJ mol^{-1} (Farina et al., 2010; Lane et al., 2008b; Pye and Seinfeld, 2010) is typically assumed for modeling OA in a CTM, which is substantially lower than that suggested by our TD observations (~100 KJ mol^{-1}). An increase of assumed ΔH_{vap} value can increase atmospheric OA burden and lifetime for a particular input volatility distribution (Farina et al., 2010), especially at low ambient temperatures and high altitudes. Finally, a value of $\gamma_e \geq 0.1$ indicates a gas-particle repartitioning timescale (Saleh et al., 2013) on the order of minutes to an hour under atmospherically relevant conditions ($N_p \sim$ 1000-5000 cm^{-3}). Therefore, the equilibrium phase-partitioning assumption typically made in CTMs should be reasonable for a prediction timestep of ~ 1 hour.

Acknowledgements

We thank Satoshi Takahama and his research group at EPFL for their help and support during the SOAS campaign, Paul Shepson's group (Purdue University) for BVOC data, SEARCH Network for temperature, relative humidity, mixing height, CO, NO_x data from the Centreville site. Operation of the SEARCH network and analysis of its data collection are sponsored by the Southern Co. and Electric Power Research Institute.

Funding was provided by start-up support from North Carolina State University, Raleigh, USA. AK acknowledges funding by USEPA (grant 83541101). Contents of this publication are solely the responsibility of the authors and do not necessarily represent the official views of the USEPA. Further, USEPA does not endorse the purchase of any commercial products or services mentioned in the publication. KY and YZ acknowledge funding from the National Science Foundation EaSM program (AGS-1049200) for WRF/Chem simulations and high-performance computing support from Stampede, provided as an Extreme Science and Engineering Discovery Environment (XSEDE) digital service by the Texas Advanced Computing Center (TACC) (http://www.tacc.utexas.edu), which is supported by National Science Foundation grant number ACI-1053575 and Yellowstone (ark:/85065/d7wd3xhc) provided by NCAR's Computational and Information Systems Laboratory, sponsored by the National Science Foundation and Information Systems Laboratory. LX and NLN acknowledge National Science Foundation grant 1242258 and US Environmental Protection Agency STAR grant RD-83540301.

References

Ackermann, I. J., Hass, H., Memmesheimer, M., Ebel, A., Binkowski, F. S. and Shankar, U.: Modal aerosol dynamics model for Europe: development and first applications, Atmos. Environ., 32(17), 2981–2999, doi:10.1016/S1352-2310(98)00006-5, 1998.

Ahmadov, R., McKeen, S. A., Robinson, A. L., Bahreini, R., Middlebrook, A. M., de Gouw, J. A., Meagher, J., Hsie, E.-Y., Edgerton, E., Shaw, S. and Trainer, M.: A volatility basis set model for summertime secondary organic aerosols over the eastern United States in 2006, J. Geophys. Res. Atmospheres, 117(D6), D06301, doi:10.1029/2011JD016831, 2012.

Bilde, M., Barsanti, K., Booth, M., Cappa, C. D., Donahue, N. M., Emanuelsson, E. U., McFiggans, G., Krieger, U. K., Marcolli, C., Topping, D., Ziemann, P., Barley, M., Clegg, S., Dennis-Smither, B., Hallquist, M., Hallquist, Å. M., Khlystov, A., Kulmala, M., Mogensen, D., Percival, C. J., Pope, F., Reid, J. P., Ribeiro da Silva, M. A. V., Rosenoern, T., Salo, K., Soonsin, V. P., Yli-Juuti, T., Prisle, N. L., Pagels, J., Rarey, J., Zardini, A. A. and Riipinen, I.: Saturation Vapor Pressures and Transition Enthalpies of Low-Volatility Organic Molecules of Atmospheric Relevance: From Dicarboxylic Acids to Complex Mixtures, Chem. Rev., 115(10), 4115–4156, doi:10.1021/cr5005502, 2015.

Boyd, C. M., Sanchez, J., Xu, L., Eugene, A. J., Nah, T., Tuet, W. Y., Guzman, M. I. and Ng, N. L.: Secondary organic aerosol formation from the β-pinene+NO3 system: effect of humidity and peroxy radical fate, Atmos Chem Phys, 15(13), 7497–7522, doi:10.5194/acp-15-7497-2015, 2015.

Budisulistiorini, S. H., Li, X., Bairai, S. T., Renfro, J., Liu, Y., Liu, Y. J., McKinney, K. A., Martin, S. T., McNeill, V. F., Pye, H. O. T., Nenes, A., Neff, M. E., Stone, E. A., Mueller, S., Knote, C., Shaw, S. L., Zhang, Z., Gold, A. and Surratt, J. D.: Examining the effects of anthropogenic emissions on isoprene-derived secondary organic aerosol formation during the 2013 Southern Oxidant and Aerosol Study (SOAS) at the Look Rock, Tennessee ground site, Atmos Chem Phys, 15(15), 8871–8888, doi:10.5194/acp-15-8871-2015, 2015.

Burtscher, H., Baltensperger, U., Bukowiecki, N., Cohn, P., Hüglin, C., Mohr, M., Matter, U., Nyeki, S., Schmatloch, V., Streit, N. and Weingartner, E.: Separation of volatile and non-volatile aerosol fractions by thermodesorption: instrumental development and applications, J. Aerosol Sci., 32(4), 427–442, doi:10.1016/S0021-8502(00)00089-6, 2001.

Canagaratna, M. R., Jimenez, J. L., Kroll, J. H., Chen, Q., Kessler, S. H., Massoli, P., Hildebrandt Ruiz, L., Fortner, E., Williams, L. R., Wilson, K. R., Surratt, J. D., Donahue, N. M., Jayne, J. T. and Worsnop, D. R.: Elemental ratio measurements of organic compounds using aerosol mass spectrometry: characterization, improved calibration, and implications, Atmos Chem Phys, 15(1), 253–272, doi:10.5194/acp-15-253-2015, 2015.

Cappa, C. D.: A model of aerosol evaporation kinetics in a thermodenuder, Atmospheric Meas. Tech., 3(3), 579–592, doi:10.5194/amt-3-579-2010, 2010.

Cappa, C. D. and Jimenez, J. L.: Quantitative estimates of the volatility of ambient organic aerosol, Atmos Chem Phys, 10(12), 5409–5424, doi:10.5194/acp-10-5409-2010, 2010.

Carlton, A. G. and Turpin, B. J.: Particle partitioning potential of organic compounds is highest in the Eastern US and driven by anthropogenic water, Atmos Chem Phys, 13(20), 10203–10214, doi:10.5194/acp-13-10203-2013, 2013.

Cerully, K. M., Bougiatioti, A., Hite Jr., J. R., Guo, H., Xu, L., Ng, N. L., Weber, R. and Nenes, A.: On the link between hygroscopicity, volatility, and oxidation state of ambient and water-soluble aerosols in the southeastern United States, Atmos Chem Phys, 15(15), 8679–8694, doi:10.5194/acp-15-8679-2015, 2015.

Donahue, N. M., Robinson, A. L., Stanier, C. O. and Pandis, S. N.: Coupled Partitioning, Dilution, and Chemical Aging of Semivolatile Organics, Environ. Sci. Technol., 40(8), 2635–2643, doi:10.1021/es052297c, 2006.

Donahue, N. M., Kroll, J. H., Pandis, S. N. and Robinson, A. L.: A two-dimensional volatility basis set – Part 2: Diagnostics of organic-aerosol evolution, Atmos Chem Phys, 12(2), 615–634, doi:10.5194/acp-12-615-2012, 2012.

Ehn, M., Thornton, J. A., Kleist, E., Sipilä, M., Junninen, H., Pullinen, I., Springer, M., Rubach, F., Tillmann, R., Lee, B., Lopez-Hilfiker, F., Andres, S., Acir, I.-H., Rissanen, M., Jokinen, T., Schobesberger, S., Kangasluoma, J., Kontkanen, J., Nieminen, T., Kurtén, T., Nielsen, L. B., Jørgensen, S., Kjaergaard, H. G., Canagaratna, M., Maso, M. D., Berndt, T., Petäjä, T., Wahner, A., Kerminen, V.-M., Kulmala, M., Worsnop, D. R., Wildt, J. and Mentel, T. F.: A large source of low-volatility secondary organic aerosol, Nature, 506(7489), 476–479, doi:10.1038/nature13032, 2014.

El-Sayed, M. M. H., Amenumey, D. and Hennigan, C. J.: Drying-Induced Evaporation of Secondary Organic Aerosol during Summer, Environ. Sci. Technol., 50(7), 3626–3633, doi:10.1021/acs.est.5b06002, 2016.

Epstein, S. A., Riipinen, I. and Donahue, N. M.: A Semiempirical Correlation between Enthalpy of Vaporization and Saturation Concentration for Organic Aerosol, Environ. Sci. Technol., 44(2), 743–748, doi:10.1021/es902497z, 2010.

Farina, S. C., Adams, P. J. and Pandis, S. N.: Modeling global secondary organic aerosol formation and processing with the volatility basis set: Implications for anthropogenic secondary organic aerosol, J. Geophys. Res. Atmospheres, 115(D9), D09202, doi:10.1029/2009JD013046, 2010.

Faulhaber, A. E., Thomas, B. M., Jimenez, J. L., Jayne, J. T., Worsnop, D. R. and Ziemann, P. J.: Characterization of a thermodenuder-particle beam mass spectrometer system for the study of organic aerosol volatility and composition, Atmospheric Meas. Tech., 2(1), 15–31, doi:10.5194/amt-2-15-2009, 2009.

Gantt, B., He, J., Zhang, X., Zhang, Y. and Nenes, A.: Incorporation of advanced aerosol activation treatments into CESM/CAM5: model evaluation and impacts on aerosol indirect effects, Atmos Chem Phys, 14(14), 7485–7497, doi:10.5194/acp-14-7485-2014, 2014.

Goldstein, A. H. and Galbally, I. E.: Known and Unexplored Organic Constituents in the Earth's Atmosphere, Environ. Sci. Technol., 41(5), 1514–1521, doi:10.1021/es072476p, 2007.

Goldstein, A. H., Koven, C. D., Heald, C. L. and Fung, I. Y.: Biogenic carbon and anthropogenic pollutants combine to form a cooling haze over the southeastern United States, Proc. Natl. Acad. Sci., 106(22), 8835–8840, doi:10.1073/pnas.0904128106, 2009.

Grieshop, A. P., Donahue, N. M. and Robinson, A. L.: Is the gas-particle partitioning in alpha-pinene secondary organic aerosol reversible?, Geophys. Res. Lett., 34(14), L14810, doi:10.1029/2007GL029987, 2007.

Grieshop, A. P., Miracolo, M. A., Donahue, N. M. and Robinson, A. L.: Constraining the Volatility Distribution and Gas-Particle Partitioning of Combustion Aerosols Using Isothermal Dilution and Thermodenuder Measurements, Environ. Sci. Technol., 43(13), 4750–4756, doi:10.1021/es8032378, 2009.

Guenther, A. B., Jiang, X., Heald, C. L., Sakulyanontvittaya, T., Duhl, T., Emmons, L. K. and Wang, X.: The Model of Emissions of Gases and Aerosols from Nature version 2.1 (MEGAN2.1): an extended and updated framework for modeling biogenic emissions, Geosci Model Dev, 5(6), 1471–1492, doi:10.5194/gmd-5-1471-2012, 2012.

Häkkinen, S. A. K., Äijälä, M., Lehtipalo, K., Junninen, H., Backman, J., Virkkula, A., Nieminen, T., Vestenius, M., Hakola, H., Ehn, M., Worsnop, D. R., Kulmala, M., Petäjä, T. and Riipinen, I.: Long-term volatility measurements of submicron atmospheric aerosol in Hyytiälä, Finland, Atmos Chem Phys, 12(22), 10771–10786, doi:10.5194/acp-12-10771-2012, 2012.

Hallquist, M., Wenger, J. C., Baltensperger, U., Rudich, Y., Simpson, D., Claeys, M., Dommen, J., Donahue, N. M., George, C., Goldstein, A. H., Hamilton, J. F., Herrmann, H., Hoffmann, T., Iinuma, Y., Jang, M., Jenkin, M. E., Jimenez, J. L., Kiendler-Scharr, A., Maenhaut, W., McFiggans, G., Mentel, T. F., Monod, A., Prévôt, A. S. H., Seinfeld, J. H., Surratt, J. D., Szmigielski, R. and Wildt, J.: The formation, properties and impact of secondary organic aerosol: current and emerging issues, Atmos Chem Phys, 9(14), 5155–5236, doi:10.5194/acp-9-5155-2009, 2009.

He, J. and Zhang, Y.: Improvement and further development in CESM/CAM5: gas-phase chemistry and inorganic aerosol treatments, Atmos Chem Phys, 14(17), 9171–9200, doi:10.5194/acp-14-9171-2014, 2014.

Hennigan, C. J., Bergin, M. H., Russell, A. G., Nenes, A. and Weber, R. J.: Gas/particle partitioning of water-soluble organic aerosol in Atlanta, Atmos Chem Phys, 9(11), 3613–3628, doi:10.5194/acp-9-3613-2009, 2009.

Hu, W., Palm, B. B., Day, D. A., Campuzano-Jost, P., Krechmer, J. E., Peng, Z., de Sá, S. S., Martin, S. T., Alexander, M. L., Baumann, K., Hacker, L., Kiendler-Scharr, A., Koss, A. R., de Gouw, J. A., Goldstein, A. H., Seco, R., Sjostedt, S. J., Park, J.-H., Guenther, A. B., Kim, S., Canonaco, F., Prévôt, A. S. H., Brune, W. H. and Jimenez, J. L.: Volatility and lifetime against OH heterogeneous reaction of ambient Isoprene Epoxydiols-Derived Secondary Organic Aerosol (IEPOX-SOA), Atmospheric Chem. Phys. Discuss., 1–35, doi:10.5194/acp-2016-418, 2016.

Hu, W. W., Campuzano-Jost, P., Palm, B. B., Day, D. A., Ortega, A. M., Hayes, P. L., Krechmer, J. E., Chen, Q., Kuwata, M., Liu, Y. J., de Sá, S. S., McKinney, K., Martin, S. T., Hu, M., Budisulistiorini, S. H., Riva, M., Surratt, J. D., St. Clair, J. M., Isaacman-Van Wertz, G., Yee, L. D., Goldstein, A. H., Carbone, S., Brito, J., Artaxo, P., de Gouw, J. A., Koss, A., Wisthaler, A., Mikoviny, T., Karl, T., Kaser, L., Jud, W., Hansel, A., Docherty, K. S., Alexander, M. L., Robinson, N. H., Coe, H., Allan, J. D., Canagaratna, M. R., Paulot, F. and Jimenez, J. L.: Characterization of a real-time tracer for isoprene epoxydiols-derived secondary organic aerosol (IEPOX-SOA) from aerosol mass spectrometer measurements, Atmos Chem Phys, 15(20), 11807–11833, doi:10.5194/acp-15-11807-2015, 2015.

Huffman, J. A., Ziemann, P. J., Jayne, J. T., Worsnop, D. R. and Jimenez, J. L.: Development and Characterization of a Fast-Stepping/Scanning Thermodenuder for Chemically-Resolved Aerosol Volatility Measurements, Aerosol Sci. Technol., 42(5), 395–407, doi:10.1080/02786820802104981, 2008.

Huffman, J. A., Docherty, K. S., Aiken, A. C., Cubison, M. J., Ulbrich, I. M., DeCarlo, P. F., Sueper, D., Jayne, J. T., Worsnop, D. R., Ziemann, P. J. and Jimenez, J. L.: Chemically-resolved aerosol volatility measurements from two megacity field studies, Atmos Chem Phys, 9(18), 7161–7182, doi:10.5194/acp-9-7161-2009, 2009.

Jimenez, J. L., Canagaratna, M. R., Donahue, N. M., Prevot, A. S. H., Zhang, Q., Kroll, J. H., DeCarlo, P. F., Allan, J. D., Coe, H., Ng, N. L., Aiken, A. C., Docherty, K. S., Ulbrich, I. M., Grieshop, A. P., Robinson, A. L., Duplissy, J., Smith, J. D., Wilson, K. R., Lanz, V. A., Hueglin, C., Sun, Y. L., Tian, J., Laaksonen, A., Raatikainen, T., Rautiainen, J., Vaattovaara, P., Ehn, M., Kulmala, M., Tomlinson, J. M., Collins, D. R., Cubison, M. J., Dunlea, J., Huffman, J. A., Onasch, T. B., Alfarra, M. R., Williams, P. I., Bower, K., Kondo, Y., Schneider, J., Drewnick, F., Borrmann, S., Weimer, S., Demerjian, K., Salcedo, D., Cottrell, L., Griffin, R., Takami, A., Miyoshi, T., Hatakeyama, S., Shimono, A., Sun, J. Y., Zhang, Y. M., Dzepina, K., Kimmel, J. R., Sueper, D., Jayne, J. T., Herndon, S. C., Trimborn, A. M., Williams, L. R., Wood, E. C., Middlebrook, A. M., Kolb, C. E., Baltensperger, U. and Worsnop, D. R.: Evolution of Organic Aerosols in the Atmosphere, Science, 326(5959), 1525–1529, doi:10.1126/science.1180353, 2009.

Jokinen, T., Berndt, T., Makkonen, R., Kerminen, V.-M., Junninen, H., Paasonen, P., Stratmann, F., Herrmann, H., Guenther, A. B., Worsnop, D. R., Kulmala, M., Ehn, M. and Sipilä, M.: Production of extremely low volatile organic compounds from biogenic emissions: Measured yields and atmospheric implications, Proc. Natl. Acad. Sci., 112(23), 7123–7128, doi:10.1073/pnas.1423977112, 2015.

Kokkola, H., Yli-Pirilä, P., Vesterinen, M., Korhonen, H., Keskinen, H., Romakkaniemi, S., Hao, L., Kortelainen, A., Joutsensaari, J., Worsnop, D. R., Virtanen, A. and Lehtinen, K. E. J.: The role of low volatile organics on secondary organic aerosol formation, Atmos Chem Phys, 14(3), 1689–1700, doi:10.5194/acp-14-1689-2014, 2014.

Kolesar, K. R., Li, Z., Wilson, K. R. and Cappa, C. D.: Heating-Induced Evaporation of Nine Different Secondary Organic Aerosol Types, Environ. Sci. Technol., 49(20), 12242–12252, doi:10.1021/acs.est.5b03038, 2015a.

Kolesar, K. R., Chen, C., Johnson, D. and Cappa, C. D.: The influences of mass loading and rapid dilution of secondary organic aerosol on particle volatility, Atmos Chem Phys, 15(16), 9327–9343, doi:10.5194/acp-15-9327-2015, 2015b.

Kroll, J. H. and Seinfeld, J. H.: Chemistry of secondary organic aerosol: Formation and evolution of low-volatility organics in the atmosphere, Atmos. Environ., 42(16), 3593–3624, doi:10.1016/j.atmosenv.2008.01.003, 2008.

Kroll, J. H., Donahue, N. M., Jimenez, J. L., Kessler, S. H., Canagaratna, M. R., Wilson, K. R., Altieri, K. E., Mazzoleni, L. R., Wozniak, A. S., Bluhm, H., Mysak, E. R., Smith, J. D., Kolb, C. E. and Worsnop, D. R.: Carbon oxidation state as a metric for describing the chemistry of atmospheric organic aerosol, Nat. Chem., 3(2), 133–139, doi:10.1038/nchem.948, 2011.

Kroll, J. H., Lim, C. Y., Kessler, S. H. and Wilson, K. R.: Heterogeneous Oxidation of Atmospheric Organic Aerosol: Kinetics of Changes to the Amount and Oxidation State of Particle-Phase Organic Carbon, J. Phys. Chem. A, 119(44), 10767–10783, doi:10.1021/acs.jpca.5b06946, 2015.

Lane, T. E., Donahue, N. M. and Pandis, S. N.: Effect of NOx on Secondary Organic Aerosol Concentrations, Environ. Sci. Technol., 42(16), 6022–6027, doi:10.1021/es703225a, 2008a.

Lane, T. E., Donahue, N. M. and Pandis, S. N.: Simulating secondary organic aerosol formation using the volatility basis-set approach in a chemical transport model, Atmos. Environ., 42(32), 7439–7451, doi:10.1016/j.atmosenv.2008.06.026, 2008b.

Lappalainen, H. K., Sevanto, S., Bäck, J., Ruuskanen, T. M., Kolari, P., Taipale, R., Rinne, J., Kulmala, M. and Hari, P.: Day-time concentrations of biogenic volatile organic compounds in a boreal forest canopy and their relation to environmental and biological factors, Atmos Chem Phys, 9(15), 5447–5459, doi:10.5194/acp-9-5447-2009, 2009.

Lee, B. H., Kostenidou, E., Hildebrandt, L., Riipinen, I., Engelhart, G. J., Mohr, C., DeCarlo, P. F., Mihalopoulos, N., Prevot, A. S. H., Baltensperger, U. and Pandis, S. N.: Measurement of the ambient organic aerosol volatility distribution: application during the Finokalia Aerosol Measurement Experiment (FAME-2008), Atmos Chem Phys, 10(24), 12149–12160, doi:10.5194/acp-10-12149-2010, 2010.

Lee, B.-H., Pierce, J. R., Engelhart, G. J. and Pandis, S. N.: Volatility of secondary organic aerosol from the ozonolysis of monoterpenes, Atmos. Environ., 45(14), 2443–2452, doi:10.1016/j.atmosenv.2011.02.004, 2011.

Lehtinen, K., Korhonen, H., Maso, M. D. and Kulmala, M.: On the concept of condensation sink diameter, Boreal Env. Res, 8, 405–411, 2003.

Liao, H., Henze, D. K., Seinfeld, J. H., Wu, S. and Mickley, L. J.: Biogenic secondary organic aerosol over the United States: Comparison of climatological simulations with observations, J. Geophys. Res. Atmospheres, 112(D6), D06201, doi:10.1029/2006JD007813, 2007.

Lopez-Hilfiker, F. D., Mohr, C., D'Ambro, E. L., Lutz, A., Riedel, T. P., Gaston, C. J., Iyer, S., Zhang, Z., Gold, A., Surratt, J. D., Lee, B. H., Kurten, T., Hu, W. W., Jimenez, J., Hallquist, M. and Thornton, J. A.: Molecular Composition and Volatility of Organic Aerosol in the Southeastern U.S.: Implications for IEPOX Derived SOA, Environ. Sci. Technol., 50(5), 2200–2209, doi:10.1021/acs.est.5b04769, 2016.

Marais, E. A., Jacob, D. J., Jimenez, J. L., Campuzano-Jost, P., Day, D. A., Hu, W., Krechmer, J., Zhu, L., Kim, P. S., Miller, C. C., Fisher, J. A., Travis, K., Yu, K., Hanisco, T. F., Wolfe, G. M., Arkinson, H. L., Pye, H. O. T., Froyd, K. D., Liao, J. and McNeill, V. F.: Aqueous-phase mechanism for secondary organic aerosol formation from isoprene: application to the southeast United States and co-benefit of SO2 emission controls, Atmos Chem Phys, 16(3), 1603–1618, doi:10.5194/acp-16-1603-2016, 2016.

Matsui, H., Koike, M., Kondo, Y., Takami, A., Fast, J. D., Kanaya, Y. and Takigawa, M.: Volatility basis-set approach simulation of organic aerosol formation in East Asia: implications for anthropogenic–biogenic interaction and controllable amounts, Atmos Chem Phys, 14(18), 9513–9535, doi:10.5194/acp-14-9513-2014, 2014.

May, A. A., Levin, E. J. T., Hennigan, C. J., Riipinen, I., Lee, T., Collett, J. L., Jimenez, J. L., Kreidenweis, S. M. and Robinson, A. L.: Gas-particle partitioning of primary organic aerosol emissions: 3. Biomass burning, J. Geophys. Res. Atmospheres, 118(19), 2013JD020286, doi:10.1002/jgrd.50828, 2013.

Murphy, B. N., Donahue, N. M., Fountoukis, C. and Pandis, S. N.: Simulating the oxygen content of ambient organic aerosol with the 2D volatility basis set, Atmos Chem Phys, 11(15), 7859–7873, doi:10.5194/acp-11-7859-2011, 2011.

Ng, N. L., Chhabra, P. S., Chan, A. W. H., Surratt, J. D., Kroll, J. H., Kwan, A. J., McCabe, D. C., Wennberg, P. O., Sorooshian, A., Murphy, S. M., Dalleska, N. F., Flagan, R. C. and Seinfeld, J. H.: Effect of NOx level on secondary organic aerosol

(SOA) formation from the photooxidation of terpenes, Atmos Chem Phys, 7(19), 5159–5174, doi:10.5194/acp-7-5159-2007, 2007.

Ng, N. L., Herndon, S. C., Trimborn, A., Canagaratna, M. R., Croteau, P. L., Onasch, T. B., Sueper, D., Worsnop, D. R., Zhang, Q., Sun, Y. L. and Jayne, J. T.: An Aerosol Chemical Speciation Monitor (ACSM) for Routine Monitoring of the Composition and Mass Concentrations of Ambient Aerosol, Aerosol Sci. Technol., 45(7), 780–794, doi:10.1080/02786826.2011.560211, 2011a.

Ng, N. L., Canagaratna, M. R., Jimenez, J. L., Zhang, Q., Ulbrich, I. M. and Worsnop, D. R.: Real-Time Methods for Estimating Organic Component Mass Concentrations from Aerosol Mass Spectrometer Data, Environ. Sci. Technol., 45(3), 910–916, doi:10.1021/es102951k, 2011b.

Offenberg, J. H., Kleindienst, T. E., Jaoui, M., Lewandowski, M. and Edney, E. O.: Thermal properties of secondary organic aerosols, Geophys. Res. Lett., 33(3), L03816, doi:10.1029/2005GL024623, 2006.

Paciga, A., Karnezi, E., Kostenidou, E., Hildebrandt, L., Psichoudaki, M., Engelhart, G. J., Lee, B.-H., Crippa, M., Prévôt, A. S. H., Baltensperger, U. and Pandis, S. N.: Volatility of organic aerosol and its components in the Megacity of Paris, Atmos Chem Phys Discuss, 15(16), 22263–22289, doi:10.5194/acpd-15-22263-2015, 2015.

Pankow, J. F.: An absorption model of gas/particle partitioning of organic compounds in the atmosphere, Atmos. Environ., 28(2), 185–188, doi:10.1016/1352-2310(94)90093-0, 1994.

Pathak, R. K., Presto, A. A., Lane, T. E., Stanier, C. O., Donahue, N. M. and Pandis, S. N.: Ozonolysis of α-pinene: parameterization of secondary organic aerosol mass fraction, Atmos Chem Phys, 7(14), 3811–3821, doi:10.5194/acp-7-3811-2007, 2007.

Pouliot, G., Denier van der Gon, H. A. C., Kuenen, J., Zhang, J., Moran, M. D. and Makar, P. A.: Analysis of the emission inventories and model-ready emission datasets of Europe and North America for phase 2 of the AQMEII project, Atmos. Environ., 115, 345–360, doi:10.1016/j.atmosenv.2014.10.061, 2015.

Presto, A. A., Huff Hartz, K. E. and Donahue, N. M.: Secondary Organic Aerosol Production from Terpene Ozonolysis. 2. Effect of NOx Concentration, Environ. Sci. Technol., 39(18), 7046–7054, doi:10.1021/es050400s, 2005.

Pye, H. O. T. and Seinfeld, J. H.: A global perspective on aerosol from low-volatility organic compounds, Atmos Chem Phys, 10(9), 4377–4401, doi:10.5194/acp-10-4377-2010, 2010.

Pye, H. O. T., Luecken, D. J., Xu, L., Boyd, C. M., Ng, N. L., Baker, K. R., Ayres, B. R., Bash, J. O., Baumann, K., Carter, W. P. L., Edgerton, E., Fry, J. L., Hutzell, W. T., Schwede, D. B. and Shepson, P. B.: Modeling the Current and Future Roles of Particulate Organic Nitrates in the Southeastern United States, Environ. Sci. Technol., 49(24), 14195–14203, doi:10.1021/acs.est.5b03738, 2015.

Ranjan, M., Presto, A. A., May, A. A. and Robinson, A. L.: Temperature Dependence of Gas–Particle Partitioning of Primary Organic Aerosol Emissions from a Small Diesel Engine, Aerosol Sci. Technol., 46(1), 13–21, doi:10.1080/02786826.2011.602761, 2012.

Riipinen, I., Pierce, J. R., Donahue, N. M. and Pandis, S. N.: Equilibration time scales of organic aerosol inside thermodenuders: Evaporation kinetics versus thermodynamics, Atmos. Environ., 44(5), 597–607, doi:10.1016/j.atmosenv.2009.11.022, 2010.

Saha, P. K. and Grieshop, A. P.: Exploring divergent volatility properties from yield and thermodenuder measurements of secondary organic aerosol from α-pinene ozonolysis, Environ. Sci. Technol., doi:10.1021/acs.est.6b00303, 2016.

Saha, P. K., Khlystov, A. and Grieshop, A. P.: Determining Aerosol Volatility Parameters Using a "Dual Thermodenuder" System: Application to Laboratory-Generated Organic Aerosols, Aerosol Sci. Technol., 49(8), 620–632, doi:10.1080/02786826.2015.1056769, 2015.

Saleh, R., Shihadeh, A. and Khlystov, A.: On transport phenomena and equilibration time scales in thermodenuders, Atmos Meas Tech, 4(3), 571–581, doi:10.5194/amt-4-571-2011, 2011.

Saleh, R., Khlystov, A. and Shihadeh, A.: Determination of Evaporation Coefficients of Ambient and Laboratory-Generated Semivolatile Organic Aerosols from Phase Equilibration Kinetics in a Thermodenuder, Aerosol Sci. Technol., 46(1), 22–30, doi:10.1080/02786826.2011.602762, 2012.

Saleh, R., Donahue, N. M. and Robinson, A. L.: Time Scales for Gas-Particle Partitioning Equilibration of Secondary Organic Aerosol Formed from Alpha-Pinene Ozonolysis, Environ. Sci. Technol., 47(11), 5588–5594, doi:10.1021/es400078d, 2013.

Schichtel, B. A., Malm, W. C., Bench, G., Fallon, S., McDade, C. E., Chow, J. C. and Watson, J. G.: Fossil and contemporary fine particulate carbon fractions at 12 rural and urban sites in the United States, J. Geophys. Res. Atmospheres, 113(D2), D02311, doi:10.1029/2007JD008605, 2008.

Seinfeld, J. H. and Pankow, J. F.: Organic Atmospheric Particulate Material, Annu. Rev. Phys. Chem., 54(1), 121–140, doi:10.1146/annurev.physchem.54.011002.103756, 2003.

Shrivastava, M., Fast, J., Easter, R., Gustafson Jr., W. I., Zaveri, R. A., Jimenez, J. L., Saide, P. and Hodzic, A.: Modeling organic aerosols in a megacity: comparison of simple and complex representations of the volatility basis set approach, Atmos Chem Phys, 11(13), 6639–6662, doi:10.5194/acp-11-6639-2011, 2011.

Shrivastava, M., Zelenyuk, A., Imre, D., Easter, R., Beranek, J., Zaveri, R. A. and Fast, J.: Implications of low volatility SOA and gas-phase fragmentation reactions on SOA loadings and their spatial and temporal evolution in the atmosphere, J. Geophys. Res. Atmospheres, 118(8), 3328–3342, doi:10.1002/jgrd.50160, 2013.

Sindelarova, K., Granier, C., Bouarar, I., Guenther, A., Tilmes, S., Stavrakou, T., Müller, J.-F., Kuhn, U., Stefani, P. and Knorr, W.: Global data set of biogenic VOC emissions calculated by the MEGAN model over the last 30 years, Atmos Chem Phys, 14(17), 9317–9341, doi:10.5194/acp-14-9317-2014, 2014.

Stanier, C. O., Donahue, N. and Pandis, S. N.: Parameterization of secondary organic aerosol mass fractions from smog chamber data, Atmos. Environ., 42(10), 2276–2299, doi:10.1016/j.atmosenv.2007.12.042, 2008.

Tarvainen, V., Hakola, H., Hellén, H., Bäck, J., Hari, P. and Kulmala, M.: Temperature and light dependence of the VOC emissions of Scots pine, Atmos Chem Phys, 5(4), 989–998, doi:10.5194/acp-5-989-2005, 2005.

Vaden, T. D., Imre, D., Beránek, J., Shrivastava, M. and Zelenyuk, A.: Evaporation kinetics and phase of laboratory and ambient secondary organic aerosol, Proc. Natl. Acad. Sci., doi:10.1073/pnas.1013391108, 2011.

Wang, K., Zhang, Y., Yahya, K., Wu, S.-Y. and Grell, G.: Implementation and initial application of new chemistry-aerosol options in WRF/Chem for simulating secondary organic aerosols and aerosol indirect effects for regional air quality, Atmos. Environ., 115, 716–732, doi:10.1016/j.atmosenv.2014.12.007, 2015.

Warneke, C., de Gouw, J. A., Del Negro, L., Brioude, J., McKeen, S., Stark, H., Kuster, W. C., Goldan, P. D., Trainer, M., Fehsenfeld, F. C., Wiedinmyer, C., Guenther, A. B., Hansel, A., Wisthaler, A., Atlas, E., Holloway, J. S., Ryerson, T. B., Peischl, J., Huey, L. G. and Hanks, A. T. C.: Biogenic emission measurement and inventories determination of biogenic emissions in the eastern United States and Texas and comparison with biogenic emission inventories, J. Geophys. Res. Atmospheres, 115(D7), D00F18, doi:10.1029/2009JD012445, 2010.

Weber, R. J., Sullivan, A. P., Peltier, R. E., Russell, A., Yan, B., Zheng, M., de Gouw, J., Warneke, C., Brock, C., Holloway, J. S., Atlas, E. L. and Edgerton, E.: A study of secondary organic aerosol formation in the anthropogenic-influenced southeastern United States, J. Geophys. Res. Atmospheres, 112(D13), D13302, doi:10.1029/2007JD008408, 2007.

Wilson, J., Imre, D., Beránek, J., Shrivastava, M. and Zelenyuk, A.: Evaporation Kinetics of Laboratory-Generated Secondary Organic Aerosols at Elevated Relative Humidity, Environ. Sci. Technol., 49(1), 243–249, doi:10.1021/es505331d, 2015.

Xu, L., Suresh, S., Guo, H., Weber, R. J. and Ng, N. L.: Aerosol characterization over the southeastern United States using high-resolution aerosol mass spectrometry: spatial and seasonal variation of aerosol composition and sources with a focus on organic nitrates, Atmos Chem Phys, 15(13), 7307–7336, doi:10.5194/acp-15-7307-2015, 2015a.

Xu, L., Guo, H., Boyd, C. M., Klein, M., Bougiatioti, A., Cerully, K. M., Hite, J. R., Isaacman-VanWertz, G., Kreisberg, N. M., Knote, C., Olson, K., Koss, A., Goldstein, A. H., Hering, S. V., Gouw, J. de, Baumann, K., Lee, S.-H., Nenes, A., Weber, R. J. and Ng, N. L.: Effects of anthropogenic emissions on aerosol formation from isoprene and monoterpenes in the southeastern United States, Proc. Natl. Acad. Sci., 112(1), 37–42, doi:10.1073/pnas.1417609112, 2015b.

Xu, L., Williams, L. R., Young, D. E., Allan, J. D., Coe, H., Massoli, P., Fortner, E., Chhabra, P., Herndon, S., Brooks, W. A., Jayne, J. T., Worsnop, D. R., Aiken, A. C., Liu, S., Gorkowski, K., Dubey, M. K., Fleming, Z. L., Visser, S., Prévôt, A. S. H. and Ng, N. L.: Wintertime aerosol chemical composition, volatility, and spatial variability in the greater London area, Atmos Chem Phys, 16(2), 1139–1160, doi:10.5194/acp-16-1139-2016, 2016.

Yahya, K., Wang, K., Saha, P. K., Grieshop, A. P. and Zhang, Y.: Application and evaluation of WRF/Chem during the 2013 Southern Oxidant and Aerosol Study (SOAS), Prep., 2016a.

Yahya, K., Glotfelty, T., Wang, K., Zhang, Y. and Nenes, A.: Modeling Regional Air Quality and Climate: Improving Organic Aerosol and Aerosol Activation Processes in WRF/Chem, Prep., 2016b.

Yarwood, G., Jung, J., Whitten, G., Heo, G., Mellberg, J. and Estes, M.: Updates to the Carbon Bond Mechanism for Version 6 (CB6)." Presented at the 9th Annual CMAS Conference, Chapel Hill., 2010.

Zhang, Q., Jimenez, J. L., Canagaratna, M. R., Allan, J. D., Coe, H., Ulbrich, I., Alfarra, M. R., Takami, A., Middlebrook, A. M., Sun, Y. L., Dzepina, K., Dunlea, E., Docherty, K., DeCarlo, P. F., Salcedo, D., Onasch, T., Jayne, J. T., Miyoshi, T.,

Shimono, A., Hatakeyama, S., Takegawa, N., Kondo, Y., Schneider, J., Drewnick, F., Borrmann, S., Weimer, S., Demerjian, K., Williams, P., Bower, K., Bahreini, R., Cottrell, L., Griffin, R. J., Rautiainen, J., Sun, J. Y., Zhang, Y. M. and Worsnop, D. R.: Ubiquity and dominance of oxygenated species in organic aerosols in anthropogenically-influenced Northern Hemisphere midlatitudes, Geophys. Res. Lett., 34(13), L13801, doi:10.1029/2007GL029979, 2007.

Zhang, X., Cappa, C. D., Jathar, S. H., McVay, R. C., Ensberg, J. J., Kleeman, M. J. and Seinfeld, J. H.: Influence of vapor wall loss in laboratory chambers on yields of secondary organic aerosol, Proc. Natl. Acad. Sci., 111(16), 5802–5807, doi:10.1073/pnas.1404727111, 2014.

Zhang, X., McVay, R. C., Huang, D. D., Dalleska, N. F., Aumont, B., Flagan, R. C. and Seinfeld, J. H.: Formation and evolution of molecular products in α-pinene secondary organic aerosol, Proc. Natl. Acad. Sci., 201517742, doi:10.1073/pnas.1517742112, 2015.

Zobrist, B., Marcolli, C., Pedernera, D. A. and Koop, T.: Do atmospheric aerosols form glasses?, Atmos Chem Phys, 8(17), 5221–5244, doi:10.5194/acp-8-5221-2008, 2008.

Table 1: Best fit OA volatility parameter values extracted from this study along with several previous field and lab studies

Study	Centreville (this study)		Raleigh (this study)		FAME (Lee et al., 2010)		MILAGRO (Cappa and Jimenez, 2010)				AP-SOA (Saha and Grieshop, 2016)
Campaign average C_{OA} (µg m^{-3})	5.2		6.7		2.8		17				5
Note	a	b	a	b			c	d	c	d	e
γ_e	0.5	0.5	0.5	0.5	0.05	1	1	1	0.1	0.1	0.1
ΔH_{vap} (KJ mol^{-1})	100	100	100	100	80	80	100	100	100	100	[80,11][‡]
logC*(µg m^{-3})	f_i										
-6							0.06		0.04		
-5							0.06		0.04		
-4	0.14	0.18	0.14	0.16			0.06	0.27	0.04	0.21	0.03
-3	0.05	0.05	0.06	0.05		0.2	0.07	0.11	0.04	0.07	0.07
-2	0.06	0.08	0.08	0.13	0.2	0.2	0.07	0.11	0.05	0.09	0.03
-1	0.15	0.13	0.12	0.20	0.2	0.3	0.08	0.12	0.06	0.10	0.12
0	0.29	0.33	0.28	0.20	0.3	0.3	0.10	0.15	0.1	0.18	0.18
1	0.31	0.23	0.32	0.26	0.3		0.16	0.24	0.2	0.35	0.57
2							0.34		0.43		
Mean C* (µg m^{-3})	0.21	0.12	0.20	0.10	0.50	0.05	0.32	0.03	1.5	0.1	1.16
C^*_{eff} (µg m^{-3})	1.8	1.4	2.0	1.5	1.3	0.3	9.4	1.9	13.8	2.8	3.5

[a]Campaign average dual-TD data fit with campaign average C_{OA} and d_p.

[b] Unified fit of individual measurement from whole campaign (*MFR*, C_{OA}, *dp*; 20-30 minute resolution data).

[c] The f_i distribution derived from $C_{i,tot} = a_1+a_2\exp[a_3(\log(C^*)-3)]$; $f_i = C_{i,tot}/\Sigma C_{i,tot}$; a_1, a_2, and a_3 coefficients were taken from table 1 of Cappa and Jimenez (2010). $\log_{10}C^*$ bin ranged from -6 to +2, as in Cappa and Jimenez (2010).

[d] Same as c, but only considered $\log_{10}C^*$ bin range of -4 to +1 to be consistent with the bin ranges used in this study. To do so, materials in $\log_{10}C^* < -4$ bins are assigned to -4 bin, material at $\log_{10}C^* = 2$ bin is excluded, and distribution is renormalized to make $\Sigma f_i = 1$.

[e] Chamber generated SOA from low-C_{OA} α-pinene ozonolysis experiment applying renormalization approach described in note e to the distribution given in Saha and Grieshop (2016) SI, table S.5.

[‡] ΔH_{vap} (KJ mol^{-1}) = 80-11logC*(µg m^{-3})

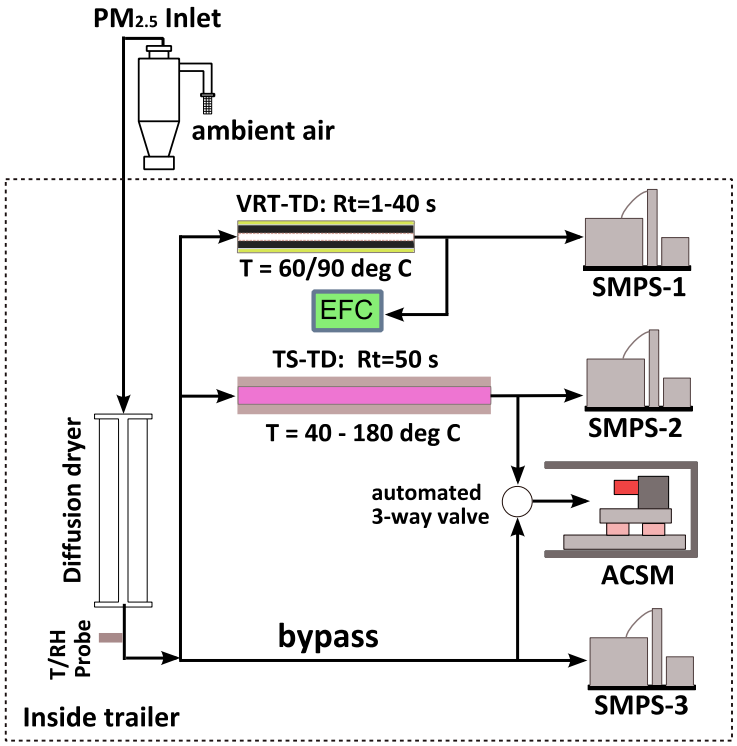

Figure 1: Dual thermodenuder aerosol volatility measurement setup used during field campaigns at two sites in the southeastern U.S. TS-TD: Temperature stepping TD, VRT-TD: Variable residence time TD, Rt: Residence time, EFC: Extra flow control, ACSM: Aerosol chemical speciation monitor, SMPS: Scanning mobility particle sizer.

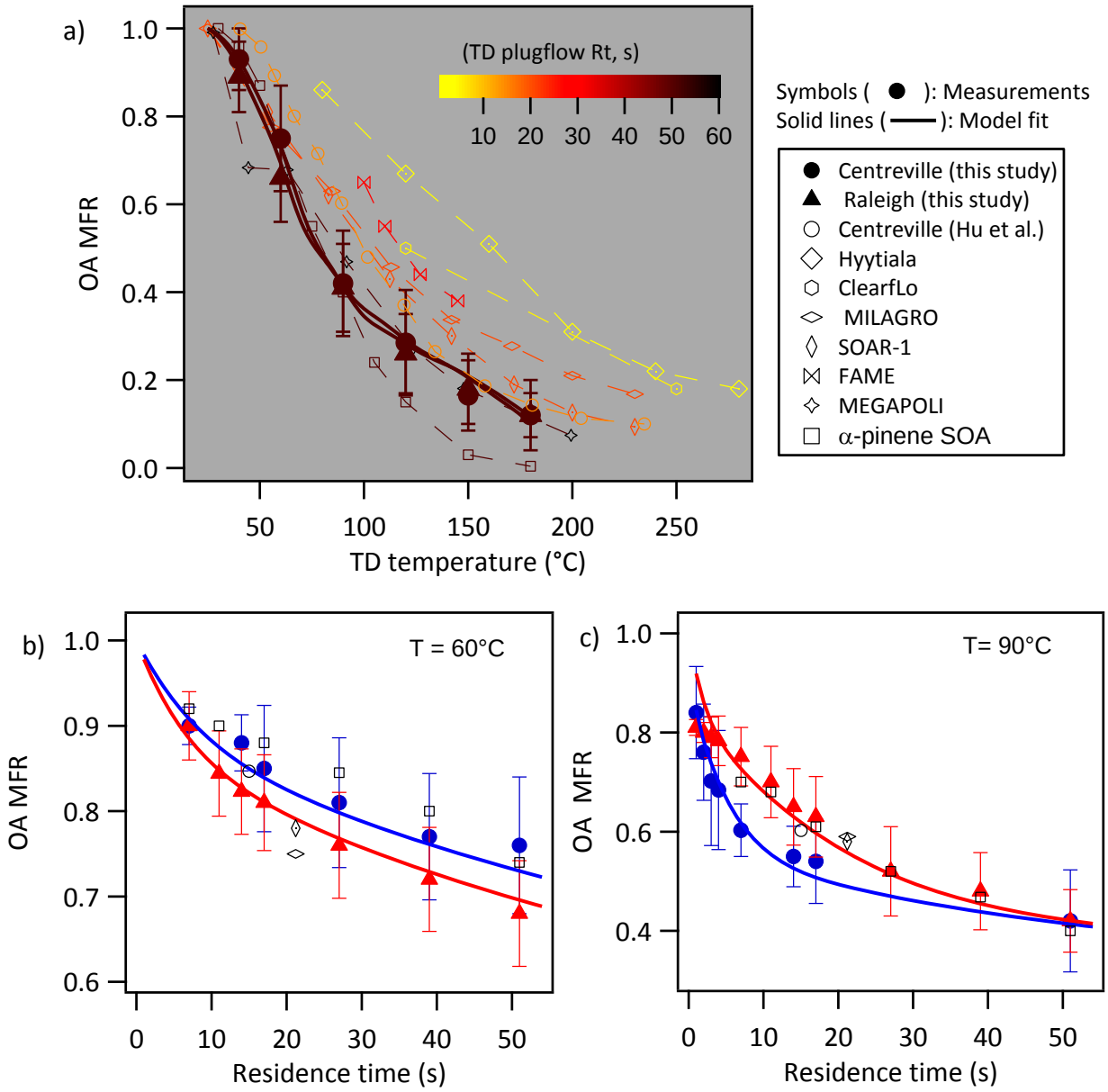

Figure 2: Measured (solid symbols) and modeled (solid thick lines) campaign average organic aerosol (OA) mass fraction remaining (MFR) as a function of TD temperatures (T) and residence times (Rt). The solid symbol shows mean value and error bar is ± one standard deviation of all campaign data at each (T, Rt) condition. Model lines are shown using the 'best fit' volatility parameter values from campaign average TD data fit (parameter values listed in Table 1). TD measurement data from the Centreville site collected by the University of Colorado group at SOAS-2013 (Hu et al., 2016) are also shown. Measurements from several previous field studies are shown with various open symbols: Hyytiala/2008-2010, Finland (Häkkinen et al., 2012); ClearfLo/2012, London (Xu et al., 2016); MILAGRO/2006, Mexico City (Huffman et al., 2009); SOAR-1/2005, Riverside, California (Huffman et al., 2009); FAME/2008, Finokalia, Greece (Lee et al., 2010); MEGAPOLI/2009-10, Paris, France (Paciga et al., 2015). Chamber alpha-pinene SOA (dark ozonolysis, COA ~ 5 µg m-3, VMD ~ 140 nm) evaporation data are shown from Saha and Grieshop (2016). In panel-a, data are color coded by TD residence times used during measurements. Legend shown next to panel (a) applies to all panels (a-c).

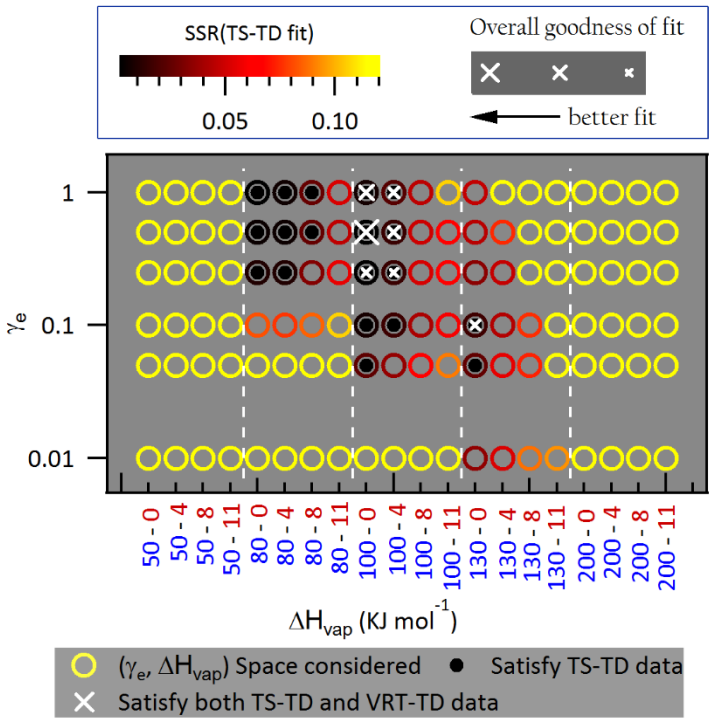

Figure 3: Extraction process of OA gas-particle partitioning parameter (ΔH_{vap}, γ_e and f_i) values**.** *A* f_i distribution was solved for each combination of (ΔH_{vap}, γ_e) via evaporation kinetic model fits to campaign-average dual-TD observations during the Centreville campaign. A relationship of ΔH_{vap} = intercept-slope ($\log_{10}C^*$ @ *298K*) was assumed (e.g., 50-0 on x-axis represents intercept =50 and slope = 0). Symbols and colors represent the goodness of fit. Points with filled inner circles recreate TS-TD observations and points with a white cross (x) recreate both TD data sets to within observational variability. Crosses represent the overall goodness of fit including both TS-TD and VRT-TD observations, with larger size corresponding to a better fit.

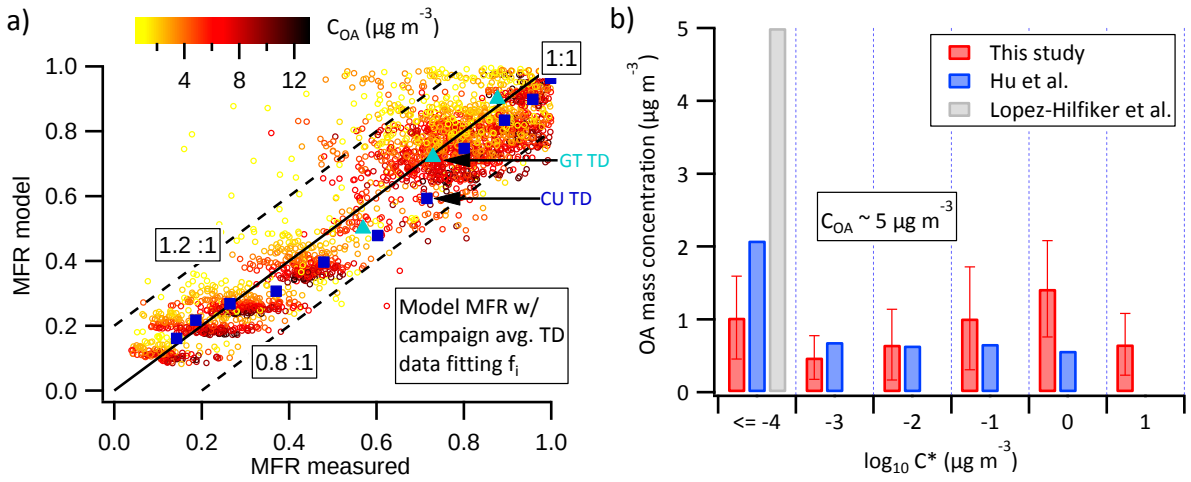

Figure 4: (a) Comparison of individual observations from the Centreville campaign and corresponding modeled MFRs applying the extracted f_i distribution from the campaign-average fit (r^2 = 0.83; RMSE: 0.11). MFR data collected by other groups during the Centreville campaign are also shown: University of Colorado TD (CU TD; blue squares) (Hu et al., 2016) and Georgia-Tech TD (GT TD; cyan triangles) (Cerully et al., 2015) along with corresponding MFRs modeled applying volatility parameterizations from this study with the campaign average C_{OA} and d_p. Fig. S9 shows an extended data figure of panel a, including similar plot using the f_i distribution from the unified fit and analysis results for the Raleigh data set. (b) Comparison of the SOAS campaign-average OA volatility distribution (showing only condensed phase) derived from this study (dual-TDs; kinetic evaporation model fits), Hu et al.(2016) (TD; method of Faulhaber et al.(2009)), and Lopez-Hilfiker et al.(2016) (FIGAERO-CIMS). Error bars on data from this study are ± one standard deviation of distributions extracted over the campaign period (Fig.6).

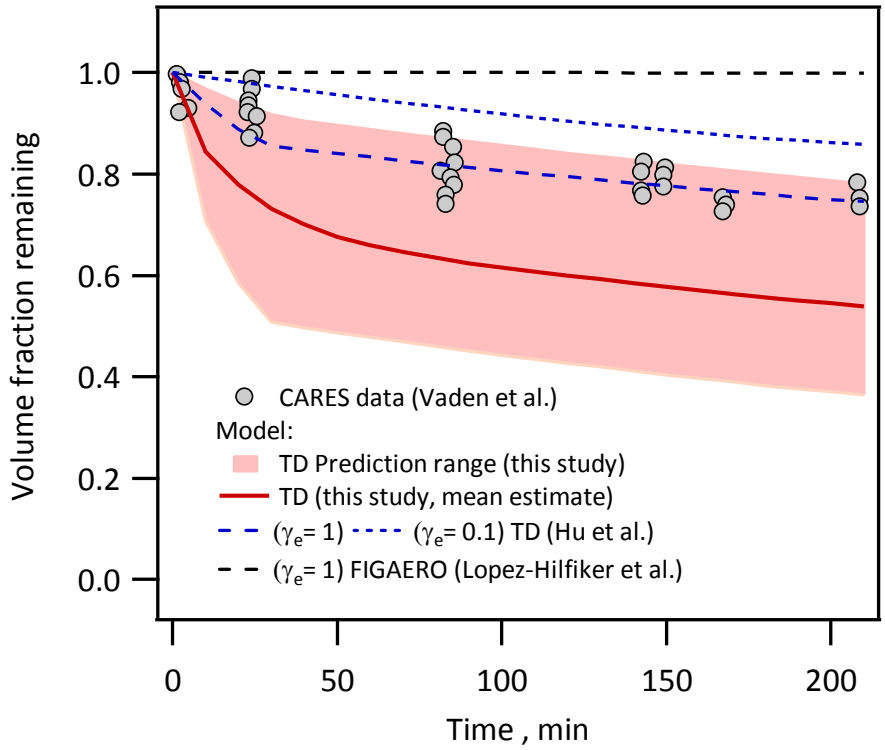

Figure 5: Isothermal evaporation kinetics of OA at 25˚C (room temperature) upon continuous stripping of vapors. Shaded region shows the evaporation kinetic model prediction range applying TD-derived volatility parameter values from this study; solid line shows the mean estimate. Dashed lines show model predictions using the OA volatility distribution derived using alternative approaches during the Centreville campaign (Hu et al., 2016; Lopez-Hilfiker et al., 2016). Symbols show experimental data from Vaden et al. (2011) collected during the CARES-2010 field campaign in California.

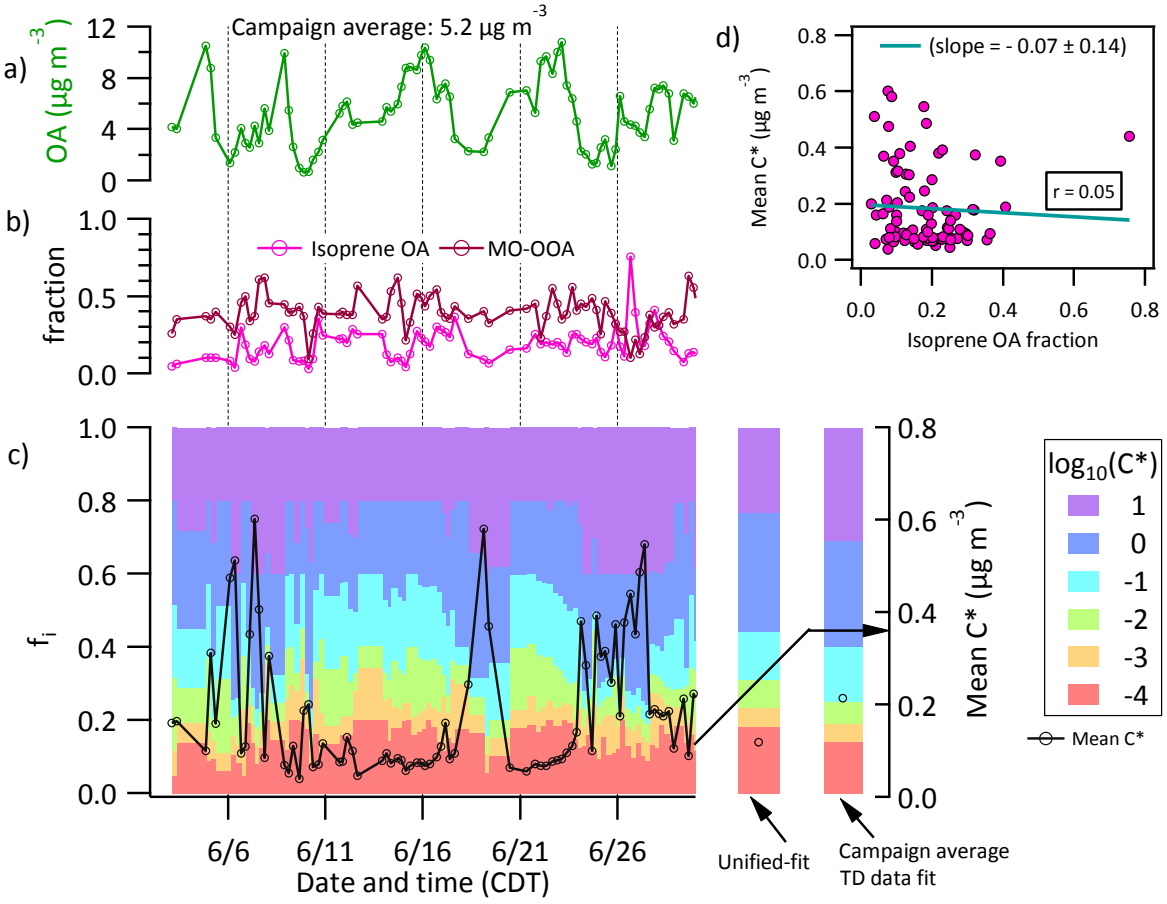

Figure 6: Time series of (a) ambient organic aerosol concentrations; C_{OA}, (b) fractional contribution of isoprene OA and more-oxidized oxygenated OA (MO-OOA) to total OA determined from PMF analysis, and (c) OA volatility distribution (f_i) and mean C* (open black circles) during the Centreville campaign. All data are averaged over ~ 6 hours (the time resolution of f_i distribution). Panel (d) shows a scatter plot of mean C* verses isoprene-OA fraction in C_{OA}. Fig. S10 shows similar analysis results for the Raleigh data set.

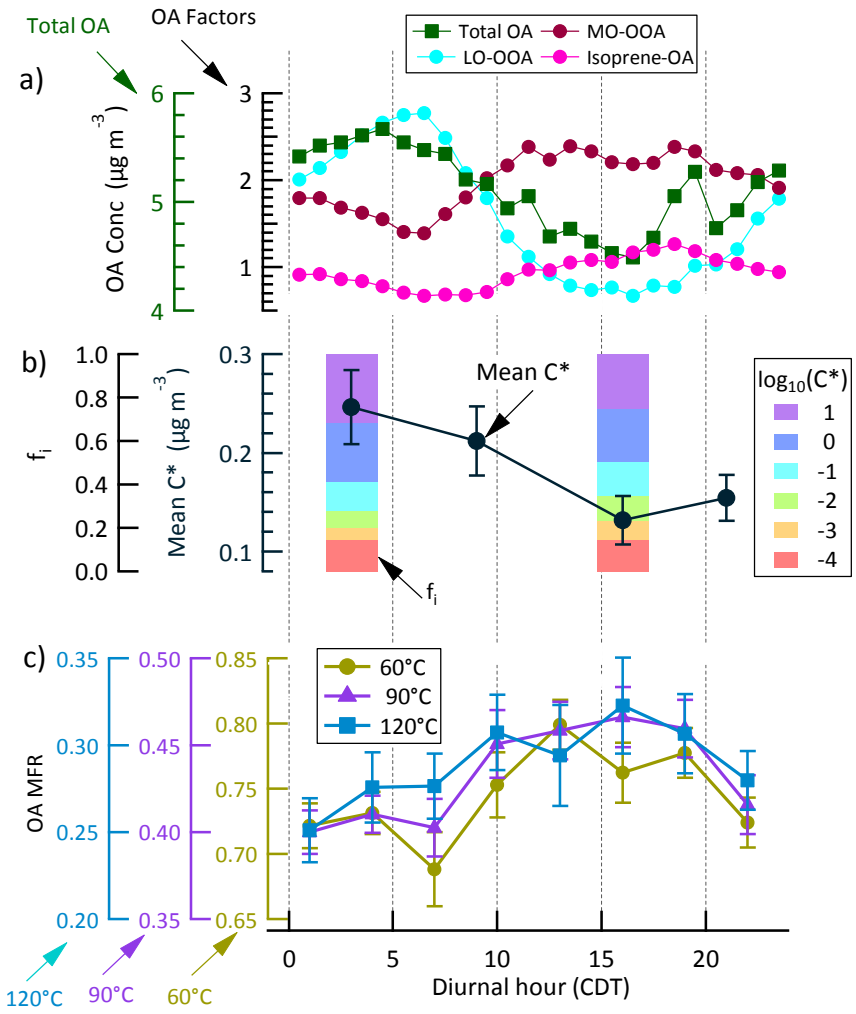

Figure 7: Campaign average diurnal trends for the Centreville measurements of: (a) concentrations of total OA and OA factors, (b) OA volatility (f_i and mean C*) (c) OA MFR after heating at 60, 90 and 120 ˚C with a TD residence time of 50 s. Fig. S11 shows similar analysis results for the Raleigh data set. PMF factors in panel-a are LO-OOA: less-oxidized oxygenated OA; MO-OOA: more-oxidized oxygenated OA; Isoprene-OA: isoprene-derived OA (for details on OA factors analysis see Xu et al., 2015a, 2015b).

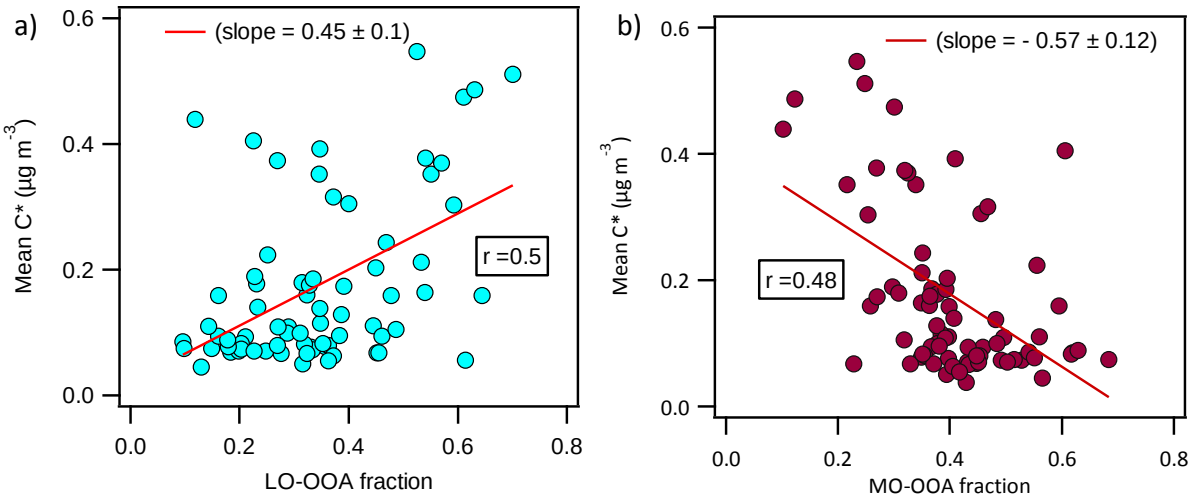

Figure 8: Scatter plot of mean C* verses (a) LO-OOA fraction, and (b) MO-OOA fraction in total OA concentration during the Centreville campaign.

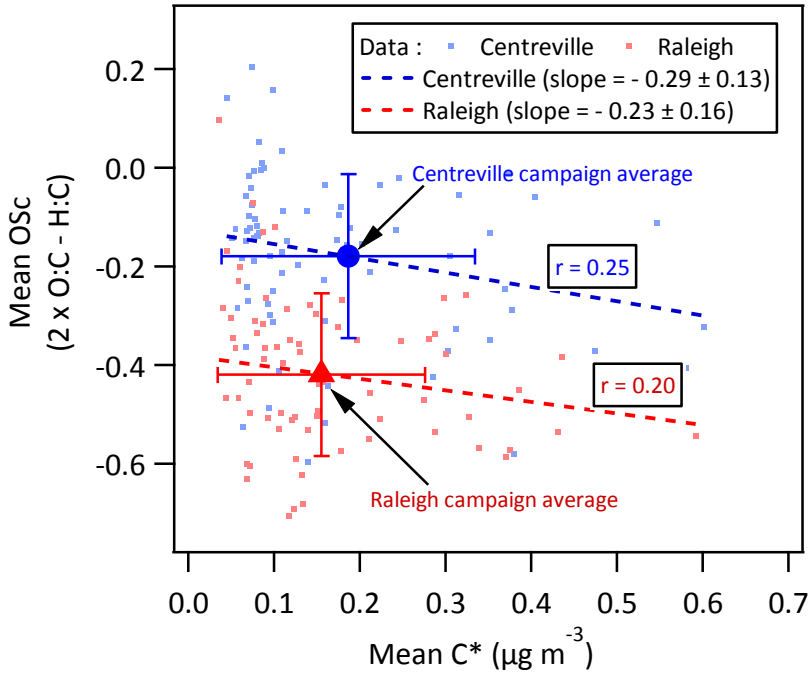

Figure 9: Mean oxidation state ($\overline{OS_c}$) versus mean volatility($\overline{C^*}$) measured during the Centreville and Raleigh campaigns. Dots are campaign data, dashed lines are linear regression fits of data, and symbols are the campaign average with error bar showing ±one standard deviation.

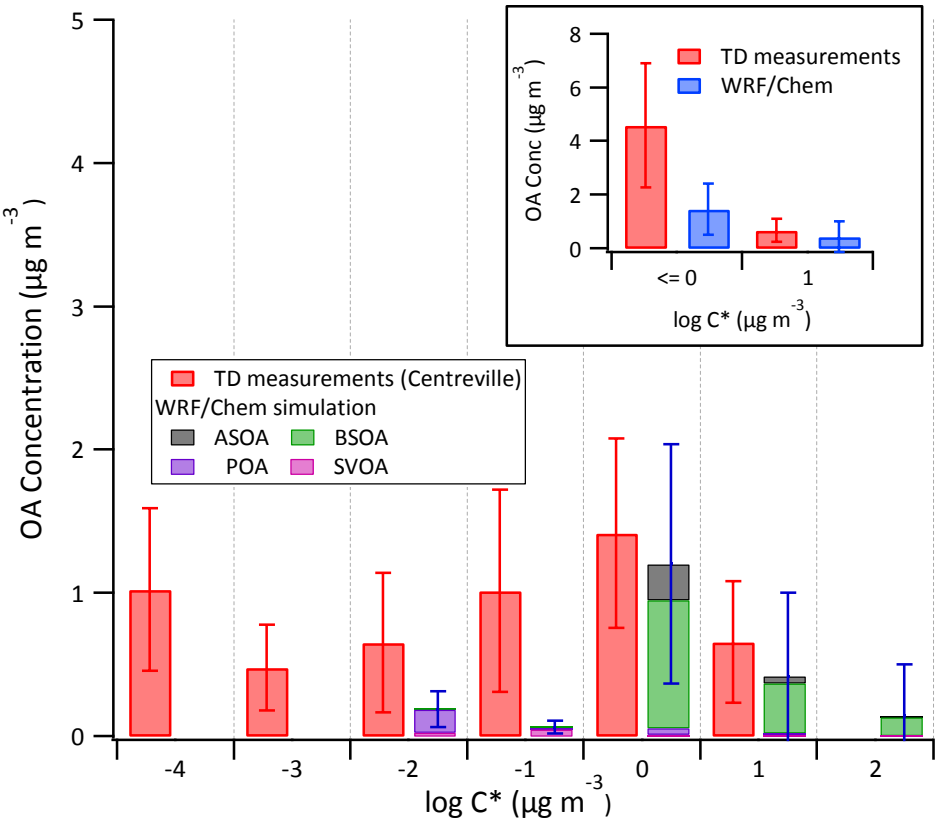

Figure 10: Comparison between measured OA volatility distributions and those simulated in WRF/Chem over the Centerville region. Bar height is mean, and error bar is ± one standard deviation of distributions extracted from measurements and simulations for June 2013. The inset shows a two-bin comparison (bin-1: C*≤1 µg m^{-3} and bin-2: C*=10 µg m^{-3}). Simulated OA components include ASOA (anthropogenic-SOA), BSOA (biogenic-SOA), POA (primary-OA), and SVOA (semi-volatile OA/oxidized POA).

Supplementary Information (SI) of
Quantifying the volatility of organic aerosol in the southeastern U.S.

Provat K. Saha[1], Andrey Khlystov[2], KhairunnisaYahya[3], Yang Zhang[3], Lu Xu[4], Nga L. Ng[4,5] , and Andrew P. Grieshop[1]

[1]Department of Civil, Construction and Environmental Engineering, North Carolina State University, Raleigh, NC, USA
[2]Division of Atmospheric Sciences, Desert Research Institute, Reno, Nevada, USA
[3]Department of Marine Earth and Atmospheric Sciences, North Carolina State University, Raleigh, NC, USA
[4]School of Chemical and Biomolecular Engineering, Georgia Institute of Technology, Atlanta, GA, USA
[5]School of Earth and Atmospheric Sciences, Georgia Institute of Technology, Atlanta, GA, USA

Correspondence to: Andrew P. Grieshop (apgriesh@ncsu.edu)

S1. Estimation of approximate equivalent OA MFR for VRT-TD/SMPS data

We assumed that measured total volume of submicron aerosol (V_{tot}) by SMPS (10-600 nm) is comprised of the volume of organic (V_{org}) and ammonium sulfate (V_{as}). Since the sample was sufficiently dried (RH < 30-40%) before traveling to instruments, the contribution of water to V_{tot} was neglected. Contributions of nitrate and chloride aerosol were also neglected.

$$V_{tot} = V_{org} + V_{as} \tag{S-1}$$

Apply the mass-volume relationship, the mass of organic aerosol (m_{org}) can be written as

$$m_{org} = \left(V_{tot} - \frac{m_{as}}{\rho_{as}} \right) \rho_{org} \tag{S-2}$$

Where, ρ_{org} and ρ_{as} are the densities of organic aerosol and ammonium sulfate aerosol, respectively.

Organic aerosol mass fraction remaining (OA MFR) at a TD temperature and residence time (T, Rt) is

$$MFR_{org}\ (T,\ \mathrm{Rt}) = \frac{m_{org,\ TD\ (T,Rt)}}{m_{org,\ BP}} \tag{S-3}$$

Where, 'TD' refers to thermodenuder and 'BP' for bypass.

Replacing m_{org} in Eq.S3 with Eq. S2

$$MFR_{org}(T,\ \mathrm{Rt}) = \frac{\left(V_{tot,\ TD(T,\ \mathrm{Rt})} - \frac{m_{as,\ TD(T,Rt)}}{\rho_{as}} \right) \rho_{org,\ TD(T,Rt)}}{\left(V_{tot,\ BP} - \frac{m_{as,\ BP}}{\rho_{as}} \right) \rho_{org,\ BP}} \tag{S-4}$$

Here, V_{tot} is in $\mu m^3\ cm^{-3}$ and mass of ammonium sulfate (m_{as}) is in $\mu g\ m^{-3}$. ρ_{as} is considered 1.77 gm cm^{-3}. Change in ρ_{org} after heating at moderate temperature (<100˚C) is assumed to be small ($\rho_{org,BP} \sim \rho_{org,TD}$). It is assumed that ammonium sulfate did

not evaporate at a TD temperature < 100˚C ($m_{as,BP} \sim m_{as,TD}$). Note, in MFR calculation, particle loss in TD due to diffusional and inertial and thermophoresis deposition were applied separately via empirically estimated correction factors as a function of temperature and residence time (Saha et al., 2015). Relative transmission of V_{tot} and different aerosol species (e.g., organic, sulfate, nitrate, and ammonium) are assumed to be the same.

To estimate mass of ammonium sulfate mass (m_{as}), we assumed a stoichiometric relationship between sulfate and ammonium. Therefore, m_{as} is calculated as $\frac{132}{96} \times m_{SO4}$; $\sim 1.375 \times m_{SO4}$.

$$MFR_{org}(T, Rt) = \frac{\left(V_{tot,\,TD\,(T,\,Rt)} - \frac{1.375 \times m_{SO_4,\,BP}}{\rho_{as}}\right)}{\left(V_{tot,\,BP} - \frac{1.375 \times m_{SO_4,\,BP)}}{\rho_{as}}\right)} \quad \text{(S-5)}$$

Eq.S-5 was applied to estimate an approximate OA MFR for VRT-TD data at 60 ˚C and 90˚C, where $m_{SO4,\,BP}$ is used from ACSM measurements.

In Eq. S-5, contribution of ammonium nitrate (AN) aerosol to V_{tot} is neglected, which has a relatively minor influence on the estimated OA MFR at both of our measurement sites. This is because the overall contribution of AN in PM_1 was small (Fig. S6). The observed evaporation of ambient AN aerosol is much less than the laboratory generated pure AN aerosol (Huffman et al., 2009) and its observed evaporation is quite similar to the OA evaporation (Fig. S2). Since evaporation of AN under VRT-TD operating conditions would be a function of temperature and residence time, an exclusion of contribution of AN from V_{tot} is not as straightforward as for AS. However, we explore the overall influences of AN on the estimated OA MFR by examining an extreme case. In this analysis, we considered the Raleigh data set, where relatively more NO_3 contribution in PM_1 was measured (Fig. S6, S7) and the highest operating Rt of VRT-TD (40 s), where maximum bias is expected. Estimated OA MFR using Eq. S-5 (neglecting AN contribution) at 60 ˚C and Rt = 40 s was 0.72 ± 0.06 (base case). In a sensitivity case, we included the contribution of AN ($V_{tot}= V_{org}+V_{as}+V_{an}$) and assumed that evaporation of NO_3 measured in TS-TD (60˚C, Rt = 50 s) is same in VRT-TD for the above condition. The estimated mean OA MFR from sensitivity case was 0.735, which is within ~ 2% of our base case estimation and falls well within the variability range. At 90 ˚C and Rt = 40 s, estimated mean OA MFR in sensitivity case was 0.498 versus 0.48 ± 0.078 in base case, which is within 4 %.

S2. Estimation of condensation sink diameter (d_{cs})

The condensation sink diameter is estimated following Lehtinen et al., 2003. The condensation sink diameter is the diameter where a monodisperse population of particles of number concentration N_{tot} can be placed to obtain the same total condensation sink (CS) as for a poly-disperse distribution of particles with total number concentration N_{tot} (Lehtinen et al., 2003).

Mathematically, $2\pi D d_{cs} F(d_{cs}) N_{tot} = 2\pi D \sum F(d_{p,i}) d_{p,i} N_i = CS$ (S-6)

Where, D is the diffusion coefficient, F is the Fuchs and Sutugin correction factor, N_i is the number concentration of particles in size bin of $d_{p,i}$

S3. Supplementary Figures

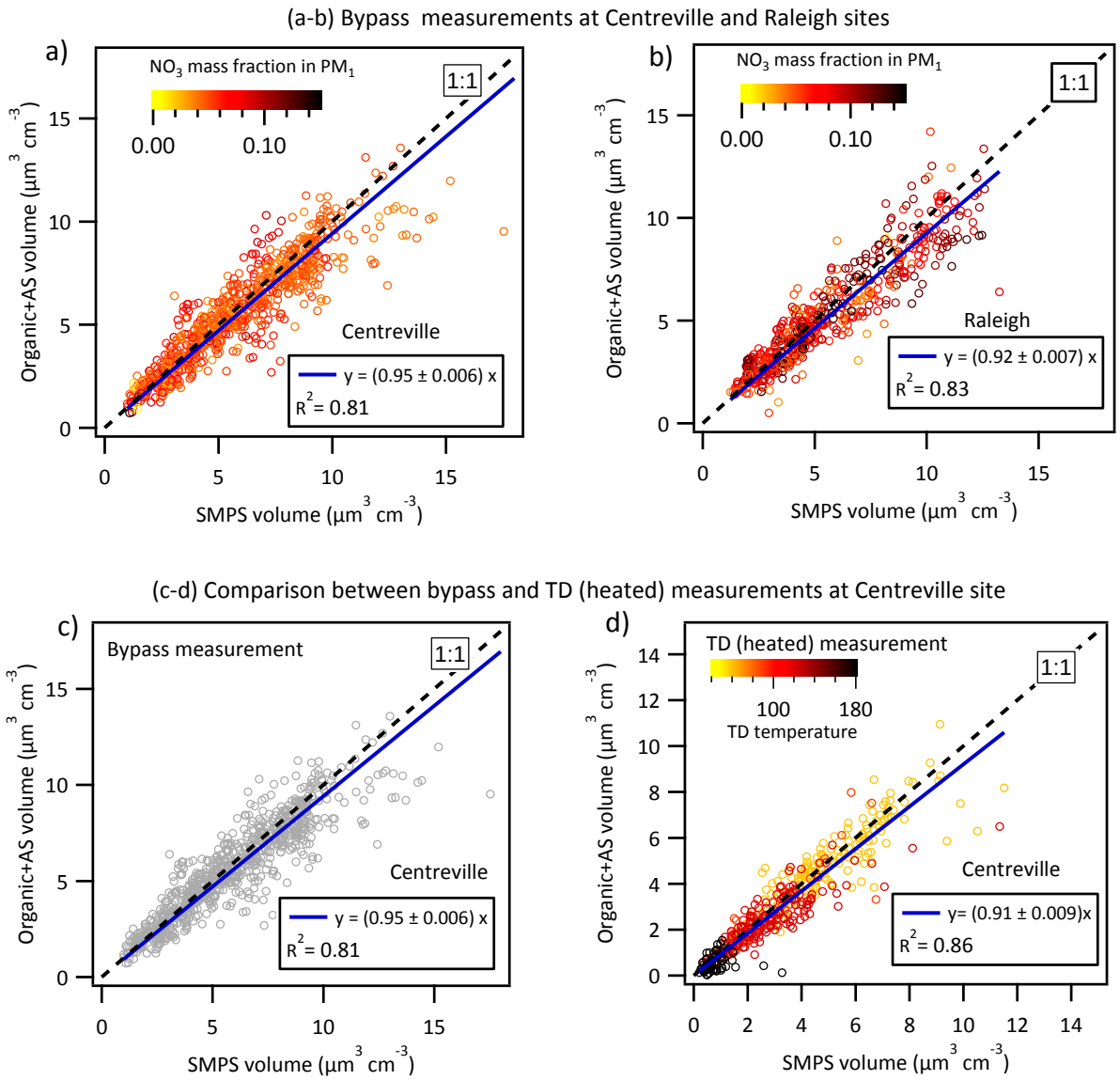

Figure S1: Comparison of submicron ambient aerosol volume concentrations measured by SMPS (10-600 nm) with the volume concentrations of organic aerosol (OA) + ammonium sulfate (AS) aerosol measured by ACSM. Both bypass and TD (heated) ACSM data were analyzed using a collection efficiency (CE) of 0.5 (Ng et al., 2011a) for all species. OA volume are calculated from the measured OA mass concentrations (m_{org}) and an effective density of OA of 1.4 g cm^{-3} , estimated from a parameterization using elemental composition (O:C; H:C) (Kuwata et al., 2012). AS mass concentration (m_{as}) is calculated as $\frac{132}{96} \times m_{SO4}$, where m_{SO4} is the mass concentration of sulfate (SO_4). AS volume is calculated assuming density of 1.77 g cm^{-3}.

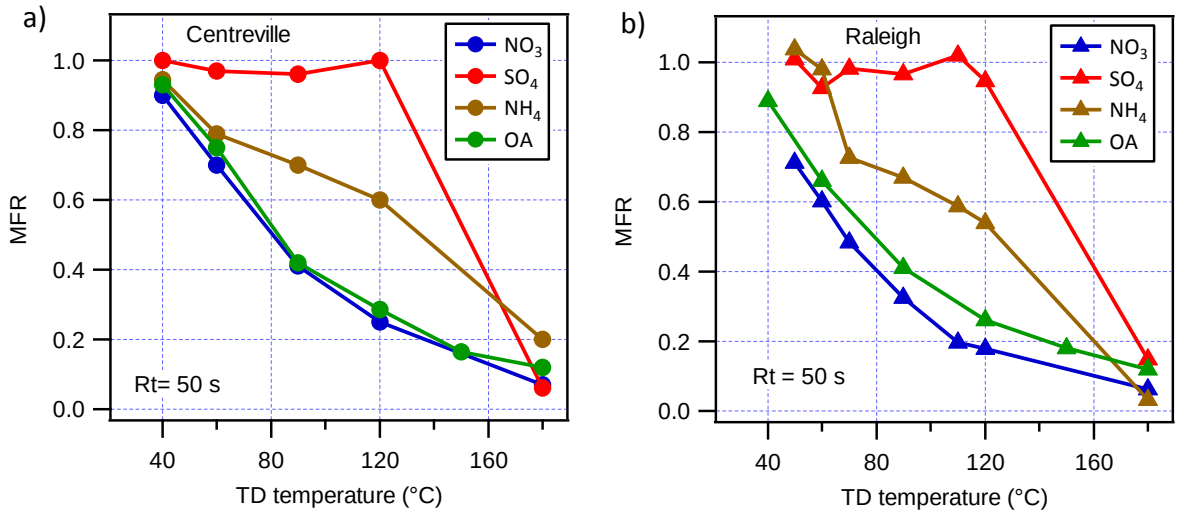

Figure S2: Campaign average mass thermogram (mass fraction remaining; MFR versus temperature) of NR-PM_1 species (OA, sulfate, nitrate, ammonium) from ACSM measurements via the TS-TD during the (a) Centreville and (b) Raleigh campaigns.

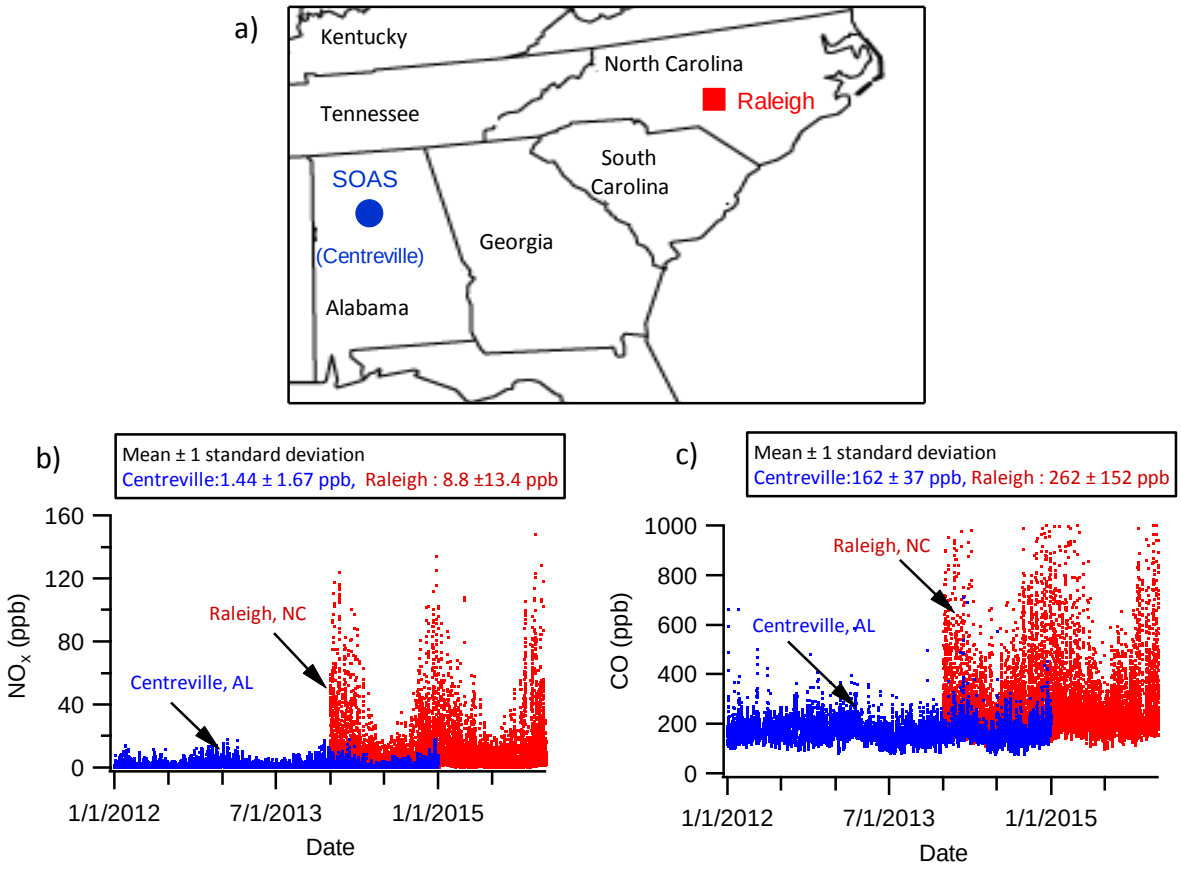

Figure S3: (a) Geographical locations of measurement sites and long-term trends of ambient (b) NO_x and (c) CO concentrations in the study areas. Centreville data are shown from SEARCH site (atmospheric-research.com/studies/SEARCH/) at Centreville (same location of the SOAS main ground site at Centreville). Raleigh data are shown from a monitoring station at Millbrook, Raleigh (35.856 ˚N, 78.574˚W, which is ~ 12 km northeast of the NCSU measurement site) operated by North Carolina Department of Environment and Natural Resources (NC DENR).

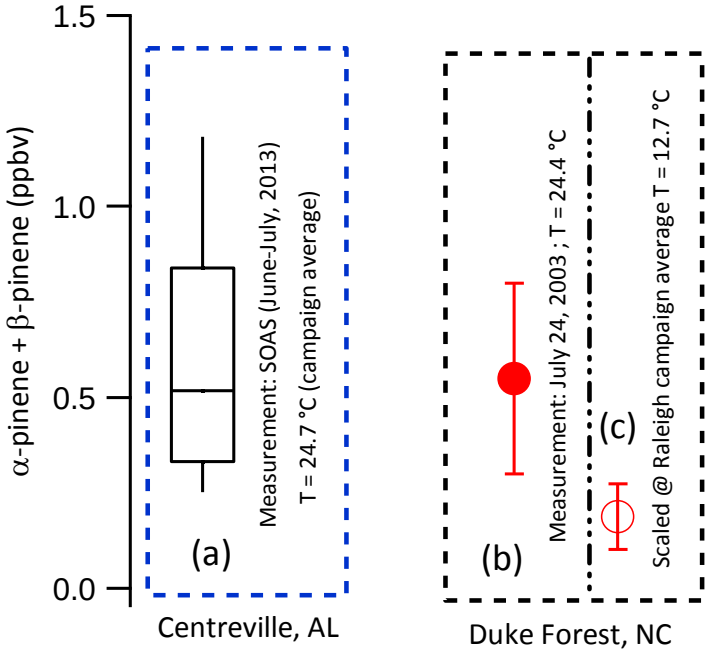

Figure S4: Comparison of ambient α-pinene + β-pinene concentration across two study areas. (a) Centreville data were collected during the SOAS campaign at Centreville, June-July, 2013 by Shepson's Group (Purdue University); (b) Duke Forest data were collected during CELTIC (Chemical Emission, Loss, Transformation and Interactions within Canopies) field campaign in 2003, reported from Stroud et al.(2005). Duke Forest site (35.98˚N, 79.09˚W) is about 40 km to the Northwest from the NCSU site. (c) Duke forest data are shown after scaling by a temperature adjustment factor, using the campaign- average temperature during our Raleigh measurements (October – November, 2013). The temperature adjustment factor for monoterpenes is estimated as, Ct = e0.09 (T-303), where T is in K (Warneke et al., 2010).

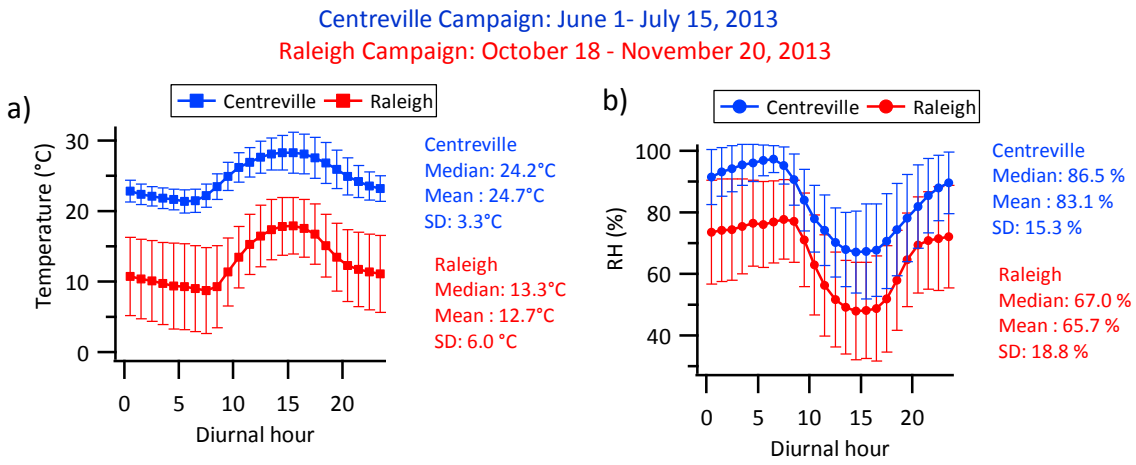

Figure S5: Diurnal trends of ambient temperature and relative humidity (RH) during the Centreville and Raleigh field campaign. Symbol is the mean value and error bar is ± one standard deviation of hourly data.

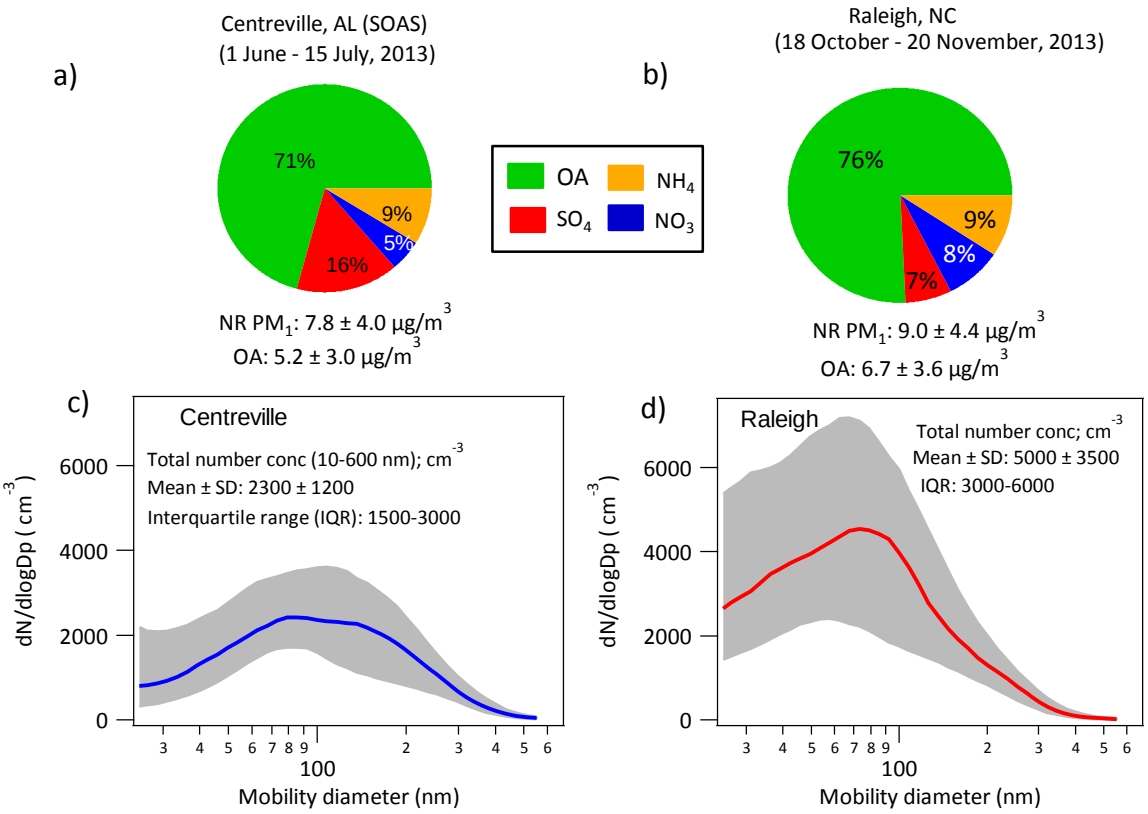

Figure S6: (a-b) Submicron aerosol compositions and (c-d) size distributions measured in ambient (bypass) condition. Non-refractory submicron aerosol (NR PM_1) composition data are measured by ACSM and number size distribution by SMPS. In panel b and c, solid lines show campaign median and shaded regions show interquartile range (25^{th} to 75^{th} percentile). Mean ± one standard deviation (SD) of organic aerosol (OA), PM_1 mass concentrations, and integrated number concentrations (10-600 nm) are reported.

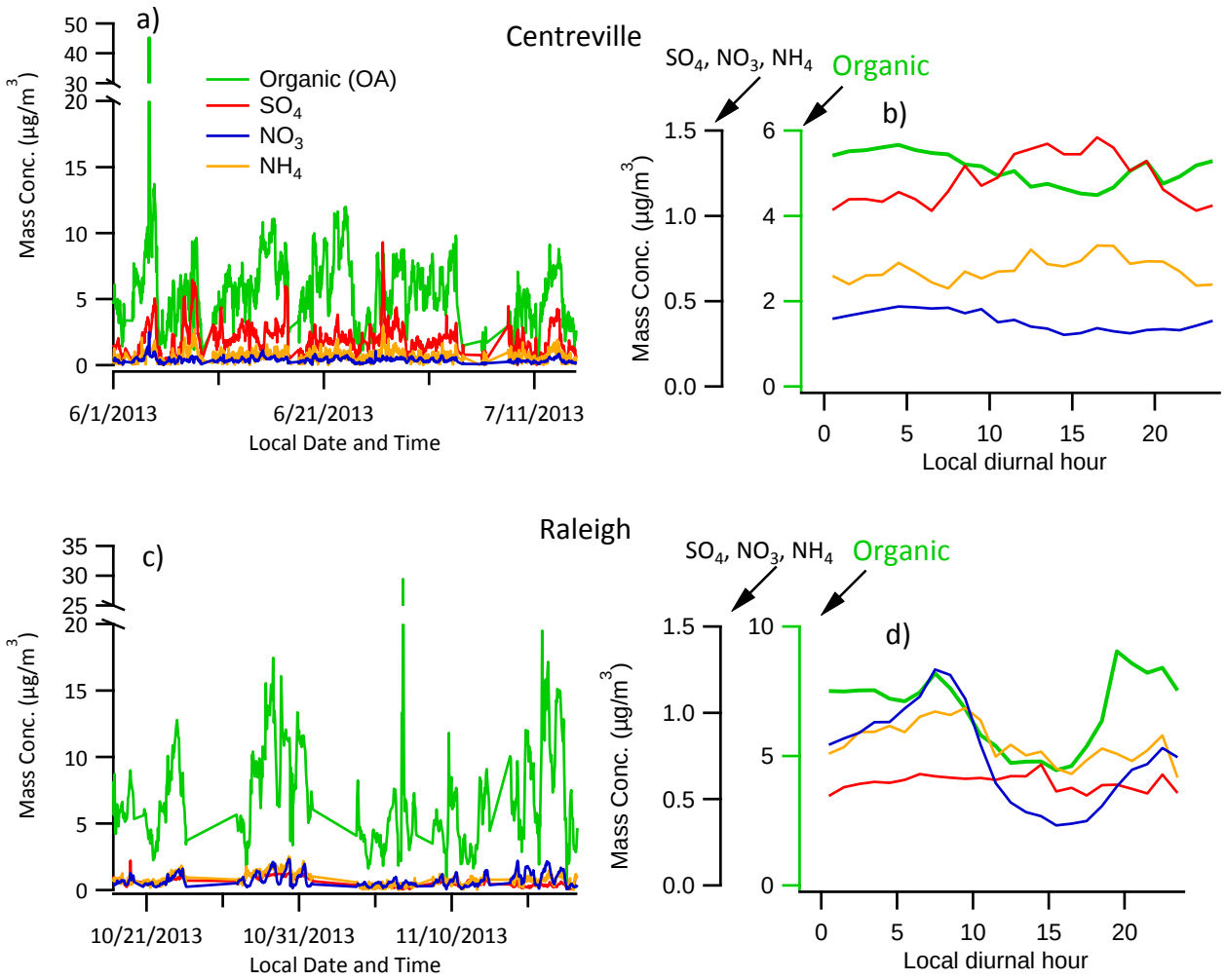

Figure S7: Time series and mean diurnal profiles of ambient submicron aerosol species concentrations (organics, sulfate; SO_4, nitrate; NO_3, and ammonium; NH_4) measured by ACSM. All ACSM data are analyzed with an assumed collection efficiency (CE) of 0.5.

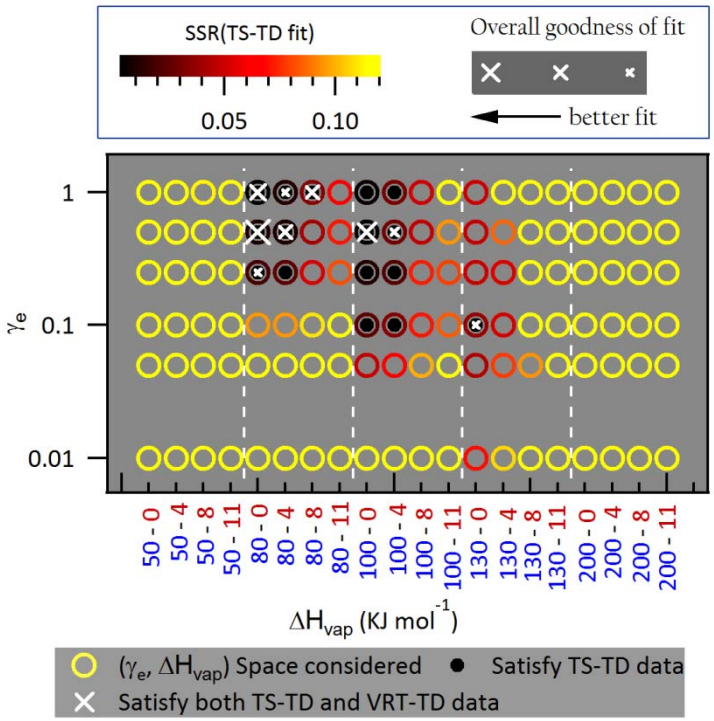

Figure S8: Similar to figure 3 in the main text showing analysis results for Raleigh data set. Extraction of OA gas-particle partitioning parameter (ΔH_{vap}, γ_e and f_i) values via evaporation kinetic model fits to campaign-average dual-TD observations. ΔH_{vap} = intercept-slope ($\log_{10}C^*$) relationship was used (e.g., 50-0 on x-axis represents intercept =50 and slope = 0). Symbols and colors represent the goodness of fit. Points with filled inner circles recreate TS-TD observations and points with a white cross (x) recreate both TD data sets to within observational variability. Crosses represent the overall goodness of fit including both TS-TD and VRT-TD observations, with larger size corresponding to a better fit.

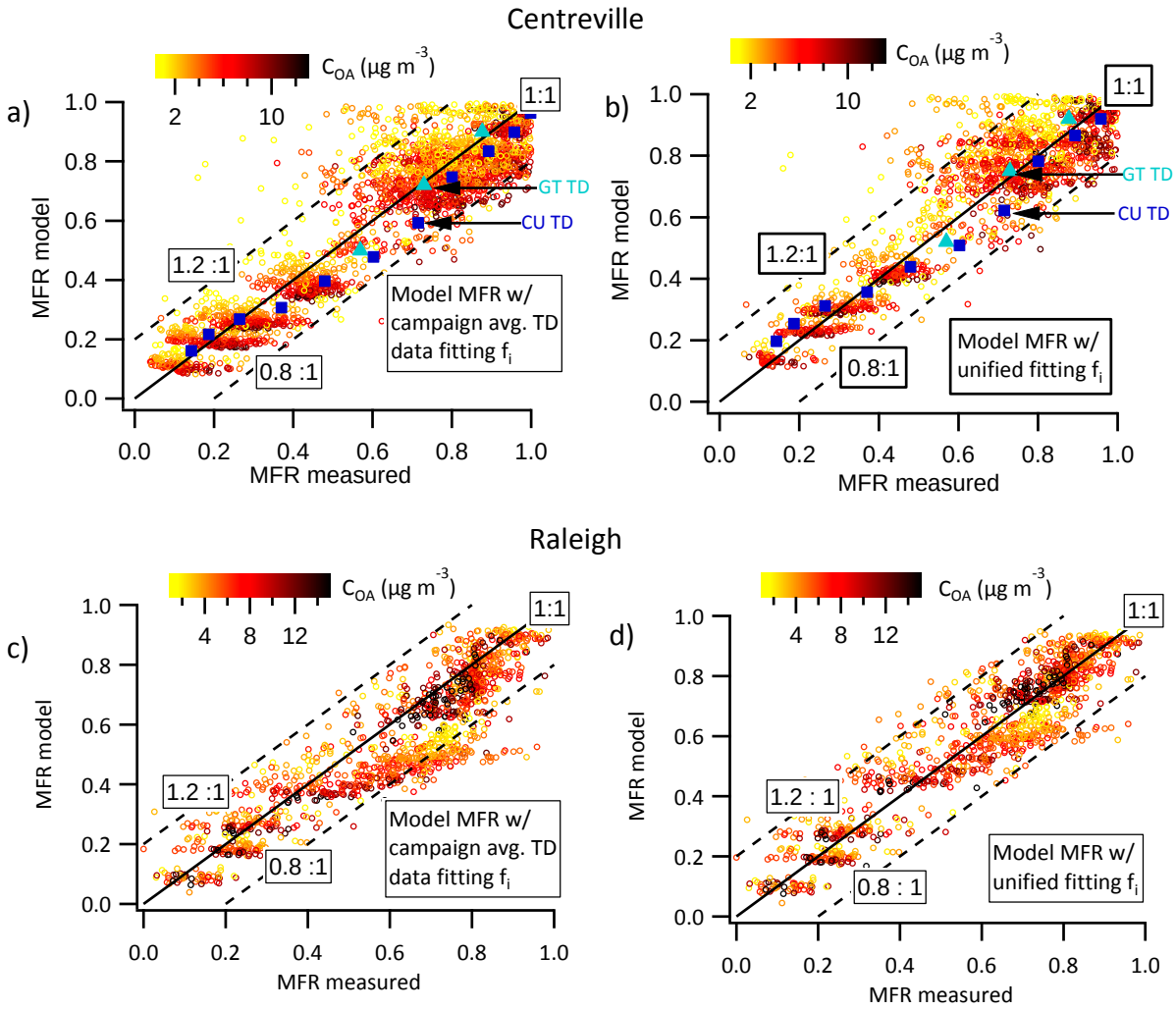

Fig S9: Comparison of individual observations and corresponding modeled MFRs applying the extracted f_i distribution from the campaign-average fit and unified fit with $\gamma_e = 0.5$ and $\Delta H_{vap} = 100$ kj mol^{-1} (see Table 1 in main text for f_i distributions). (a-b) Centreville data set, (c-d) Raleigh data set. Panel a is same as Fig. 4 (a) in main text. The coefficient of determination (r^2) and root mean squared error (RMSE) for the panel (a) $r^2 = 0.83$; RMSE = 0.11; (b) $r^2 = 0.81$; RMSE = 0.11; (c) $r^2 = 0.82$; RMSE = 0.12; and (d) $r^2 = 0.86$; RMSE = 0.09.

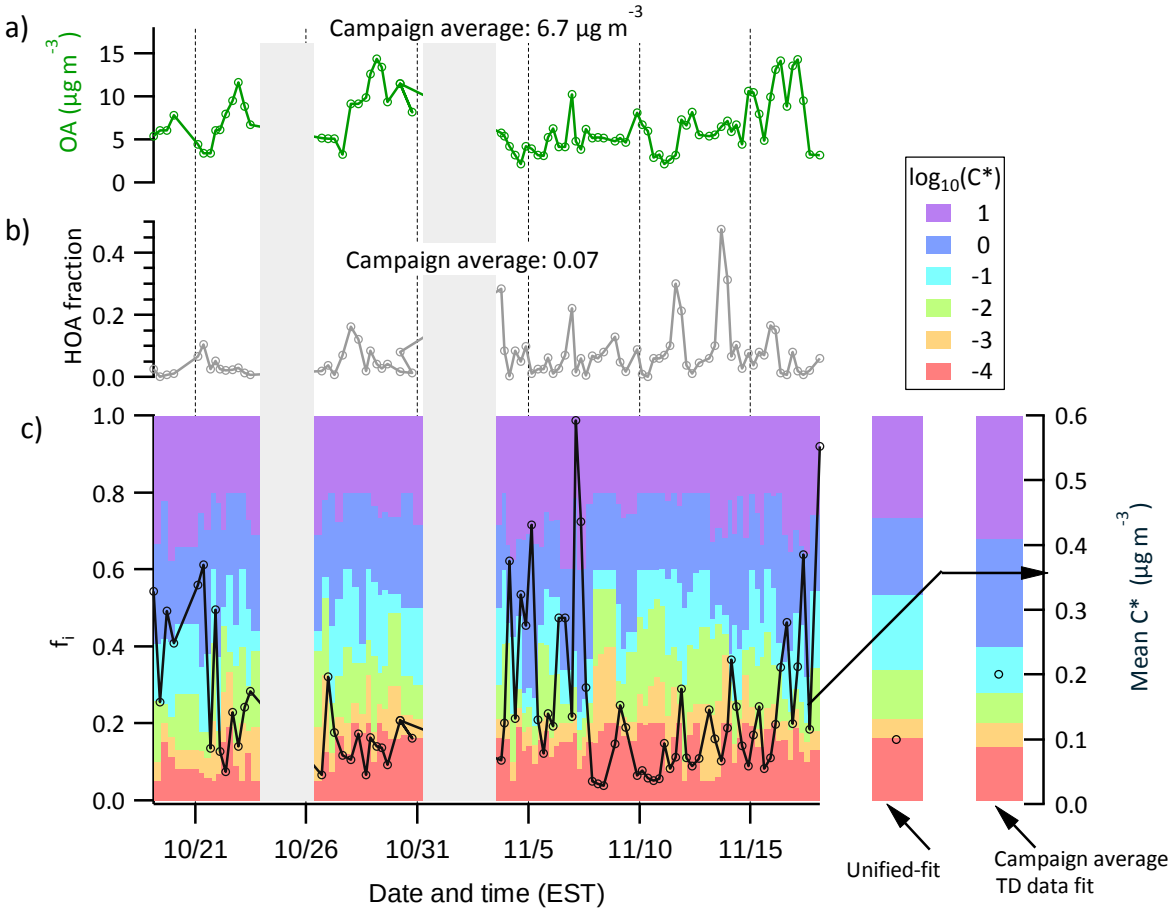

Figure S10: Similar to figure 6 in the main text showing analysis results for Raleigh data set. Time series of (a) ambient OA concentrations (C_{OA}), (b) hydrocarbon-like OA (HOA) fractional contribution to C_{OA}, and (c) OA volatility distribution (f_i) and $\overline{C^*}$ (open black circles).Tracer m/z based rough HOA are estimated as ~ 13.4 × (C_{57} − 0.1 × C_{44}), where C_{57} and C_{44} are the equivalent mass concentration of tracer ion m/z 57 and 44, respectively (Ng et al., 2011b).

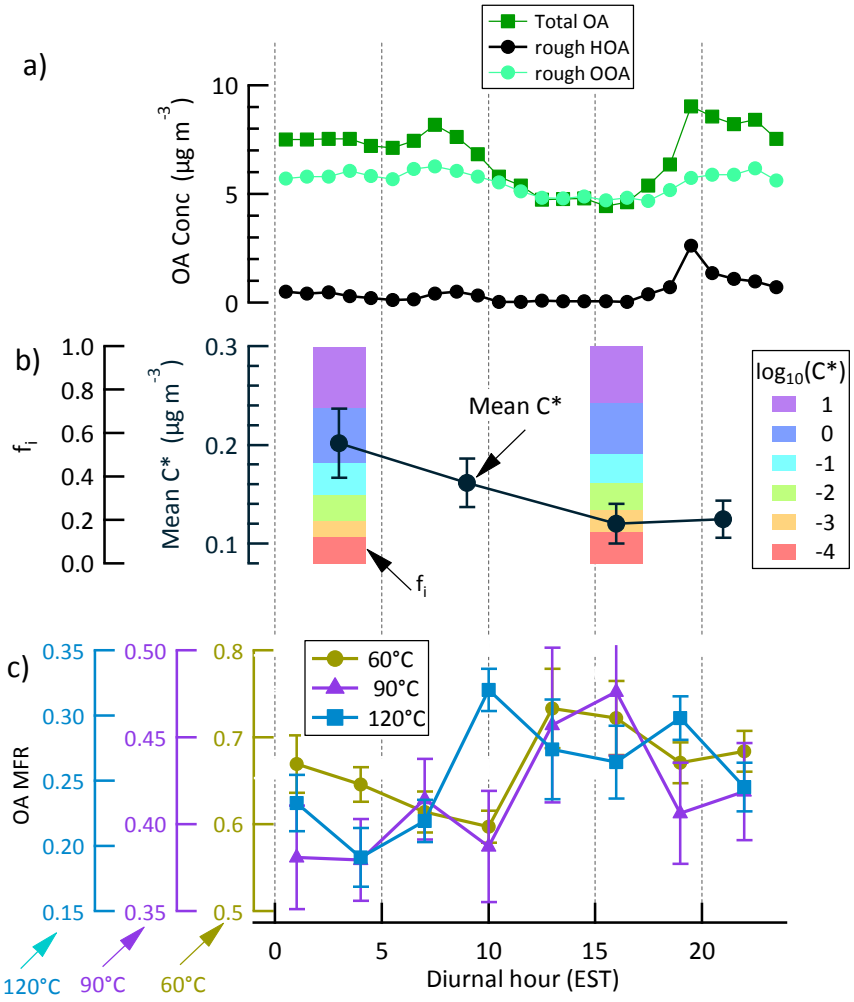

Figure S11: Similar to figure 7 in the main text showing analysis results for Raleigh data set. Campaign average diurnal trends of: (a) concentration of total OA and rough OA factors, (b) OA volatility (f_i and $\overline{C^*}$), (c) OA MFR after heating at 60, 90 and 120 ˚C with a TD residence time of 50 s. Tracer m/z based rough OA components are estimated following Ng et al.(2011) as: hydrocarbon-like OA (HOA ~ $13.4 \times (C_{57} - 0.1 \times C_{44})$) and oxygenated OA (OOA ~ $6.6 \times C_{44}$) , where C_{57} and C_{44} are the equivalent mass concentration of tracer ion m/z 57 and 44, respectively.

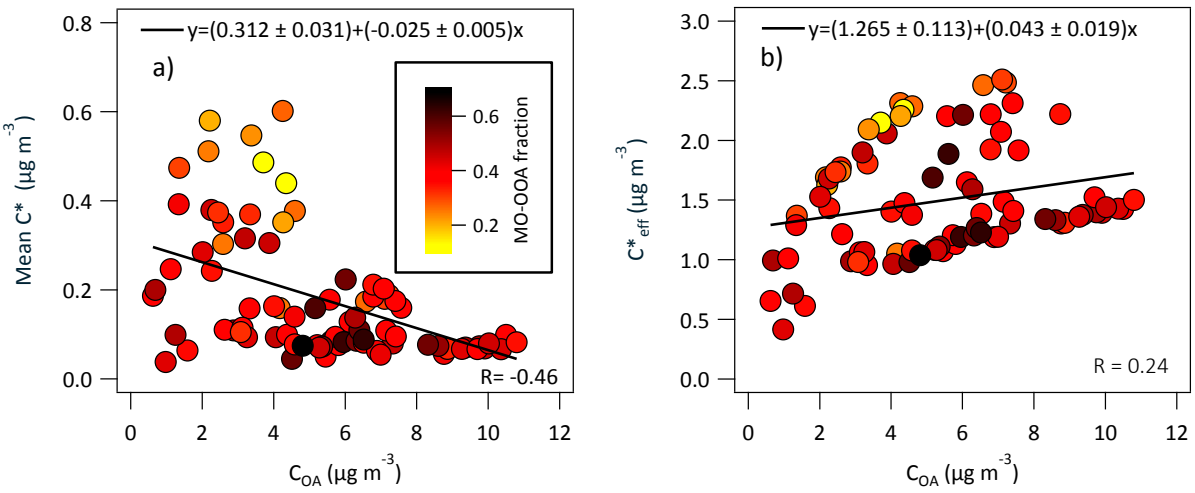

Figure S12: Scatter plot of (a) mean C* vs. ambient OA loading (C_{OA}); (b) C^*_{eff} vs. ambient OA loading (C_{OA}). Results are shown from the Centreville campaign.

5

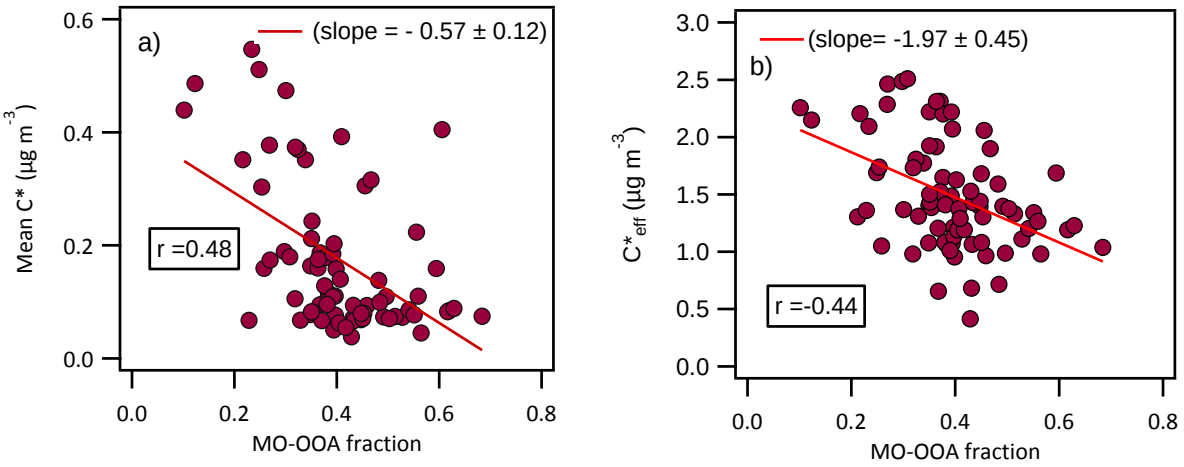

Figure S13: Scatter plot of (a) mean C* vs. MO-OOA fraction in C_{OA}; (b) C^*_{eff} vs. MO-OOA fraction in C_{OA}. Results are shown from the

10 Centreville campaign.

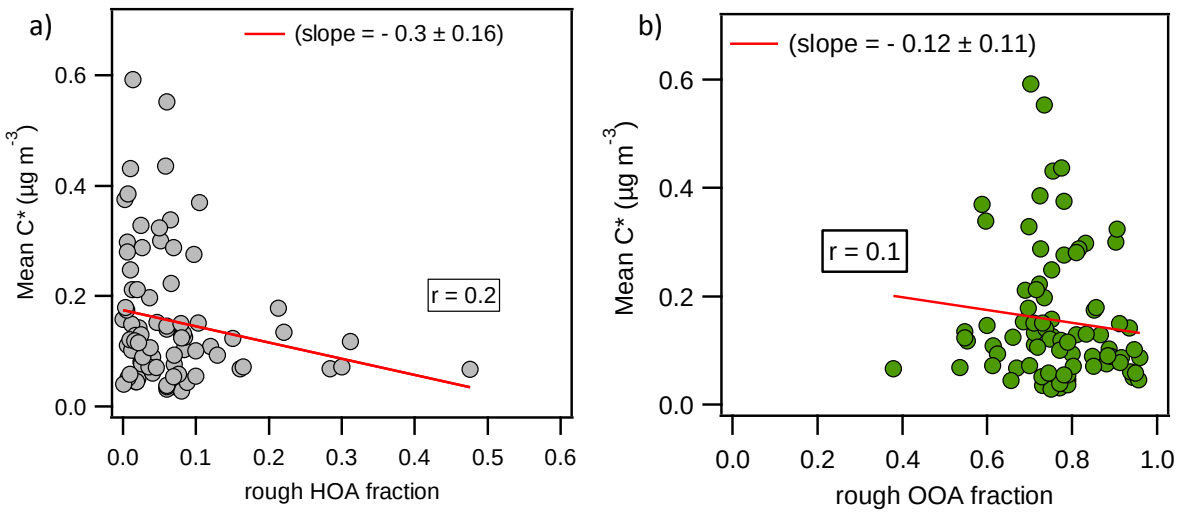

Figure S14: Similar to figure 8 in the main text showing analysis results for Raleigh data set. Scatter plot of mean C* verses (a) rough HOA fraction, and (b) rough OOA fraction in total OA concentration during the Raleigh campaign. For rough HOA and OOA estimation method, see Fig S11 caption.

S4. Supplementary Tables

Table S1: TD kinetic model input parameters

Parameters	Value	Notes
Density (kg m^{-3})	1400	Kuwata et al., 2012 parameterization
Diffusion coefficient (m^2 s^{-1})	3.5 E-06	Cappa and Jimenez (2010)
Surface tension (J m^{-2})	0.08	Approximated as Pimelic acid, Bilde et al.(2003)
Molecular weight (MW)	MW_i (g mol^{-1}) =169-28 ($\log_{10}C^*_i$)	Approximated from Di-carboxylic acid

Table S2: Statistical correlation (Pearson R value) between isoprene-OA fraction to C_{OA} and f_i's in any particular C^* bin

$\log_{10}C^*$ bin	-4	-3	-2	-1	0	10	mean C^*	C^*_{eff}
Pearson R value	0.02	0.29	-0.07	-0.06	-0.14	0.04	-0.06	0.19

References

Bilde, M., Svenningsson, B., Mønster, J., and Rosenørn, T. (2003). Even−Odd Alternation of Evaporation Rates and Vapor Pressures of C3−C9 Dicarboxylic Acid Aerosols. Environ. Sci. Technol. *37*, 1371–1378.

Cappa, C.D., and Jimenez, J.L. (2010). Quantitative estimates of the volatility of ambient organic aerosol. Atmos Chem Phys *10*, 5409–5424.

Huffman, J.A., Docherty, K.S., Aiken, A.C., Cubison, M.J., Ulbrich, I.M., DeCarlo, P.F., Sueper, D., Jayne, J.T., Worsnop, D.R., Ziemann, P.J., et al. (2009). Chemically-resolved aerosol volatility measurements from two megacity field studies. Atmos Chem Phys *9*, 7161–7182.

Kuwata, M., Zorn, S.R., and Martin, S.T. (2012). Using Elemental Ratios to Predict the Density of Organic Material Composed of Carbon, Hydrogen, and Oxygen. Environ. Sci. Technol. *46*, 787–794.

Lehtinen, K., Korhonen, H., Maso, M. D. and Kulmala, M.: On the concept of condensation sink diameter, Boreal Env. Res, 8, 405–411, 2003.

Ng, N.L., Herndon, S.C., Trimborn, A., Canagaratna, M.R., Croteau, P.L., Onasch, T.B., Sueper, D., Worsnop, D.R., Zhang, Q., Sun, Y.L., et al. (2011a). An Aerosol Chemical Speciation Monitor (ACSM) for Routine Monitoring of the Composition and Mass Concentrations of Ambient Aerosol. Aerosol Sci. Technol. *45*, 780–794.

Ng, N.L., Canagaratna, M.R., Jimenez, J.L., Zhang, Q., Ulbrich, I.M., and Worsnop, D.R. (2011b). Real-Time Methods for Estimating Organic Component Mass Concentrations from Aerosol Mass Spectrometer Data. Environ. Sci. Technol. *45*, 910–916.

Saha, P.K., Khlystov, A., and Grieshop, A.P. (2015). Determining Aerosol Volatility Parameters Using a "Dual Thermodenuder" System: Application to Laboratory-Generated Organic Aerosols. Aerosol Sci. Technol. *49*, 620–632.

Stroud, C., Makar, P., Karl, T., Guenther, A., Geron, C., Turnipseed, A., Nemitz, E., Baker, B., Potosnak, M., and Fuentes, J.D. (2005). Role of canopy-scale photochemistry in modifying biogenic-atmosphere exchange of reactive terpene species: Results from the CELTIC field study. J. Geophys. Res. Atmospheres *110*, D17303.

Warneke, C., de Gouw, J.A., Del Negro, L., Brioude, J., McKeen, S., Stark, H., Kuster, W.C., Goldan, P.D., Trainer, M., Fehsenfeld, F.C., et al. (2010). Biogenic emission measurement and inventories determination of biogenic emissions in the eastern United States and Texas and comparison with biogenic emission inventories. J. Geophys. Res. Atmospheres *115*, D00F18.